VORTEX DYNAMO IN ROTATING MEDIA†

Michael I. Kopp[a]*, Volodymyr V. Yanovsky[a,b]

aInstitute for Single Cristals, Nat. Academy of Science Ukraine, Nauky Ave. 60, Kharkiv 61072,Ukraine
bV.N. Karazin Kharkiv National University, 4, Svoboda Sq., Kharkiv, 61022, Ukraine
*Corresponding Author e-mail: michaelkopp0165@gmail.com
Received April 9, 2023; accepted April 24, 2023

The review highlights the main achievements in the theory of the vortex dynamo in rotating media. Various models of a vortex dynamo in rotating media are discussed: a homogeneous viscous fluid, a temperature-stratified fluid, a moist atmosphere, and a stratified nanofluid. The main analytical and numerical results for these models obtained by the method of multiscale asymptotic expansions are presented. The main attention is paid to models with a non-spiral external force. For a rotating moist atmosphere, characteristic estimates of the spatial and temporal scales of the generated vortex structures are obtained. New effects of the vortex dynamo in a rotating stratified nanofluid, which arise due to thermophoresis and Brownian motion of nanoparticles, are shown. The results of the analysis of the nonlinear equations of the vortex dynamo in the stationary regime are presented in the form of spiral kinks, periodic nonlinear waves, and solitons.

Keywords: *dynamo theory; large-scale instability; Coriolis force; multiscale asymptotic expansions; α - effect; solitons; kinks*
PACS: 47.32.C, 47.32.cd, 47.90.+a

1. INTRODUCTION

The review is devoted to modern problems with the vortex dynamo theory. This is an extensive area of research that includes the generation and nonlinear evolution of large-scale vortex structures. The focus of the review will be on the influence of the rotation of turbulent media on the generation of structures. The reason for the importance of this factor is both the widespread nature and the nontriviality of its influence. Rotation effects play an important role in many practical and theoretical applications of fluid mechanics [1] and are especially important in geophysics and astrophysics [2]-[5], where one has to deal with such rotating objects as the Earth, Jupiter, the Sun, etc. A variety of wave and vortex motions can be excited in rotating liquids. For example, gyroscopic waves, Rossby waves, internal waves, localized vortices, and coherent vortex structures. Large-scale vortex structures are of the greatest interest because they carry out efficient transfer of energy and momentum. Large-scale structures are understood to mean structures whose characteristic scale is much greater than the scale of turbulence or the scale of the external force that excites this turbulence. The study of the problem of generation of large-scale vortex structures (LSVS) is of great importance for a number of geophysical and astrophysical problems, such as the problem of the origin of Jupiter's Great Spot, Venus superrotation, vortex structures in solar prominences, the spiral structure of galaxies, etc. [6]-[7]. Geophysical problems include studies on the generation of LSVSs such as tropical cyclones (typhoons), tornadoes, etc. These LSVS play an important role in the global circulation of the atmosphere, which is very important for weather and climate [8]-[9] forecasts on our planet. The actual effect of LSVS generation in turbulence is called the vortex dynamo.

According to the Kolmogorov-Obukhov local theory of turbulence, large-scale violations of homogeneity and isotropy are restored on small scales of turbulent flow. In this regard, the question arises: can such turbulence enhance large-scale perturbations? In magnetohydrodynamics, the answer to this question was obtained earlier. It was shown in [10] that initially homogeneous, isotropic, and mirror-symmetric turbulence cannot enhance large-scale magnetic fields. However, if the mirror symmetry of turbulence is broken, then such a medium can enhance the large-scale magnetic field. The process of amplification of a large-scale field occurs under the action of a turbulent e.m.f. proportional to the average magnetic field $\vec{\mathcal{E}} = \alpha \vec{\overline{H}}$, and the coefficient α is proportional to the average helicity $\alpha \sim \overline{\vec{v}^t rot \vec{v}^t}$ of the velocity field. The phenomenon of generation of large-scale magnetic fields by homogeneous isotropic but mirror-asymmetric (helical) turbulence discovered in [10] was called the α -effect. On the basis of this effect, the dynamo theory [11]-[12] was constructed by the efforts of many researchers and explains the origin of magnetic fields in various astrophysical objects: the Earth, planets, the Sun, galaxies, etc. Helical turbulence is characterized by a violation of the mirror symmetry of the turbulent velocity field, for which the correlation $\overline{\vec{v}^t rot \vec{v}^t}$ is non-zero. Such a turbulent velocity field is characterized by the fact that right-handed and left-handed vortices are observed with different probabilities, i.e., there are more vortices of one sign than another.

The concept of a vortex dynamo was first developed in [13]–[14], where a hypothesis was put forward that helical turbulence is capable of generating large vortices. This hypothesis was based on the similarity of the equations of induction of a magnetic field and a vortex in hydrodynamics. It was hypothesized in [13] that helical turbulence is capable of generating large eddies similarly to a large-scale magnetic field in magnetohydrodynamics. The physical essence of this phenomenon lies in the inverse cascade of energy transfer from small vortices to larger ones. However, it

was shown in [15] that there is no effect on generating large-scale vortices by homogeneous isotropic helical turbulence in an incompressible fluid. The reason for the negative effect lies in the certain symmetry of the Reynolds stress tensor in the averaged Navier-Stokes equation. The Reynolds stresses are a linear functional of the mean velocity field (for weak fields), which can be represented as a series

$$\overline{v_k^t \nabla_k v_i^t} = \nabla_k \left(\overline{v_k^t v_i^t} \right) = T_i^{(0)} + T_{ik}^{(1)} V_k + T_{ikl}^{(2)} \nabla_k V_l + \cdots,$$

where the expansion coefficients of the tensors $T^{(n)}$ are expressed in terms of the moments of the turbulent fields. If the tensor $\overline{v_k^t v_i^t}$ is symmetric in indices, then the tensor $T_{ikl}^{(2)}$ must also be symmetric in indices i, k and not be expressed in terms of the antisymmetric tensor ε_{ikl}. The tensor of the third rank cannot be constructed only from Kronecker tensors δ_{ik}; therefore, the hydrodynamic α-effect is absent in the homogeneous isotropic turbulence of an incompressible fluid. However, a reverse energy cascade in helical turbulence is possible. This requires an additional symmetry break of the Reynolds stresses. The effect of generating large-scale eddies is associated with the appearance of the term $\alpha\vec{\Omega}$:

$$\frac{\partial \vec{\Omega}}{\partial t} + \alpha\, rot\,\vec{\Omega} = \nu\Delta\vec{\Omega},$$

where $\alpha \sim \overline{\vec{v}^T rot\vec{v}^T}$ is expressed in terms of the turbulence helicity, $\vec{\Omega} = rot\vec{V}$, $\vec{V}$ is a large-scale field of fluid velocity, ν is a turbulent kinematic viscosity. This effect is called the hydrodynamic alpha effect. The further development of the vortex dynamo theory was based on the search for additional factors that break the symmetry of the equations. These factors, in addition to the compressibility of the medium, are, for example, an inhomogeneous flow [16], a temperature gradient in a gravity field [17], and a specific water content and temperature gradient in a gravity field [18].

It should be noted that free convection, or heat and mass transfer of matter in the gravity field, plays a special role in the processes of LSVS generation in the atmosphere of the Earth and other planets. The occurrence of LSVS in convective systems was studied both within the laminar theory [19] and in the turbulent one [15]-[18]. The most developed is the turbulent theory (vortex dynamo), which shows the existence of large-scale instability in convective systems with small-scale helical turbulence [17]-[18], which results in the formation of one convective cell, which is interpreted as a huge tropical cyclone-type vortex. This theory was confirmed in a number of numerical and analytical calculations [20]. Large-scale vortex instability in rotating turbulent flows has been studied in many papers [21]-[24]. So, when considering rotating convective systems, attempts were made to apply the results obtained to the theory of the occurrence of tropical cyclones. The linear theory of the vortex dynamo [15]-[24] is best developed within the framework of the statistical approach, which also uses the second-order correlation approximation. Thus, the question arose about the mechanisms of saturation of large-scale instability and the emergence of stationary vortex structures. However, the construction of a nonlinear theory of the vortex dynamo within the framework of the statistical theory has great difficulties associated with the problem of closure of the averaged equations.

The nonlinear theory of the vortex dynamo was developed within the framework of a dynamic approach based on the method of multiscale asymptotic expansions. In [25], for the first time, the method of multiscale asymptotic expansions was applied to describe the generation of LSVSs in non-reflective, invariant turbulence. In this work, it was shown that parity violation in small-scale turbulence (external small-scale forces) leads to large-scale instability, the so-called anisotropic kinetic alpha effect (AKA effect). In another work [26], the inverse energy cascade and nonlinear saturation of the instability were studied. The instability of the hydrodynamic α-effect, obtained within the framework of the dynamic approach, can be interpreted as a new type of parametric instability arising from a special type of pumping (external force). Under the action of an external small-scale periodic force $\vec{F}_0$, fluctuations of the velocity field $\vec{v}_0$ arise, the nonlinear interaction of which affects large-scale velocity perturbations $\vec{W}$. The Reynolds stresses $R_{ij} = \overline{v_i v_j}$ (where averaged over the period) are modified by large-scale perturbations, and in the linear approximation, the gradient series can be expanded into a Taylor series [27]:

$$R_{ij} = -\alpha_{ijl} W_l - \nu_{ijlm} \nabla_l W_m + \ldots$$

The first term is known as the anisotropic kinetic α-effect (AKA) [25], which describes the generation of LSVSs. Thus, an external force that creates a small-scale parity violation can lead to non-trivial changes in the large-scale flow. In contrast to [25], in [27], a small-scale force was considered that creates a parity-invariant turbulent flow. In this case, the AKA effect is absent, and the dynamics of small large-scale perturbations $\vec{W}$ is determined by the turbulent viscosity. Although parity violation is a more general concept than helicity, it is helicity $\overline{\vec{v} rot\vec{v}} \neq 0$ that is a widespread mechanism for parity violation in hydrodynamic flow. In [28]-[29], a nonlinear theory of the convective vortex dynamo was developed, where the method of multiscale asymptotic expansions was applied. Paper [28] is a more complete

version of [29], which presents the linear theory of LSVS generation in more detail. The small Reynolds number of small-scale motions is a parameter of the asymptotic expansions.

This method makes it possible to single out the main order of the emergence of instability from the entire hierarchy of perturbations. Nonlinear stabilization of large-scale convective instability, considered in [28]-[29], leads to the formation of helical vortex solitons or kinks of a new type in the fluid, despite stable stratification. The structure of the equations in [28]-[29] describing the instability in the linear approximation is similar to the AKA effect equation. But, unlike the AKA effect, α is a function of the Rayleigh number Ra. This means that in an unstratified fluid, $Ra = 0$, the instability disappears. In addition, in [28]-[29] helical turbulence was assumed to be given, in contrast to [25]-[26].

Using the method of multiscale asymptotic expansions, in [30], a large-scale vortex instability was obtained in a rotating viscous fluid under the action of an external small-scale helical force. In this work, the nonlinear stage of instability and the generation of vortex kinks of a new type were also investigated. The paper [30] was generalized to the case of a rotating moist atmosphere in [31], where it was shown that taking into account the effects of stratification in a rotating atmosphere, such as temperature heating and an additional source of condensation heat release, enhances large-scale vortex disturbances. It was shown in [31] that the helicity of the small-scale velocity field is due not only to the action of the Coriolis force, as in a homogeneous medium [30], but also to the stratification of the moist atmosphere. This circumstance leads to the appearance of a new instability of the α-effect type, as a result of which large-scale vortex structures are generated.

The origin of helical turbulence in natural conditions is usually associated with the influence of the Coriolis force on the turbulent motion of the medium [10], which was initially uniform, isotropic and mirror-symmetric. Thus, a problem arises in the origin of helicity itself. The natural hypothesis is that helicity itself arises as a result of the action of the Coriolis force on convective turbulence. In this case, large-scale instabilities in the atmosphere should appear self-consistently, without additional assumptions. For the first time, the question of the generation of large-scale vortex fields under the action of a small-scale force with zero helicity $\vec{F}_0 rot \vec{F}_0 = 0$ in a rotating homogeneous medium, i.e., without taking into account convective phenomena, was considered in [32]-[33], and taking into account convective phenomena in [34]-[36]. It was also demonstrated that nonlinear Beltrami waves and localised vortex structures such as kinks emerge as a result of the development of a large-scale instability in an obliquely rotating fluid.

The generation of the LSVS by a large-scale instability of the hydrodynamic α-effect has a threshold character and depends on the magnitude of the helicity. In this connection, the search for large-scale helical vortex instability based on atmospheric data was started in [37]. An extensive review of studies aimed at applying the theoretical hypothesis of a turbulent vortex dynamo to the study of tropical cyclogenesis is presented in [38]. The review presents the results of a numerical simulation of the spiral self-organization of humid-convective atmospheric turbulence during the formation of tropical cyclones. Particular attention is paid here to the influence of the initial conditions on the generation of helicity in the first hours of the experiments. These studies contributed to the application of the vortex dynamo theory for diagnosing the onset of cyclogenesis in a favorable tropical environment.

The question of the appearance of helicity, leading to the appearance of a LSVS, is central to any formalism. An important difference between these formalisms is that in statistical turbulence, it is difficult to correctly separate small-scale motions from large-scale ones, which leads to the problem of the influence of some scales on others and requires the use of additional hypotheses. However, this can be done consistently in the multiscale formalism. The difference in averaging over small-scale turbulent fluctuations (in the statistical theory) and small-scale motions (in the multiscale method) rather indicates the closeness of these theories. Therefore, it can be assumed that the average helicity arising in the statistical theory is quite similar to the average helicity in the multiscale method.

Next, we discuss in more detail the new types of large-scale instabilities and localized vortex structures in rotating turbulent media considered in our papers [30]-[36].

2. LARGE-SCALE INSTABILITY OF A ROTATING FLUID WITH A SMALL-SCALE FORCE

Let's start with a discussion of large-scale instability in a rotating viscous fluid under the action of a small-scale external force, which was first considered in [30]. The small-scale external force simulates the action of small-scale turbulence and maintains turbulent fluctuations at a certain stationary level. It was shown in [30] that, as a result of the development of a large-scale instability in a rotating fluid, nonlinear large-scale helical vortex structures such as Beltrami vortices or localized kinks with an internal helical structure arise.

2.1. Basic equations and statement of the problem

Consider the equations of motion of an incompressible rotating fluid with an external force in a rotating coordinate system

$$\frac{\partial \vec{V}}{\partial t} + (\vec{V}\nabla)\vec{V} = -\frac{1}{\rho_0}\nabla P + 2[\vec{V}\times\vec{\Omega}] + \nu\Delta\vec{V} + \vec{F}_0 \tag{1}$$

$$div\vec{V} = 0 \tag{2}$$

Here, $\vec{\Omega}$ is the constant angular velocity of rotation of the fluid, v is the viscosity, and ρ_0 is the constant density of the fluid. The vector of angular velocity of rotation $\vec{\Omega}$ is directed along the axis OZ, and the external force $\vec{F}_0$ acts in a plane that is perpendicular to the axis of rotation (see Fig. 1).
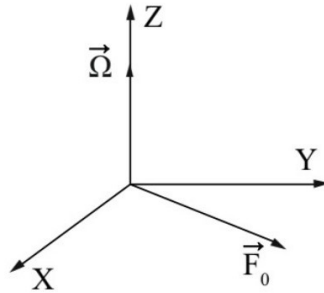

Figure 1. The angular velocity vector $\vec{\Omega}$ is directed perpendicular to the plane (X, Y) in which the external force $\vec{F}_0$ is located.

Let us denote the characteristic amplitude of the force f_0, and its characteristic spatial and temporal scales, respectively, as λ_0 and t_0. The external force has the following properties:

$$\vec{F}_0 = f_0 \vec{F}_0 \left(\frac{\vec{x}}{\lambda_0}, \frac{t}{t_0} \right), div\vec{F}_0 = 0, \vec{F}_0 rot\vec{F}_0 \neq 0. \tag{3}$$

The main role of this force is the creation of small-scale helical fluctuations in the velocity field $\vec{v}_0$ with a small Reynolds number $R = \dfrac{v_0 t_0}{\lambda_0} \ll 1$, or, in other words, the maintenance of stationary small-scale helical turbulence. It is obvious that the characteristic speed caused by an external force has the same characteristic scales:

$$\vec{v}_0 = \vec{v}_0 \left(\frac{\vec{x}}{\lambda_0}, \frac{t}{t_0} \right)$$

Let's maintain the old notation of variables but replace the dimensioned variables in the system of equations (1) and (2) with dimensionless variables for convenience:

$$\vec{x} \rightarrow \frac{\vec{x}}{\lambda_0}, \quad t \rightarrow \frac{t}{t_0}, \quad \vec{V} \rightarrow \frac{\vec{V}}{v_0}, \quad \vec{F}_0 \rightarrow \frac{\vec{F}_0}{f_0}, \quad P \rightarrow \frac{P}{\rho_0 P_0}, \quad t_0 = \frac{\lambda_0^2}{v}, \quad P_0 = \frac{v_0 v}{\lambda_0}, \quad f_0 = \frac{v_0 v}{\lambda_0^2}, \quad v_0 = \frac{f_0 \lambda_0^2}{v}.$$

Then, in dimensionless variables, equations (1)-(2) take the form:

$$\frac{\partial \vec{V}}{\partial t} + R(\vec{V} \cdot \nabla)\vec{V} = -\nabla P + [\vec{V} \times \vec{D}] + \Delta \vec{V} + \vec{F}_0, \tag{4}$$

$$div\vec{V} = 0. \tag{5}$$

Here, $R = \dfrac{\lambda_0 v_0}{v}$ is the Reynolds number of small-scale pulsations, $D_i = \dfrac{2\Omega_i \lambda_0^2}{v}$ is the dimensionless rotation parameter on the scale λ_0 ($i = 1, 2, 3$), associated with the Taylor number $Ta_i = D_i^2$, and which is a characteristic of the degree of influence of Coriolis forces over viscous forces.

In what follows, the Reynolds number $R \ll 1$ will be assumed to be small, and we will construct an asymptotic expansion from this small parameter. We consider the parameter D to be independent of the asymptotic expansion scheme. Of course, the Reynolds number on a large scale can be large. Consider the following formulation of the problem: we will consider the external force as small-scale and high-frequency. This force leads to small scale velocity fluctuations. After averaging, the rapidly oscillating fluctuations disappear. However, due to small non-linear interactions, non-zero terms may appear after averaging in some orders of perturbation theory. This means that these terms are not oscillatory, i.e., they are on a large scale. From a formal point of view, these members are secular. The difference from zero of such "constant" contributions leads to a rapid collapse of the asymptotic expansions. Therefore, the conditions for the conservation of the asymptotic expansion are based on the vanishing of the secular terms. This leads to conditions for the solvability of equations for large-scale perturbations. We discuss these equations below.

2.2. The method of multiscale asymptotic expansions and the equation for the large-scale velocity field

We denote the small-scale variables $x_0 = (\vec{x}_0, t_0)$, and the large-scale $X = (\vec{X}, T)$ ones. Denote the derivative $\dfrac{\partial}{\partial x_0^i}$ by ∂_i, and the derivative $\dfrac{\partial}{\partial t_0}$ by ∂_t. To designate large-scale spatial and temporal derivatives, the following notation will be used:

$$\frac{\partial}{\partial X_i} \equiv \nabla_i, \quad \frac{\partial}{\partial T} \equiv \partial_T$$

The spatial and temporal derivatives now turn into the corresponding derivatives with respect to both fast small-scale variables and slow large-scale variables. Therefore, we replace the spatial and temporal derivatives in equations (4)-(5) with operators of the form:

$$\frac{\partial}{\partial x_i} \to \partial_i + R^2 \nabla_i, \quad \frac{\partial}{\partial t} \to \partial_t + R^4 \partial_T \tag{6}$$

To construct a nonlinear theory, we represent the variables $\vec{V}, P$ in the form of asymptotic series:

$$\vec{V}(x,t) = \frac{1}{R}\vec{W}_{-1}(X) + \vec{v}_0(x_0) + R\vec{v}_1 + R^2\vec{v}_2 + R^3\vec{v}_3 + \cdots \tag{7}$$

$$P(x,t) = \frac{1}{R^3}P_{-3} + \frac{1}{R^2}P_{-2} + \frac{1}{R}P_{-1} + P_0 + R(P_1 + \overline{P}_1(X)) + R^2 P_2 + R^3 P_3 + \cdots$$

Substituting the expansions (6)-(7) into the system of equations (4)-(5) and collecting together the terms with R the same orders up to the power inclusive R^3, we obtain the equations of the multiscale asymptotic expansion. Let us pay attention to the analysis of rather deep orders of equations with respect to a small parameter, which is necessary to obtain equations for large-scale motions. This is typical for this method. There is only one equation in order R^{-3}:

$$\partial_i P_{-3} = 0 \quad \Rightarrow \quad P_{-3} = P_{-3}(X) \tag{8}$$

In order R^{-2}, we have the equation:

$$\partial_i P_{-2} = 0 \quad \Rightarrow \quad P_{-2} = P_{-2}(X) \tag{9}$$

In order R^{-1}, we get a system of equations:

$$\partial_t W_{-1}^i + W_{-1}^k \partial_k W_{-1}^i = -\partial_i P_{-1} - \nabla_i P_{-3} + \partial_k^2 W_{-1}^i + \varepsilon_{ijk} W_j D_k e_k, \quad \partial_i W_{-1}^i = 0 \tag{10}$$

Averaging equations (10) over fast variables gives the secular equation,

$$-\nabla_i P_{-3} + \varepsilon_{ijk} W_j D_k = 0, \tag{11}$$

which corresponds to the equation of geostrophic equilibrium.

In order zero R^0, we have the following system of equations:

$$\partial_t v_0^i + W_{-1}^k \partial_k v_0^i + v_0^k \partial_k W_{-1}^i = -\partial_i P_0 - \nabla_i P_{-2} + \partial_k^2 v_0^i + \varepsilon_{ijk} v_0^j D_k + F_0^i \tag{12}$$

$$\partial_i v_0^i = 0$$

These equations give one secular equation:

$$\nabla P_{-2} = 0 \quad \Rightarrow \quad P_{-2} = const \tag{13}$$

Consider a first-order R^1 approximation:

$$\partial_t v_1^i + W_{-1}^k \partial_k v_1^i + v_0^k \partial_k v_0^i + v_1^k \partial_k W_{-1}^i + W_{-1}^k \nabla_k W_{-1}^i = -\nabla_i P_{-1} - \partial_i (P_1 + \overline{P}_1) + \partial_k^2 v_1^i + 2\partial_k \nabla_k W_{-1}^i + \varepsilon_{ijk} v_1^j D_k, \tag{14}$$

$$\partial_i v_1^i + \nabla_i W_{-1}^i = 0$$

Secular equations follow from this system of equations:

$$W_{-1}^k \nabla_k W_{-1}^i = -\nabla_i P_{-1} \tag{15}$$

$$\nabla_i W^i_{-1} = 0 \tag{16}$$

Secular equations (15)-(16) satisfy the following field geometry:

$$\vec{W}_{-1} = \left(W^x_{-1}(Z), W^y_{-1}(Z), 0 \right), \quad P_{-1} = const \tag{17}$$

For the second order R^2, we get the equations:

$$\partial_t v^i_2 + W^k_{-1}\partial_k v^i_2 + v^k_0\partial_k v^i_1 + W^k_{-1}\nabla_k v^i_0 + v^k_0\nabla_k W^i_{-1} + v^k_1\partial_k v^i_0 + v^k_2\partial_k W^i_{-1} = -\nabla_i P_2 - \nabla_i P_0 + \partial^2_k v^i_2 + 2\partial_k \nabla_k v^i_0 + \varepsilon_{ijk} v^j_2 D_k, \tag{18}$$

$$\partial_i v^i_2 + \nabla_i v^i_0 = 0$$

It is easy to see that there are no secular terms in this order. Finally, we come to the most important order R^3. In this order, the equations are:

$$\partial_t v^i_3 + \partial_T W^i_{-1} + W^k_{-1}\partial_k v^i_3 + v^k_0\partial_k v^i_2 + W^k_{-1}\nabla_k v^i_1 + v^k_0\nabla_k v^i_0 + v^k_1\partial_k v^i_1 + v^k_1\nabla_k W^i_{-1} +$$

$$+ v^k_2\partial_k v^i_0 + v^k_3\partial_k W^i_{-1} = -\partial_i P_3 - \nabla_i \left(P_1 + \overline{P}_1 \right) + \partial^2_k v^i_3 + 2\partial_k \nabla_k v^i_1 + \Delta W^i_{-1} + \varepsilon_{ijk} v^j_3 D_k, \tag{19}$$

$$\partial_i v^i_3 + \nabla_i v^i_1 = 0$$

Averaging these equations over fast variables, we obtain the main secular equation describing the evolution of large-scale perturbations:

$$\partial_T W^i_{-1} - \Delta W^i_{-1} + \nabla_k \left(\overline{v^k_0 v^i_0} \right) = -\nabla_i \overline{P}_1 \tag{20}$$

Equation (20) describes the evolution of a large-scale vortex field $\vec{W}$, but the final closure of equation (20) will be carried out after calculating the Reynolds stress $\nabla_k \left(\overline{v^k_0 v^i_0} \right)$. To do this, it is necessary to find solutions for the small-scale velocity field $\vec{v}_0$.

2.3. Velocity field in zero approximation

Let us write the equation of the asymptotic expansion in the zeroth approximation (12) in the following form:

$$\widehat{D}_0 v^i_0 = -\partial_i P_0 + \varepsilon_{ijk} v^j_0 D_k + F^i_0, \tag{21}$$

where the operator $\widehat{D}_0$ is introduced

$$\widehat{D}_0 = \partial_t - \partial^2_k + W^k_{-1}\partial_k.$$

The pressure P_0 is found in the condition $\partial_i v^i_0 = 0$:

$$P_0 = \widehat{P}_1 u_0 + \widehat{P}_2 v_0 + \widehat{P}_3 w_0 \tag{22}$$

Here we introduced the notation for the operators

$$\widehat{P}_1 = \frac{D_2\partial_z - D_3\partial_y}{\partial^2}, \quad \widehat{P}_2 = \frac{D_3\partial_x - D_1\partial_z}{\partial^2}, \quad \widehat{P}_3 = \frac{D_1\partial_y - D_2\partial_x}{\partial^2},$$

and velocities $v^x_0 = u_0$, $v^y_0 = v_0$, $v^z_0 = w_0$. Then, excluding the pressure from (21), we obtain a system of equations for finding the zero-order velocity field:

$$\left(\widehat{D}_0 + \widehat{p}_{1x} \right) u_0 + \left(\widehat{p}_{2x} - D_3 \right) v_0 + \left(\widehat{p}_{3x} + D_2 \right) w_0 = F^x_0$$

$$\left(D_3 + \widehat{p}_{1y} \right) u_0 + \left(\widehat{D}_0 + \widehat{p}_{2y} \right) v_0 + \left(\widehat{p}_{3y} - D_1 \right) w_0 = F^y_0 \tag{23}$$

$$\left(\widehat{p}_{1z} - D_2 \right) u_0 + \left(\widehat{p}_{2z} + D_1 \right) v_0 + \left(\widehat{D}_0 + \widehat{p}_{3z} \right) w_0 = F^z_0$$

The tensor components $\widehat{p}_{ij}$ are as follows:

$$\hat{p}_{1x} = \frac{D_2\partial_x\partial_z - D_3\partial_x\partial_y}{\partial^2}, \quad \hat{p}_{2x} = \frac{D_3\partial_x^2 - D_1\partial_x\partial_z}{\partial^2}, \quad \hat{p}_{3x} = \frac{D_1\partial_x\partial_y - D_2\partial_x^2}{\partial^2},$$

$$\hat{p}_{1y} = \frac{D_2\partial_y\partial_z - D_3\partial_y^2}{\partial^2}, \quad \hat{p}_{2y} = \frac{D_3\partial_y\partial_x - D_1\partial_y\partial_z}{\partial^2}, \quad \hat{p}_{3y} = \frac{D_1\partial_y^2 - D_2\partial_y\partial_x}{\partial^2}, \tag{24}$$

$$\hat{p}_{1z} = \frac{D_2\partial_z^2 - D_3\partial_z\partial_y}{\partial^2}, \quad \hat{p}_{2z} = \frac{D_3\partial_z\partial_x - D_1\partial_z^2}{\partial^2}, \quad \hat{p}_{3z} = \frac{D_1\partial_z\partial_y - D_2\partial_z\partial_x}{\partial^2}.$$

In accordance with the problem statement, we choose the coordinate system so that the axis OZ coincides with the direction of the angular velocity of rotation. Then the components of the rotation parameter are $D_1 = D_2 = 0, D_3 = D$. To solve the system of equations (23), it is necessary to specify the force $\vec{F}_0$ explicitly. Taking into account condition (3), we choose an external force in a rotating coordinate system in the following form:

$$\vec{F}_0 = f_0\left(\vec{i}\cos\phi_2 + \vec{j}\cos\phi_1\right), \quad F_0^z = 0, \tag{25}$$

where f_0 is the amplitude of the external force,

$$\phi_1 = \vec{k}_1\vec{x} - \omega_0 t, \quad \phi_2 = \vec{k}_2\vec{x} - \omega_0 t, \quad \vec{k}_1 = \vec{k}_0(1,0,1), \quad \vec{k}_2 = \vec{k}_0(0,1,1).$$

Thus, the external force is given in the plane (X, Y) orthogonal to the axis of rotation, and the divergence of this force is zero. We seek the solution of the system of equations (23) according to the Cramer rule:

$$u_0 = \frac{1}{\Delta}\left\{\left[\left(\hat{D}_0 + \hat{p}_{2y}\right)\left(\hat{D}_0 + \hat{p}_{3z}\right) - \left(\hat{p}_{2z} + D_1\right)\left(\hat{p}_{3y} - D_1\right)\right]F_0^x + \left[\left(\hat{p}_{3x} + D_2\right)\left(\hat{p}_{2z} + D_1\right) - \left(\hat{p}_{2x} - D_3\right)\left(\hat{D}_0 + \hat{p}_{3z}\right)\right]F_0^y\right\} \tag{26}$$

$$v_0 = \frac{1}{\Delta}\left\{\left[\left(\hat{D}_0 + \hat{p}_{1x}\right)\left(\hat{D}_0 + \hat{p}_{3z}\right) - \left(\hat{p}_{3x} + D_2\right)\left(\hat{p}_{1z} - D_2\right)\right]F_0^y + \left[\left(\hat{p}_{3y} - D_1\right)\left(\hat{p}_{1z} - D_2\right) - \left(D_3 + \hat{p}_{1y}\right)\left(\hat{D}_0 + \hat{p}_{3z}\right)\right]F_0^x\right\} \tag{27}$$

$$w_0 = \frac{1}{\Delta}\left\{\left[\left(D_3 + \hat{p}_{1y}\right)\left(\hat{p}_{2z} + D_1\right) - \left(\hat{D}_0 + \hat{p}_{2y}\right)\left(\hat{p}_{1z} - D_2\right)\right]F_0^x + \left[\left(\hat{p}_{2x} - D_3\right)\left(\hat{p}_{1z} - D_2\right) - \left(\hat{D}_0 + \hat{p}_{1x}\right)\left(\hat{p}_{2z} + D_1\right)\right]F_0^y\right\} \tag{28}$$

Here Δ is the determinant of the system of equations (23), which in its expanded form has the form:

$$\Delta = \left(\hat{D}_0 + \hat{p}_{1x}\right)\left(\hat{D}_0 + \hat{p}_{2y}\right)\left(\hat{D}_0 + \hat{p}_{3z}\right) + \left(D_3 + \hat{p}_{1y}\right)\left(\hat{p}_{2z} + D_1\right)\left(\hat{p}_{3x} + D_2\right) + \left(\hat{p}_{2x} - D_3\right)\left(\hat{p}_{3y} - D_1\right)\left(\hat{p}_{1z} - D_2\right) -$$

$$- \left(\hat{p}_{3x} + D_2\right)\left(\hat{D}_0 + \hat{p}_{2y}\right)\left(\hat{p}_{1z} - D_2\right) - \left(\hat{p}_{2z} + D_1\right)\left(\hat{p}_{3y} - D_1\right)\left(\hat{D}_0 + \hat{p}_{1x}\right) - \left(D_3 + \hat{p}_{1y}\right)\left(\hat{p}_{2x} - D_3\right)\left(\hat{D}_0 + \hat{p}_{3z}\right) \tag{29}$$

To calculate expressions (26)-(29), we write the external force (25) in complex form:

$$\vec{F}_0 = \vec{i}\frac{f_0}{2}e^{i\phi_2} + \vec{j}\frac{f_0}{2}e^{i\phi_1} + c.c. \tag{30}$$

Then all operators in formulas (26)-(29) act from the left on eigenfunctions:

$$\hat{D}_0 e^{i\phi_1} = e^{i\phi_1}\hat{D}_0\left(k_1, -\omega_0\right), \quad \hat{D}_0 e^{i\phi_2} = e^{i\phi_2}\hat{D}_0\left(k_2, -\omega_0\right), \quad \Delta e^{i\phi_1} = e^{i\phi_1}\Delta\left(k_1, -\omega_0\right), \quad \Delta e^{i\phi_2} = e^{i\phi_2}\Delta\left(k_2, -\omega_0\right) \tag{31}$$

To simplify the formulas, we set $\omega_0 = 1$, $k_0 = 1$ and introduce new notation:

$$\hat{D}_0\left(k_1, -\omega_0\right) = \hat{A}_1^* = 2 - i\left(1 - W_1\right), \quad \hat{D}_0\left(k_2, -\omega_0\right) = \hat{A}_2^* = 2 - i\left(1 - W_2\right) \tag{32}$$

Here and below, complex conjugate quantities will be denoted by an asterisk. When performing further calculations, parts of the components in the tensors $\hat{p}_{ij}\left(k_1\right)$ and $\hat{p}_{ij}\left(k_2\right)$ vanish, so we write out only the non-zero components:

$$\hat{p}_{11}\left(k_1\right) = \hat{A}_1^*, \quad \hat{p}_{12}\left(k_1\right) = -\frac{D}{2}, \quad \hat{p}_{32}\left(k_1\right) = \frac{D}{2}, \quad \hat{p}_{22}\left(k_1\right) = \hat{D}_1^*, \quad \hat{p}_{33}\left(k_1\right) = \hat{A}_1^*, \tag{33}$$

$$\hat{p}_{11}\left(k_2\right) = \hat{A}_2^*, \quad \hat{p}_{12}\left(k_2\right) = -D, \quad \hat{p}_{21}\left(k_2\right) = \frac{D}{2}, \quad \hat{p}_{22}\left(k_2\right) = \hat{A}_2^*, \quad \hat{p}_{31}\left(k_2\right) = -\frac{D}{2}, \quad \hat{p}_{33}\left(k_2\right) = \hat{A}_2^*.$$

Taking into account formulas (31)-(33), we find the determinant:

$$\Delta(k_1) = \hat{A}_1^* \left(\hat{A}_1^{*2} + \frac{D^2}{2} \right), \quad \Delta(k_2) = \hat{A}_2^* \left(\hat{A}_2^{*2} + \frac{D^2}{2} \right) \tag{34}$$

In a similar way, we find the velocity field of the zero approximation:

$$u_0 = \frac{f_0}{2} \frac{\hat{A}_2^* e^{i\phi_2}}{\hat{A}_2^{*2} + \frac{D^2}{2}} + \frac{f_0}{4} \frac{D e^{i\phi_1}}{\hat{A}_1^{*2} + \frac{D^2}{2}} + c.c., \tag{35}$$

$$v_0 = -\frac{f_0}{4} \frac{D e^{i\phi_2}}{\hat{A}_2^{*2} + \frac{D^2}{2}} + \frac{f_0}{2} \frac{\hat{A}_1^* e^{i\phi_1}}{\hat{A}_2^{*2} + \frac{D^2}{2}} + c.c., \tag{36}$$

$$w_0 = \frac{f_0}{4} \frac{D e^{i\phi_2}}{\hat{A}_2^{*2} + \frac{D^2}{2}} - \frac{f_0}{4} \frac{D e^{i\phi_1}}{\hat{A}_1^{*2} + \frac{D^2}{2}} + c.c. \tag{37}$$

The relations obtained for the velocity field in the zeroth approximation make it possible to find the Reynolds stresses necessary to close the equation.

2.4. Reynolds stresses and large-scale instability
Consider large-scale fields that satisfy the geometry of the problem within the framework of the "quasi-two-dimensional" model (17). Large-scale derivatives with respect to Z are then preferred.

$$\nabla_Z \equiv \frac{\partial}{\partial Z} \gg \frac{\partial}{\partial X}, \frac{\partial}{\partial Y}.$$

In this case, equation (20) can be written in the coordinate form:

$$\partial_T W_1 - \nabla_Z^2 W_1 + \nabla_Z \left(\overline{v_0^z v_0^x} \right) = 0, \quad W_1 \equiv W_{-1}^x \tag{38}$$

$$\partial_T W_2 - \nabla_Z^2 W_2 + \nabla_Z \left(\overline{v_0^z v_0^y} \right) = 0, \quad W_2 \equiv W_{-1}^y \tag{39}$$

To close the equations (38)-(39) it is necessary to calculate the Reynolds stresses $\overline{w_0 u_0}$ and $\overline{w_0 v_0}$. These terms are easily calculated using formulas (35)-(37). As a result, we get:

$$\overline{w_0 u_0} = -\frac{f_0^2}{8} \frac{D^2}{16(1-W_1)^2 + \left[\frac{D^2}{2} + 4 - (1-W_1)^2 \right]^2} + \frac{f_0^2}{2} \frac{D}{16(1-W_2)^2 + \left[\frac{D^2}{2} + 4 - (1-W_2)^2 \right]^2}$$

$$\overline{w_0 v_0} = -\frac{f_0^2}{8} \frac{D^2}{16(1-W_2)^2 + \left[\frac{D^2}{2} + 4 - (1-W_2)^2 \right]^2} - \frac{f_0^2}{2} \frac{D}{16(1-W_1)^2 + \left[\frac{D^2}{2} + 4 - (1-W_1)^2 \right]^2} \tag{40}$$

Now equations (38)-(39) have a closed form:

$$\partial_T W_1 - \Delta W_1 + \frac{\partial}{\partial Z} \overline{w_0 u_0} = 0, \quad \partial_T W_2 - \Delta W_2 - \frac{\partial}{\partial Z} \overline{w_0 v_0} = 0. \tag{41}$$

For small values of $W_{1,2}$ the Reynolds stress (40) can be expanded into a series in $W_{1,2}$. As a result, we obtain the following linearized equations (41):

$$\partial_T W_1 - \nabla_Z^2 W_1 = \alpha_1 \nabla_Z W_1 - \alpha_2 \nabla_Z W_2 \tag{42}$$

$$\partial_T W_2 - \nabla_Z^2 W_2 = \alpha_1 \nabla_Z W_2 + \alpha_2 \nabla_Z W_1 \tag{43}$$

where

$$\alpha_1 = \frac{f_0^2}{8} D^2 \alpha, \quad \alpha_2 = \frac{f_0^2}{2} D\alpha, \quad \alpha = \frac{32D^2\left(10 - D^2\right)}{\left(\left(D^2 + 6\right)^2 + 64\right)^2}.$$

The solution of the linear system of equations (42)-(43) will be found in the form of plane waves with the wave vector $\vec{K} \parallel OZ$, i.e.

$$W_{1,2} = A_{W_{1,2}} \exp\left(-i\omega T + iKZ\right) \tag{44}$$

Substituting (44) into the system of equations (42)-(43), we obtain the dispersion equation:

$$\left(-i\omega + K^2 - i\alpha_1 K\right)^2 - \alpha_2^2 K^2 = 0 \tag{45}$$

Dispersion equation (45) shows the existence of unstable oscillatory solutions with the oscillation frequency

$$\omega = \frac{f_0^2}{8} D^2 \alpha K$$

and instability increment

$$\gamma = \frac{f_0^2}{2} D\alpha K - K^2$$

The instability is large-scale because the unstable term dominates the damping at large scales: $\frac{f_0^2}{2} D\alpha > K$. The maximum instability increment is $\gamma_{\max} = \alpha^2 f_0^4 D^2 / 16$ and is achieved on the wave vector $K_{\max} = \alpha f_0^2 D / 4$.

Thus, in the considered stationary small-scale "turbulent" medium, large-scale motions arise and grow exponentially. It can be expected that stabilization of this instability will occur at the nonlinear stage. We show below that, as a result of the development of instability in the system, large-scale spiraling, circularly polarized vortices of the Beltrami type are generated.

2.5. Stationary nonlinear vortex structures

Obviously, as the amplitude increases, the nonlinear terms decrease and the instability saturates. As a result, stationary, nonlinear vortex structures are formed. To find them, we put in equations (41) $\partial_T = 0$ and integrate the equations once over Z. We obtain the following system of equations:

$$\frac{d}{dZ} W_1 = \overline{w_0 u_0} + C_1$$
$$\frac{d}{dZ} W_2 = \overline{w_0 v_0} + C_2 \tag{46}$$

From equations (46), follow:

$$\frac{dW_1}{dW_2} = \frac{\overline{w_0 u_0} + C_1}{\overline{w_0 v_0} + C_2} \tag{47}$$

Integrating the system of equations (47), we get:

$$\int \overline{w_0 v_0}\, dW_1 + C_2 W_1 = \int \overline{w_0 u_0}\, dW_2 + C_1 W_2 \tag{48}$$

The integrals in expression (48) are calculated through elementary functions, which give the expression for the first integral of motion J of equations (47):

$$J = \frac{D^2}{8} \frac{W_1}{\left[4 + \frac{1}{2}D^2 - \left(W_2 - 1\right)^2\right]^2 + 16\left(W_2 - 1\right)^2} + \frac{1}{2^{5/2}\left(D^2 + 8\right)} \ln \frac{\left(W_1 - 1\right)^2 + D\sqrt{2}\left(W_1 - 1\right) + 4 + \frac{D^2}{2}}{\left(W_1 - 1\right)^2 - D\sqrt{2}\left(W_1 - 1\right) + 4 + \frac{D^2}{2}} +$$

$$+ \frac{D}{8\left(D^2 + 8\right)} \frac{\left(W_1 - 1\right)^2 - 4 - \frac{D^2}{2}}{4\left(W_1 - 1\right)} - \frac{D^2}{8} \frac{W_2}{\left[4 + \frac{D^2}{2} - \left(W_1 - 1\right)^2\right]^2 + 16\left(W_1 - 1\right)^2} +$$

$$+\frac{1}{2^{5/2}(D^2+8)}\ln\frac{(W_2-1)^2+(W_2-1)D\sqrt{2}+4+\dfrac{D^2}{2}}{(W_2-1)^2-D\sqrt{2}(W_2-1)+4+\dfrac{D^2}{2}}+\frac{D}{8(D^2+8)}\frac{(W_2-1)^2-4-\dfrac{D^2}{2}}{4(W_2-1)}+C_1W_2+C_2W_1$$

It is clear that system (46) is analogous to a dynamical system in which the coordinate Z plays the role of time. As a result, the standard methods for studying dynamical systems apply. A phase portrait of a dynamic system is thus used to gain a qualitative understanding of all possible modes implemented in it. The phase portrait of the system (46) is depicted in Fig. 2. From which the most interesting modes of behaviour are easily noticeable. Such regimes correspond to trajectories in the phase portrait connecting hyperbolic points with stable and unstable foci.
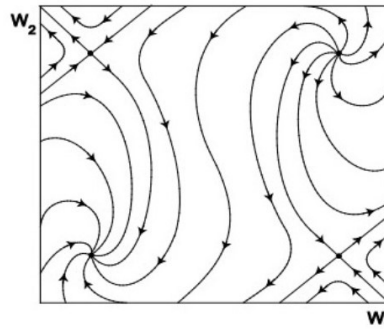
Figure 2. Phase portrait of a dynamical system (46) with parameters $D=1, C_1=-0.03, C_2=0.03$. One can see two hyperbolic singular points, as well as stable and unstable nodes.

On the left side of Fig. 3, we see the solution corresponding to the trajectory connecting the hyperbolic singular point with the stable node. On the right in Fig. 3, the solution corresponds to the trajectory connecting the unstable and stable foci. All these solutions correspond to large-scale localized vortex structures, such as kinks with rotation, which are generated by the instability considered here. The kink connecting a hyperbolic point to a stable knot contains rotations around the stable knot, as shown on the left in Fig. 3. In the kink that connects the unstable and stable foci, the velocity vector field W rotates around both singular points, as can be seen from the right side of Fig. 3. Note that, in contrast to previous works on the hydrodynamic α-effect in a rotating fluid, the method of asymptotic expansion makes it possible to construct a nonlinear theory in a natural way and study stationary nonlinear vortex kinks.
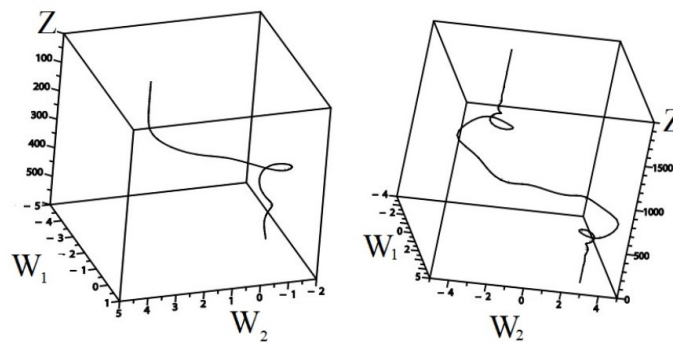

Figure 3. On the left, a kink is shown connecting a hyperbolic point to a stable knot with parameters $D=1, C_1=0.04, C_2=0.04$. When approaching a stable node, the rotation of the velocity field is observed. On the right, a kink is shown connecting the unstable and stable foci with the $D=1, C_1=0.04, C_2=0.04$ parameters. Here you can see the internal helical structure of the kink

3. NONLINEAR LARGE-SCALE VORTEX STRUCTURES IN AN OBLIQUELY ROTATING FLUID

This section presents the results of works [32]-[33], where a large-scale instability was studied that occurs in an obliquely rotating viscous fluid with small-scale turbulence. In [32]-[33], turbulence is modelled by an external small-scale and high-frequency force with a small Reynolds number. However, the main difference from the results of [30], which were presented in the previous section, is that the external force has no helicity. Therefore, the instability discussed above should be absent. The mathematical aspects of the theory [32]-[33] are based on a rigorous multiscale asymptotic expansion method. In the third order of perturbation theory, nonlinear equations were obtained for a large-scale velocity field. A study was also carried out of the linear and nonlinear stages of instability, and in the stationary mode, nonlinear periodic waves and vortex kinks were found [32]-[33].

3.1 Statement of the problem and equation for a large-scale velocity field

Let us consider a turbulent flow in an obliquely rotating viscous fluid whose axis of rotation does not coincide with the OZ axis. We will model turbulence with an external small-scale and high-frequency force $\vec{F}_0$ located in the plane (X, Y) (see Fig. 4). This force is not random and is set in a deterministic way in the following way:

$$F_0^z = 0, \quad \vec{F}_{0\perp} = f_0 \left(\vec{i} \cos \phi_2 + \vec{j} \cos \phi_1 \right),$$

$$\phi_1 = \vec{k}_1 \vec{x} - \omega_0 t, \quad \phi_2 = \vec{k}_2 \vec{x} - \omega_0 t, \quad \vec{k}_1 = \vec{k}_0 (1, 0, 0), \quad \vec{k}_2 = \vec{k}_0 (0, 1, 0) \tag{49}$$

Obviously, the non-helical external force (49) satisfies the following properties:

$$div\vec{F}_0 = 0, \quad \vec{F}_0 rot\vec{F}_0 = 0, \quad rot\vec{F}_0 \neq 0, \quad \vec{F}_0 = f_0 \vec{F}_0 \left(\frac{\vec{x}}{\lambda_0}; \frac{t}{t_0} \right) \tag{50}$$

In addition, the external force (49) is invariant with respect to the parity transformation $\vec{F}_0(\vec{x}, t) = \vec{F}_0(-\vec{x}, -t)$.
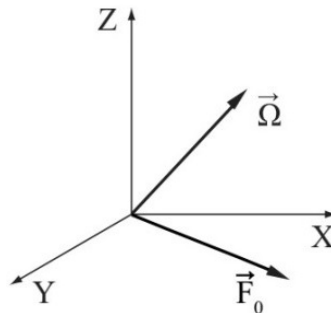

Figure 4. The angular velocity $\vec{\Omega}$ is inclined with respect to the plane (X, Y) in which the external force $\vec{F}_{0\perp}$ is located.

In the absence of rotation $\Omega = 0$, an external force $\vec{F}_0$ excites a small-scale flow $\vec{v}_0$ with a small Reynolds number $R = \frac{v_0 t_0}{\lambda_0} \ll 1$ and zero helicity $\overline{\vec{v}_0 rot\vec{v}_0} = 0$. To describe a turbulent flow in an obliquely rotating viscous incompressible fluid, we use the Navier-Stokes equations in a rotating coordinate system (1)-(2), which in a dimensionless form have the form (4)-(5). Further, the problem is to find an equation for a large-scale, slow velocity field $\vec{W}$. To do this, we also apply the method of multiscale asymptotic expansion with a small parameter R. Then, already in the third order of the perturbation theory, we obtain nonlinear equations for the large-scale components of the velocity field (W_1, W_2) in the framework of the "quasi-two-dimensional" model (17):

$$\partial_T W_1 - \nabla_Z^2 W_1 + \nabla_Z \left(\overline{v_0^z v_0^x} \right) = 0, \quad W_1 \equiv W_{-1}^x \tag{51}$$

$$\partial_T W_2 - \nabla_Z^2 W_2 + \nabla_Z \left(\overline{v_0^z v_0^y} \right) = 0, \quad W_2 \equiv W_{-1}^y \tag{52}$$

These equations are supplemented by the secular equations (11), (15), and (16). The fundamental difference between equations (51)-(52) and (38)-(39) is the Reynolds stresses, since the small-scale velocity fields v_0 included in them will be different. Naturally, to close equations (51)-(52), it is necessary to find solutions for the small-scale velocity field v_0.

3.2. Small-scale velocity field in the zeroth approximation in R

Using the results of Section 2.2, we calculate the zero-approximation velocity field, considering the geometry of the problem (see Fig. 4) and the selection of external force (49). We find expressions for the operator $\widehat{D}_0$ by representing (49) in complex form (30):

$$\widehat{D}_0(k_1, -\omega_0) = \widehat{A}_1^* = 1 - i(1 - W_1), \quad \widehat{D}_0(k_2, -\omega_0) = \widehat{A}_2^* = 1 - i(1 - W_2) \tag{53}$$

and non-zero components of the tensors $\widehat{p}_{ij}(k_1)$ and $\widehat{p}_{ij}(k_2)$:

$$\widehat{p}_{21}(k_1) = D_3, \quad \widehat{p}_{31}(k_1) = -D_2, \quad \widehat{p}_{12}(k_2) = -D_3, \quad \widehat{p}_{32}(k_2) = D_1. \tag{54}$$

Here, to simplify the formulas, it was assumed that $k_0 = 1, \omega_0 = 1, f_0 = 1$. Taking into account formulas (53)-(54), we find the determinant:

$$\Delta\left(k_1\right) = \widehat{A}_1^*\left(\widehat{A}_1^{*2} + D_1^2\right), \quad \Delta\left(k_2\right) = \widehat{A}_2^*\left(\widehat{A}_2^{*2} + D_2^2\right) \tag{55}$$

Using formulas (26)-(29) and (53)-(55) it is easy to find the zero approximation velocity field:

$$u_0 = \frac{1}{2}\frac{e^{i\phi_2}\,\widehat{A}_2^*}{\widehat{A}_2^{*2} + D_2^2} + c.c. \tag{56}$$

$$v_0 = \frac{1}{2}\frac{e^{i\phi_1}\,\widehat{A}_1^*}{\widehat{A}_1^{*2} + D_1^2} + c.c. \tag{57}$$

$$w_0 = \frac{1}{2}\frac{e^{i\phi_2}D_2}{\widehat{A}_2^{*2} + D_2^2} - \frac{1}{2}\frac{e^{i\phi_1}D_1}{\widehat{A}_1^{*2} + D_1^2} + c.c. \tag{58}$$

Note that the angular velocity component D_3 has dropped out of the expressions for the zero-approximation velocity, which is a consequence of the choice of an external force.

3.3. Reynolds stresses and large-scale instability

To close equations (51)-(52), we need to calculate the Reynolds stresses $\overline{w_0 u_0}$ and $\overline{w_0 v_0}$. These terms are easily calculated using formulas (56)-(58). As a result, we get:

$$\overline{w_0 u_0} = \frac{1}{2}\frac{D_2}{\left|A_2^2 + D_2^2\right|^2}, \quad \overline{w_0 v_0} = -\frac{1}{2}\frac{D_1}{\left|A_1^2 + D_1^2\right|^2}. \tag{59}$$

Now equations (51)-(52) are closed and take the form:

$$\partial_T W_1 - \Delta W_1 + \frac{1}{2}\frac{\partial}{\partial Z}\frac{D_2}{4\left(1 - W_2\right)^2 + \left[D_2^2 + W_2\left(2 - W_2\right)\right]^2} = 0,$$

$$\partial_T W_2 - \Delta W_2 - \frac{1}{2}\frac{\partial}{\partial Z}\frac{D_1}{4\left(1 - W_1\right)^2 + \left[D_1^2 + W_1\left(2 - W_1\right)\right]^2} = 0 \tag{60}$$

For small values W_1, W_2, equation (60) can be linearized, which gives:

$$\partial_T W_1 - \Delta W_1 - \alpha_2\,\frac{\partial}{\partial Z}W_2 = 0$$

$$\partial_T W_2 - \Delta W_2 + \alpha_1\,\frac{\partial}{\partial Z}W_1 = 0, \tag{61}$$

System (61) describes the positive feedback between the velocity components W_1, W_2, which is carried out by projections of the Coriolis force through the coefficients $\alpha_{1,2}$:

$$\alpha_1 = 2\frac{D_1\left(D_1^2 - 2\right)}{\left(4 + D_1^2\right)^2}, \quad \alpha_2 = 2\frac{D_2\left(D_2^2 - 2\right)}{\left(4 + D_2^2\right)^2}$$

The solution to the linear system (61) will be sought in the form:

$$W_1, W_2 \sim \exp\left(\gamma T + iKZ\right) \tag{62}$$

Substituting equation (62) into equation (61), we obtain the dispersion equation:

$$\gamma = \pm\sqrt{\alpha_1\alpha_2}\,K - K^2 \tag{63}$$

Dispersion equation (63) shows the existence of a large-scale instability $\alpha_1\alpha_2 > 0$ with a maximum increment $\gamma_{max} = \frac{\alpha_1\alpha_2}{4}$, with a wave vector $K_{max} = \frac{1}{2}\sqrt{\alpha_1\alpha_2}$.

As a result of the development of instability in the system, large-scale helical vortices of the Beltrami type are generated. At $\alpha_1\alpha_2 < 0$, damped oscillations with frequency $\omega_0 = \sqrt{\alpha_1\alpha_2}\,K$ appear instead of instability. As can be

seen from (63), the increment of large-scale instability γ depends on the values of D_1, D_2, i.e., on how the external forces F_0^x, F_0^y are located with respect to the perpendicular projection of the angular velocity of rotation. If one of the components D_1, D_2 vanishes or is equal to $\sqrt{2}$, then there is no instability. Instability exists in the following cases:

- $D_1 > \sqrt{2}, D_2 > \sqrt{2}$,
- $D_1, D_2 > 0, D_1 < \sqrt{2}, D_2 < \sqrt{2}$,
- $D_1 > 0, D_2 > 0, D_1^2 < 2, D_2^2 < 2$,
- $D_1 > 0, D_2 > 0, D_1^2 < 2, D_2^2 < 2$,
- $D_1 < 0, D_2 < 0, D_2^2 > 2, D_1^2 < 2$, или $D_2^2 < 2, D_1^2 < 2$,
- $D_1 > 0, D_2 < 0, D_2^2 > 2, D_1^2 < 2$, или $D_2^2 < 2, D_1^2 > 2$.

Of course, the instability should stabilise at the nonlinear stage, which we discuss below.

3.4. Stationary solutions of the nonlinear equation for a large-scale velocity field

As the perturbation amplitude W_1, W_2 increases, the nonlinear terms in (60) decrease, and the instability saturates. As a result, stationary, nonlinear vortex structures are formed. To find them in equation (63), we set $\dfrac{\partial}{\partial T} = 0$ and integrate the equations once with respect to Z. As a result, we obtain the following system of equations:

$$\frac{dW_1}{dZ} = \frac{1}{2} \frac{D_2}{4(1-W_2)^2 + \left[D_2^2 + W_2(2-W_2) \right]^2} + C_1, \qquad \frac{dW_2}{dZ} = -\frac{1}{2} \frac{D_1}{4(1-W_1)^2 + \left[D_1^2 + W_1(2-W_1) \right]^2} + C_2 \qquad (64)$$

Let's move on to some convenient variables in this system: $1 - W_1 = \widetilde{W}_1, 1 - W_2 = \widetilde{W}_2$. Then we get

$$\begin{aligned}
\frac{d\widetilde{W}_1}{dZ} &= -\frac{1}{2} \frac{D_2}{\left(D_2^2 + 1 \right)^2 + 2\left(1 - D_2^2 \right) W_2^2 + \widetilde{W}_2^4} + C_1 \\
\frac{d\widetilde{W}_2}{dZ} &= \frac{1}{2} \frac{D_1}{\left(D_1^2 + 1 \right)^2 + 2\left(1 - D_1^2 \right) \widetilde{W}_1^2 + \widetilde{W}_1^4} + C_2
\end{aligned} \qquad (65)$$

Again, considering Z as a variable analogous to time, we can use the usual methods of dynamical systems. So the system of equations (65) can be written in the Hamiltonian form:

$$\frac{d\widetilde{W}_1}{dZ} = -\frac{\partial \mathcal{H}}{\partial \widetilde{W}_2}, \quad \frac{d\widetilde{W}_2}{dZ} = \frac{\partial \mathcal{H}}{\partial \widetilde{W}_1}$$

where the Hamiltonian $\mathcal{H}$ has the form:

$$\mathcal{H} = \mathcal{H}_1\left(D_1, \widetilde{W}_1 \right) + \mathcal{H}_2\left(D_2, \widetilde{W}_2 \right) \qquad (66)$$

The function $\mathcal{H}\left(D, \widetilde{W} \right)$ is

$$\mathcal{H}\left(D, \tilde{W} \right) = \frac{D}{2} \int \frac{d\tilde{W}}{\left(D^2 + 1 \right)^2 + 2\left(1 - D^2 \right) \tilde{W}^2 + \tilde{W}^4} + C\tilde{W} \qquad (67)$$

The integral in formula (67) is calculated using elementary functions. Let's put it simply: $D_1 = D_2 = D = 1$. Then function (67) is

$$\mathcal{H}\left(\widetilde{W} \right) = \frac{1}{16} \left\{ \ln \frac{\widetilde{W}^2 + 2\widetilde{W} + 2}{\widetilde{W}^2 - 2\widetilde{W} + 2} + arctg \frac{2\widetilde{W}}{2 - \widetilde{W}^2} \right\} + C\widetilde{W} \qquad (68)$$

The amounts $\mathcal{H}_1\left(\widetilde{W}_1 \right) + \mathcal{H}_2\left(\widetilde{W}_2 \right)$ can be combined into one formula. Then the Hamiltonian is

$$\mathcal{H} = \frac{1}{16} \ln \frac{\left(\widetilde{W}_1^2 + 2\widetilde{W}_1 + 2 \right)\left(\widetilde{W}_2^2 + 2\widetilde{W}_2 + 2 \right)}{\left(\widetilde{W}_1^2 - 2\widetilde{W}_1 + 2 \right)\left(\widetilde{W}_2^2 - 2\widetilde{W}_2 + 2 \right)} + \frac{1}{16} arctg \frac{2\widetilde{W}_2\left(\widetilde{W}_1^2 - 2 \right) + 2\widetilde{W}_1\left(\widetilde{W}_2^2 - 2 \right)}{2\left(\widetilde{W}_1 + \widetilde{W}_2 \right)^2 - \widetilde{W}_1^2 \widetilde{W}_2^2 - 4} + C_1\widetilde{W}_1 + C_2\widetilde{W}_2 \qquad (69)$$

For Hamiltonians (69), it is easy to construct a phase portrait (Fig. 5), where for constant parameters $C_1 = 0.1$, $C_2 = 0.1$. The phase portrait shows the presence of closed trajectories on the phase plane around elliptical points and separatrices that connect hyperbolic points. Obviously, closed trajectories correspond to nonlinear periodic solutions (see the left side of Fig. 6), and localized solutions, such as kinks, correspond to separatrices (see the right side of Fig. 6).
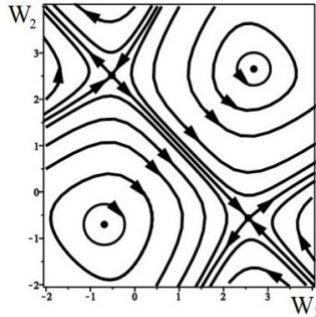

Figure. 5. The phase plane for the Hamiltonian (69) for constants $(C_1 = 0.1, C_2 = 0.1)$ is shown. One can see the presence of closed trajectories around the elliptic points and separatrices that connect the hyperbolic points.
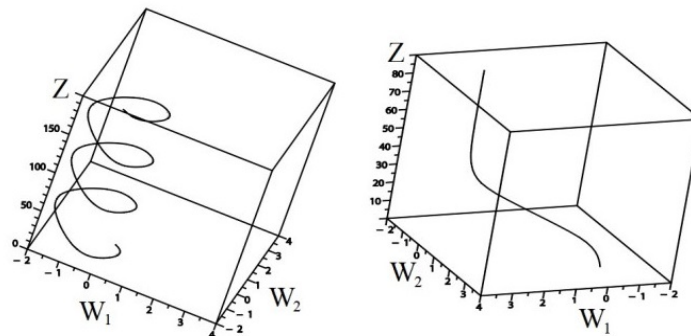
Figure. 6. The non-linear helical beltrami wave is shown on the left, which corresponds to a closed trajectory on the phase plane. The spiral is oriented along the axis Z and inclined with respect to the axis of rotation. On the right is a localized solution (kink) that corresponds to a separatrix on the phase plane. Solutions are obtained with parameters $(C_1 = 0.1, C_2 = 0.1)$.

4. NONLINEAR LARGE-SCALE VORTEX STRUCTURES IN AN OBLIQUELY ROTATING STRATIFIED FLUID

In this section, we discuss the nonlinear theory of generation of large-scale vortex structures (LSVS) in an obliquely rotating stratified medium with small-scale non-spiral turbulence, which was developed in [34]. Here turbulence was modeled by an external small-scale force with zero helicity, which creates small-scale flows with a small Reynolds number. Analytical results were obtained based on the method of multiscale asymptotic expansions. Nonlinear equations were found to describe the evolution of large-scale motions in the third order of perturbation theory. Linear instability and stationary nonlinear regimes were studied, and stationary solutions were obtained in the form of nonlinear Beltrami waves and localized vortex structures-kinks of a new type [34].

When temperature stratification is present, there are significant differences from the findings presented in works [32]-[33]. Firstly, the physical state changes completely. Accounting for temperature stratification in a gravitational field leads to free convection, resulting in the creation of vortex convective cells. The outcomes of [32]-[33] are not applicable in this scenario. Secondly, the mechanism of helicity generation is different here. Initially, non-helical external forces and the Coriolis force excite mirror-symmetric turbulence that organizes convective cells in such a way that the average helicity of small-scale motions is not zero (α -effect). Thirdly, the regime of large-scale instability is significantly altered. The increment of instability becomes much greater in the presence of convection $Ra \neq 0$.

4.1. Equations for Large Scale Fields

The Boussinesq-Oberbeck approximation describes the perturbations of velocity, temperature, and pressure in a rotating coordinate system with a constant temperature gradient. The system of equations is as follows:

Momentum equation:

$$\frac{\partial V_i}{\partial t} + V_k \frac{\partial V_i}{\partial x_k} = \nu \Delta V_i - \frac{1}{\rho} \frac{\partial P}{\partial x_i} + 2\varepsilon_{ijk} V_j \Omega_k + g e_i \beta T + F_0^i \tag{70}$$

Energy equation:

$$\frac{\partial T}{\partial t} + V_k \frac{\partial T}{\partial x_k} - A e_k V_k = \chi \Delta T \tag{71}$$

Continuity equation:

$$\frac{\partial V_i}{\partial x_i} = 0 \tag{72}$$

The system of equations (70)-(73) describes the evolution of perturbations against the background of the main equilibrium state, set by a constant temperature gradient $\nabla \overline{T} = -A\vec{e}$ (heating from below $A > 0$) and hydrostatic pressure: $\nabla \overline{P} = \overline{\rho}\vec{g} - \overline{\rho}\left[\vec{\Omega} \times \left[\vec{\Omega} \times \vec{r}\right]\right]$, where $\vec{r}$ is the radius vector of the fluid element. The vector of the angular velocity of rotation $\vec{\Omega}$ is considered constant (solid-body rotation) and inclined with respect to the plane (X, Y), as shown in Fig. 7, i.e., for the Cartesian geometry of the problem: $\vec{\Omega} = (\Omega_1, \Omega_2, \Omega_3)$; $\vec{e} = (0,0,1)$ is a unit vector in the direction of the Z axis; gravity is directed vertically downwards $\vec{g} = (0,0,-g)$; β is the coefficient of thermal expansion. Equation (70) includes an external force $\vec{F}_0$, which simulates an excitation source in the medium of small-scale and high-frequency fluctuations of the velocity field $\vec{v}_0$ with a small Reynolds number $R = \frac{v_0 t_0}{\lambda_0} \ll 1$.
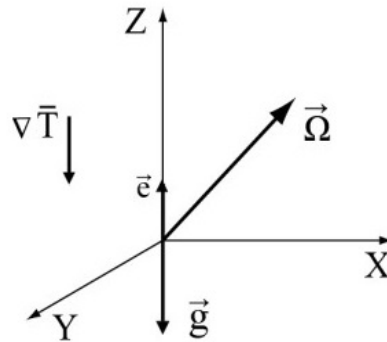

Figure 7. The angular velocity of rotation $\vec{\Omega}$ is not perpendicular to the plane (X, Y) in which the external force $\vec{F}_{0\perp}$ is located, but inclined at an angle with respect to it.

In this context, we employ an external non-helical force in the form of equation (49) and with properties (50). To simplify notation, we switch to dimensionless variables in equations (70)-(72), while retaining the notation for the dimensional variables

$$x \to \frac{x}{\lambda_0}, \quad t \to \frac{t}{t_0}, \quad \vec{V} \to \frac{\vec{V}}{v_0}, \quad \vec{F}_0 \to \frac{\vec{F}_0}{f_0}, \quad P \to \frac{P}{\rho p_0}, \quad t_0 = \frac{\lambda_0^2}{\nu}, \quad p_0 = \frac{v_0 \nu}{\lambda_0}, \quad f_0 = \frac{v_0 \nu}{\lambda_0^2}, \quad T \to \frac{T}{\lambda_0 A}.$$

In dimensionless variables, equations (70)-(72) take the form:

$$\frac{\partial V_i}{\partial t} + R V_k \frac{\partial V_i}{\partial x_k} = \Delta V_i - \frac{\partial P}{\partial x_i} + \varepsilon_{ijk} V_j D_k + e_i \widetilde{Ra} T + F_0^i \tag{73}$$

$$\frac{\partial T}{\partial t} + R V_k \frac{\partial T}{\partial x_k} - e_k V_k = Pr^{-1} \Delta T \tag{74}$$

$$\frac{\partial V_i}{\partial x_i} = 0 \tag{75}$$

New dimensionless parameters have appeared here: $\widetilde{Ra} = \frac{Ra}{Pr}$, $Ra = \frac{g\beta A \lambda_0^2}{\nu \chi}$ is the Rayleigh number on the scale λ_0, $Pr = \frac{\nu}{\chi}$ is the Prandtl number. We consider the Reynolds number $R = \frac{v_0 t_0}{\lambda_0} \ll 1$ to be a small parameter of the asymptotic expansion, and the parameters D_i and $\widetilde{Ra}$ are arbitrary and do not affect the expansion scheme. The

primary objective of this section is to obtain the solvability equations for the multiscale asymptotic expansion, which involves finding equations for large-scale perturbations. As in the previous sections, we express the spatial and temporal derivatives in equations (73)-(75) using an asymptotic expansion (6). In constructing the nonlinear theory, we represent the variables $\vec{V}$, P as an asymptotic series (7), and the temperature perturbations T as the following series:

$$T(x,t) = \frac{1}{R} T_{-1}(X) + T_0(x_0) + R T_1 + R^2 T_2 + R^3 T_3 + \cdots \tag{76}$$

To obtain the equations of the multiscale asymptotic expansion, we substitute the expansions (6)-(7), (76) into the system of equations (73)-(75) and group together the terms with the same orders in R up to the power of R^3. The algebraic structure of the asymptotic expansion in equations (73)-(75) differs from the asymptotic expansion presented in Section 2.2 due to the presence of terms related to the expansion of temperature perturbations. The fundamental secular equations, or equations for large-scale fields, are derived at the third order in R:

$$\partial_T W_{-1}^i - \Delta W_{-1}^i + \nabla_k \left(\overline{v_0^k v_0^i} \right) = -\nabla_i \overline{P_1} \tag{77}$$

$$\partial_T T_{-1} - Pr^{-1} \Delta T_{-1} = -\nabla_k \left(\overline{v_0^k T_0} \right) \tag{78}$$

Equations (77)-(78) are supplemented by secular equations:

$$-\nabla_i P_{-3} + \widetilde{Ra} e_i T_{-1} + \varepsilon_{ijk} W_j D_k = 0 , \; W_{-1}^k \nabla_k W_{-1}^i = -\nabla_i P_{-1}$$

$$W_{-1}^k \nabla_k T_{-1} = 0 , \; \nabla_i W_{-1}^i = 0 , W_{-1}^z = 0 .$$

These equations are satisfied by choosing the following geometry for the velocity field:

$$\vec{W}_{-1} = \left(W_{-1}^x(Z), \quad W_{-1}^y(Z), 0 \right), \quad T_{-1} = T_{-1}(Z), \quad P_{-1} = const \tag{79}$$

In the framework of a quasi-two-dimensional problem, when large-scale derivatives with respect to Z are preferable, i.e.

$$\nabla_Z \equiv \frac{\partial}{\partial Z} \gg \frac{\partial}{\partial X}, \frac{\partial}{\partial Y}$$

Then the system of equations (77)-(78) is simplified and takes the following form:

$$\partial_T W_1 - \nabla_Z^2 W_1 + \nabla_Z \left(\overline{v_0^z v_0^x} \right) = 0, \quad W_{-1}^x = W_1 \tag{80}$$

$$\partial_T W_2 - \nabla_Z^2 W_2 + \nabla_Z \left(\overline{v_0^z v_0^y} \right) = 0, \quad W_{-1}^y = W_2 \tag{81}$$

$$\partial_T T_{-1} - Pr^{-1} \Delta T_{-1} + \nabla_Z \left(\overline{v_0^z T_0} \right) = 0 \tag{82}$$

Equations (80)-(82) describe the evolution of large-scale vortex fields $\vec{W}$, but the final closure of these equations is achieved after calculating the Reynolds stresses $\nabla_k \left(\overline{v_0^k v_0^i} \right)$. This shows that we need to find solutions for the small-scale velocity field $\vec{v}_0$.

4.2. Solving Equations for Small-Scale Fields and Calculating Reynolds Stresses
We write the asymptotic expansion equations in the zeroth approximation in the following form:

$$\widehat{D}_W v_0^i = -\partial_i P_0 + \widetilde{Ra} e_i T_0 + \varepsilon_{ijk} v_0^j D_k + F_0^i \tag{83}$$

$$\widehat{D}_\theta T_0 = e_k v_0^k \tag{84}$$

$$\partial_i v_0^i = 0 \tag{85}$$

where the notation for the operators is introduced:

$$\widehat{D}_W = \partial_t - \partial_k^2 + W_{-1}^k \partial_k , \; \widehat{D}_\theta = \partial_t - Pr^{-1} \partial^2 + W_{-1}^k \partial_k$$

Small-scale temperature oscillations are easily found from equation (84):

$$T_0 = \frac{v_0^z}{\widehat{D}_\theta} \tag{86}$$

Substituting (86) into (83), and using the condition of solenoidality of the fields $\vec{v}_0$ and $\vec{F}_0$, we find the pressure P_0:

$$P_0 = \widehat{P}_1 u_0 + \widehat{P}_2 v_0 + \widehat{P}_3 w_0 \tag{87}$$

Here we introduce the notation for the operators

$$\widehat{P}_1 = \frac{D_2 \partial_z - D_3 \partial_y}{\partial^2}, \quad \widehat{P}_2 = \frac{D_3 \partial_x - D_1 \partial_z}{\partial^2}, \quad \widehat{P}_3 = \frac{D_1 \partial_y - D_2 \partial_x}{\partial^2} + \widetilde{Ra} \frac{\partial_z}{\widehat{D}_\theta \partial^2}$$

and velocities: $v_0^x = u_0$, $v_0^y = v_0$, $v_0^z = w_0$. Using expression (87), we can eliminate the pressure from equation (83) and, as a result, obtain a system of equations for finding the zero-order velocity field:

$$\left(\widehat{D}_W + \widehat{p}_{1x}\right) u_0 + \left(\widehat{p}_{2x} - D_3\right) v_0 + \left(\widehat{p}_{3x} + D_2\right) w_0 = F_0^x$$

$$\left(D_3 + \widehat{p}_{1y}\right) u_0 + \left(\widehat{D}_W + \widehat{p}_{2y}\right) v_0 + \left(\widehat{p}_{3y} - D_1\right) w_0 = F_0^y \tag{88}$$

$$\left(\widehat{p}_{1z} - D_2\right) u_0 + \left(\widehat{p}_{2z} + D_1\right) v_0 + \left(\widehat{D}_W - \frac{\widetilde{Ra}}{\widehat{D}_\theta} + \widehat{p}_{3z}\right) w_0 = 0$$

The components of the tensor $\widehat{p}_{ij}$ have the following form:

$$\widehat{p}_{1x} = \frac{D_2 \partial_x \partial_z - D_3 \partial_x \partial_y}{\partial^2}, \widehat{p}_{2x} = \frac{D_3 \partial_x^2 - D_1 \partial_x \partial_z}{\partial^2}, \widehat{p}_{3x} = \frac{D_1 \partial_x \partial_y - D_2 \partial_x^2}{\partial^2} + \widetilde{Ra} \frac{\partial_x \partial_z}{\widehat{D}_\theta \partial^2},$$

$$\widehat{p}_{1y} = \frac{D_2 \partial_y \partial_z - D_3 \partial_y^2}{\partial^2}, \widehat{p}_{2y} = \frac{D_3 \partial_y \partial_x - D_1 \partial_y \partial_z}{\partial^2}, \widehat{p}_{3y} = \frac{D_1 \partial_y^2 - D_2 \partial_y \partial_x}{\partial^2} + \widetilde{Ra} \frac{\partial_y \partial_z}{\widehat{D}_\theta \partial^2}, \tag{89}$$

$$\widehat{p}_{1z} = \frac{D_2 \partial_z^2 - D_3 \partial_z \partial_y}{\partial^2}, \widehat{p}_{2z} = \frac{D_3 \partial_z \partial_x - D_1 \partial_z^2}{\partial^2}, \widehat{p}_{3z} = \frac{D_1 \partial_z \partial_y - D_2 \partial_z \partial_x}{\partial^2} + \widetilde{Ra} \frac{\partial_z^2}{\widehat{D}_\theta \partial^2}$$

The solution to the system of equations (88) is easily found according to Cramer's rules (26)-(28). Then, using the complex form of the external force (49), we find the zero approximation velocity field:

$$u_0 = \frac{f_0}{2} \frac{\widehat{\mathcal{A}}_2^*}{\widehat{\mathcal{A}}_2^* \widehat{D}_{W_2}^* + D_2^2} e^{i\phi_2} + c.c. = u_{03} + u_{04} \tag{90}$$

$$v_0 = \frac{f_0}{2} \frac{\widehat{\mathcal{A}}_1^*}{\widehat{\mathcal{A}}_1^* \widehat{D}_{W_1}^* + D_1^2} e^{i\phi_1} + c.c. = v_{01} + v_{02} \tag{91}$$

$$w_0 = -\frac{f_0}{2} \frac{D_1}{\widehat{\mathcal{A}}_1^* \widehat{D}_{W_1}^* + D_1^2} e^{i\phi_1} + \frac{f_0}{2} \frac{D_2}{\widehat{\mathcal{A}}_2^* \widehat{D}_{W_2}^* + D_2^2} e^{i\phi_2} + c.c. = w_{01} + w_{02} + w_{03} + w_{04}, \tag{92}$$

where

$$\widehat{\mathcal{A}}_{1,2}^* = \widehat{D}_{W_{1,2}}^* - \frac{\widetilde{Ra}}{\widehat{D}_{\theta_{1,2}}^*}.$$

This indicates that the zero-order velocity field is not influenced by the angular velocity component D_3, as a result of the chosen external force (49). It is worth noting that the velocity components follow the subsequent relationships:

$$w_{02} = \left(w_{01}\right)^*, \ w_{04} = \left(w_{03}\right)^*, \ v_{02} = \left(v_{01}\right)^*, \ v_{04} = \left(v_{03}\right)^*, \ u_{02} = \left(u_{01}\right)^*, \ u_{04} = \left(u_{03}\right)^*.$$

In order to solve equations (80)-(81), which portray the development of large-scale vortex fields, it is crucial to compute the Reynolds stress $T^{ik} = \overline{v_0^i v_0^k}$, specifically its components:

$$T^{31} = \overline{w_0 u_0} = \overline{w_{01}(u_{01})^*} + \overline{(w_{01})^* u_{01}} + \overline{w_{03}(u_{03})^*} + \overline{(w_{03})^* u_{03}} \tag{93}$$

$$T^{32} = \overline{w_0 v_0} = \overline{w_{01}(v_{01})^*} + \overline{(w_{01})^* v_{01}} + \overline{w_{03}(v_{03})^*} + \overline{(w_{03})^* v_{03}} \tag{94}$$

By substituting the solutions for the small-scale velocity field (90)-(92) into formulas (93)-(94), we can obtain the following expressions for the correlators:

$$T^{31} = \frac{f_0^2}{4} \frac{D_2(\hat{\mathcal{A}}_2 + \hat{\mathcal{A}}_2^*)}{\left|\hat{\mathcal{A}}_2 \hat{D}_{W_2} + D_2^2\right|^2}, \qquad T^{32} = -\frac{f_0^2}{4} \frac{D_1(\hat{\mathcal{A}}_1 + \hat{\mathcal{A}}_1^*)}{\left|\hat{\mathcal{A}}_1 \hat{D}_{W_1} + D_1^2\right|^2} \tag{95}$$

If we assume the medium is the atmosphere, the Prandtl number is approximately equal to one $Pr = 1$. In this case, the expressions for the Reynolds stress components become simplified:

$$T^{31} = \frac{f_0^2}{2} D_2 \frac{(1 + \tilde{W}_2^2 - Ra)}{(1 + \tilde{W}_2^2)((1 + \tilde{W}_2^2)^2 + 2(D_2^2 - Ra)(1 - \tilde{W}_2^2) + (D_2^2 - Ra)^2)} \tag{96}$$

$$T^{32} = -\frac{f_0^2}{2} D_1 \frac{(1 + \tilde{W}_1^2 - Ra)}{(1 + \tilde{W}_1^2)((1 + \tilde{W}_1^2)^2 + 2(D_1^2 - Ra)(1 - \tilde{W}_1^2) + (D_1^2 - Ra)^2)} \tag{97}$$

By substituting (96)-(97) into (80)-(81), we can obtain closed equations for the evolution of large-scale vortex fields $\vec{W}$:

$$(\partial_T - \nabla_Z^2)\tilde{W}_1 = \frac{f_0^2}{2} D_2 \nabla_Z \left[\frac{1 + \tilde{W}_2^2 - Ra}{(1 + \tilde{W}_2^2)((1 + \tilde{W}_2^2)^2 + 2(D_2^2 - Ra)(1 - \tilde{W}_2^2) + (D_2^2 - Ra)^2)} \right] \tag{98}$$

$$(\partial_T - \nabla_Z^2)\tilde{W}_2 = -\frac{f_0^2}{2} D_1 \nabla_Z \left[\frac{1 + \tilde{W}_1^2 - Ra}{(1 + \tilde{W}_1^2)((1 + \tilde{W}_1^2)^2 + 2(D_1^2 - Ra)(1 - \tilde{W}_1^2) + (D_1^2 - Ra)^2)} \right] \tag{99}$$

These closed equations (98)-(99) can be considered as the equations of a nonlinear vortex dynamo in a stratified fluid that is rotating obliquely with a non-spiral force acting on the small-scale. If the rotation effect disappears ($\Omega = 0$) or the rotation axis coincides with the OZ axis ($\vec{\Omega} \| OZ$), the usual diffusion spreading of large-scale fields will occur. In the limit of a homogeneous fluid $Ra = 0$, equations (98)-(99) are completely equivalent to equations (60) when $f_0 = 1$.

4.3. Large scale instability

Equations (98)-(99) are used to describe the nonlinear behavior of large-scale perturbations in the vortex field. Consequently, it is important to investigate the stability of small perturbations in the field $\vec{W}$. For small values of $\vec{W} = (W_1, W_2)$, equations (98)-(99) can be simplified to a system of linear equations:

$$\begin{aligned} \partial_T W_1 - \nabla_Z^2 W_1 - \alpha_2 \nabla_Z W_2 = 0 \\ \partial_T W_2 - \nabla_Z^2 W_2 + \alpha_1 \nabla_Z W_1 = 0 \end{aligned} \tag{100}$$

where the following notation for the coefficients is introduced:

$$\alpha_1 = f_0^2 D_1 \left[\frac{(D_1^2 - Ra - 2)(2 - Ra) + Ra(4 + (D_1^2 - Ra)^2)}{(4 + (D_1^2 - Ra)^2)^2} \right],$$

$$\alpha_2 = f_0^2 D_2 \left[\frac{(D_2^2 - Ra - 2)(2 - Ra) + Ra(4 + (D_2^2 - Ra)^2)}{(4 + (D_2^2 - Ra)^2)^2} \right]. \tag{101}$$

This shows that equations (100) are similar to the equations for a vortex dynamo or hydrodynamic α-effect. To study the large-scale instability described by equation (100), we choose perturbations in the form of plane waves with the wave vector $\vec{K} \| OZ$. As a result, we find the dispersion equation:

$$\left(-i\omega + K^2\right)^2 - \alpha_1 \alpha_2 K^2 = 0 \tag{102}$$

Representing $\omega = \omega_0 + i\Gamma$, from equation (102) we find:

$$\Gamma = Im\omega = \pm\sqrt{\alpha_1 \alpha_2} K - K^2 \qquad (103)$$

Solutions (103) show the existence of instability at $\alpha_1 \alpha_2 > 0$ for large-scale vortex disturbances. If $\alpha_1 \alpha_2 < 0$, then instead of instabilities, damped oscillations occur, respectively, with frequency $\omega_0 = \sqrt{\alpha_1 \alpha_2} K$. By means of the coefficients α_1, α_2 a positive feedback is established between the velocity components, which is carried out by projections of the Coriolis force. Note that in the linear theory considered here, the coefficients α_1, α_2 do not depend on the field amplitudes but only on the rotation parameters $D_{1,2}$, the Rayleigh number Ra, and the amplitude of the external force f_0. Let us analyze the dependence of these coefficients on dimensionless parameters, assuming the dimensionless amplitude of the external force to be equal to $f_0 = 10$. Fixing the level of the dimensionless force means choosing a certain level of the stationary background of small-scale and fast oscillations. In the coefficients α_1, α_2 instead of the Cartesian projections D_1 and D_2, it is convenient to pass to their projections in the spherical coordinate system (D, ϕ, θ) (see Fig. 8).
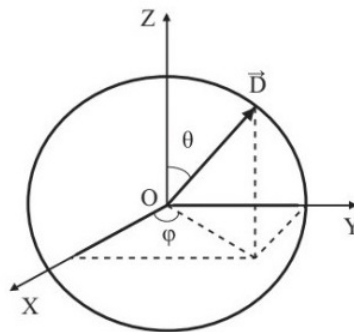

Figure 8. The conversion between the Cartesian projections of the rotation parameter D (or the rotation angular velocity vector Ω) and their projections in a spherical coordinate system is demonstrated.

The coordinate surface represented by $D = const$ forms a sphere, where θ stands for latitude ($\theta \in [0, \pi]$) and ϕ denotes longitude ($\phi \in [0, 2\pi]$). To investigate the impact of rotation and stratification on the gains α_1, α_2, we assume that D_1 and D_2 are equal, corresponding to a fixed longitude value of $\phi = \pi/4 + \pi n$, where $n = 0, 1, 2...k$, k is an integer. Under this assumption, the amplification factors for vortex disturbances are given by:

$$\alpha = \alpha_1 = \alpha_2 = f_0^2 \sqrt{2} D \sin\theta \left[\frac{4(D^2 \sin^2\theta - 2Ra - 4)(2 - Ra) + 2Ra(16 + (D^2 \sin^2\theta - 2Ra)^2)}{(16 + (D^2 \sin^2\theta - 2Ra)^2)^2} \right]$$

This implies that generating vortex disturbances at the poles ($\theta = 0, \theta = \pi$) is not efficient since $\alpha \to 0$. The left side of Fig. 9 illustrates the dependence of the coefficient α on the fluid stratification parameter (Rayleigh number Ra) at a fixed value of latitude $\theta = \pi/2$ and number $D = 2$.
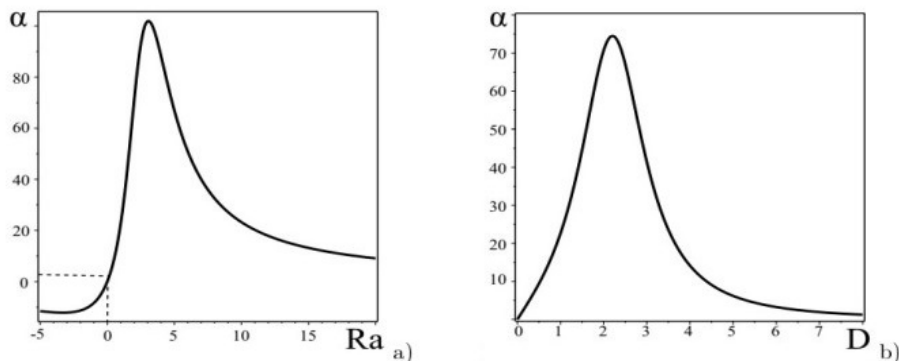

Figure 9. a) Plot of the dependence of the α-effect on the medium stratification parameter Ra (Rayleigh number); b) plot of the dependence of the α-effect on the medium rotation parameter D.

It also shows the case of a homogeneous medium, where large-scale vortex disturbances are generated by the external small-scale non-spiral force and the Coriolis force. Fig. 9 indicates that temperature stratification ($Ra \neq 0$) can result in a significant increase in the coefficient α, leading to faster generation of large-scale vortex disturbances than in a homogeneous medium. This effect is particularly significant at higher numbers. Moreover, an increase in Rayleigh numbers leads to a decrease in the values of the coefficient. We are also interested in exploring the impact of the medium rotation effect on the amplification factor or the process of generating large-scale disturbances. Therefore, we set the Rayleigh number to $Ra = 2$ at $\theta = \pi / 2$. On the right-hand side of Fig. 9, the functional relationship $\alpha(D)$ is presented. It is evident from the graph that the coefficient attains its maximum value α_{max} at a specific rotation parameter D after which it gradually diminishes with an increase in D. This implies that the α-effect is suppressed. Similar behavior was observed in the magnetohydrodynamic α-effect [39]. On the left side of Fig. 10, the combined impact of rotation and stratification on the (D, Ra) plane is depicted. The gray shaded region indicates the $\alpha > 0$

instability area. The maximum instability increment $\Gamma_{max} = \dfrac{\alpha_1 \alpha_2}{4}$ is achieved for wave numbers $K_{max} = \dfrac{\sqrt{\alpha_1 \alpha_2}}{2}$. The

graph on the right-hand side of Fig. 10 shows the dependence of the instability increment Γ on the wave numbers K, which has a conventional pattern similar to the α-effect. Consequently, a rotating stratified atmosphere experiences the generation of large-scale helical circularly polarized vortices of the Beltrami type due to the development of a large-scale instability.
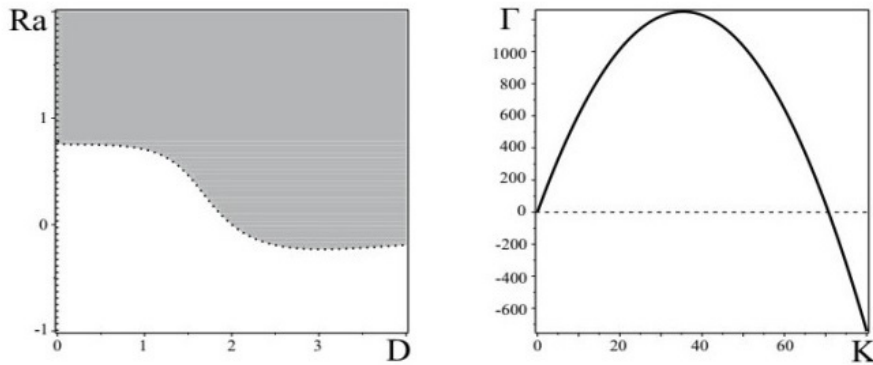

Figure 10. The image on the left displays a graph representing the (D, Ra) plane. The region indicating positive values of α (representing unstable solutions) is shaded in gray, while the region indicating negative values of α is shown in white. On the right-hand side, there is a plot showing the relationship between the increment of instability and the wave numbers K, with $D = 2$ and $Ra = 2$ as the parameters.

4.4. Stationary nonlinear vortex structures

Obviously, with an increase in the amplitude of perturbations, the nonlinear terms decrease and the instability saturates. As a result, nonlinear vortex structures are formed. To find them, we put in equations (98)-(99) $\partial_T = 0$ and integrate the equations once over Z. Furthermore, we make the assumption that the projections D_1 and D_2 hold identical values. To simplify the calculations, we assign the latitudinal angle a value of $\theta = \pi / 2$. Consequently, we derive a set of nonlinear equations in the following format:

$$\frac{d\tilde{W}_1}{dZ} = -f_0^2 D\sqrt{2} \frac{1 + \tilde{W}_2^2 - Ra}{(1 + \tilde{W}_2^2)(4(1 + \tilde{W}_2^2)^2 + 4(D^2 - 2Ra)(1 - \tilde{W}_2^2) + (D^2 - 2Ra)^2)} + C_1 \tag{104}$$

$$\frac{d\tilde{W}_2}{dZ} = f_0^2 D\sqrt{2} \frac{1 + \tilde{W}_1^2 - Ra}{(1 + \tilde{W}_1^2)(4(1 + \tilde{W}_1^2)^2 + 4(D^2 - 2Ra)(1 - \tilde{W}_1^2) + (D^2 - 2Ra)^2)} + C_2 \tag{105}$$

C_1, C_2 are integration constants that can take any value. It is important to note that the system of dynamic equations (104)-(105) is conservative, meaning it possesses a Hamiltonian. To obtain the Hamiltonian, we can express equations (104)-(105) in the Hamiltonian form.

$$\frac{d\tilde{W}_1}{dZ} = -\frac{\partial \mathcal{H}}{\partial \tilde{W}_2}, \quad \frac{d\tilde{W}_2}{dZ} = \frac{\partial \mathcal{H}}{\partial \tilde{W}_1}$$

where the Hamiltonian $\mathcal{H}$ has the form:

$$\mathcal{H} = \mathcal{H}_1(\widetilde{W}_1) + \mathcal{H}_2(\widetilde{W}_2) + C_2\widetilde{W}_1 - C_1\widetilde{W}_2 \tag{106}$$

and functions $\mathcal{H}_{1,2}$ are

$$\mathcal{H}_{1,2} = f_0^2 D\sqrt{2}\int \frac{(1+\tilde{W}_{1,2}^2 - Ra)d\tilde{W}_{1,2}}{(1+\tilde{W}_{1,2}^2)(4(1+\tilde{W}_{1,2}^2)^2 + 4(D^2 - 2Ra)(1-\tilde{W}_{1,2}^2) + (D^2 - 2Ra)^2)}$$

Assuming $D = Ra = 2$ and $f_0 = 10$ one can easily calculate the Hamiltonian (106):

$$\mathcal{H} = -\frac{25}{2}\sqrt{2}\left(\frac{\widetilde{W}_1(\widetilde{W}_1^2 + 3)}{(\widetilde{W}_1^2 + 1)^2} + \frac{\widetilde{W}_2(\widetilde{W}_2^2 + 3)}{(\widetilde{W}_2^2 + 1)^2} + arctg\widetilde{W}_1 + arctg\widetilde{W}_2\right) + C_2\widetilde{W}_1 - C_1\widetilde{W}_2$$

Equations (104)-(105) being Hamiltonian implies that the phase space can only have two types of fixed points: elliptic and hyperbolic fixed points. This can be observed through a qualitative analysis of the system by linearizing the right-hand sides of equations (104)-(105) near fixed points, determining their type, and constructing a phase portrait. Through this analysis, we have identified four fixed points, two of which are hyperbolic and two of which are elliptic. The phase portrait of the dynamic system of equations (104)-(105) with parameters $C_1 = -1$, $C_2 = 1$, $D = Ra = 2$ and $f_0 = 10$ is shown in Fig. 11, which allows us to qualitatively describe possible stationary solutions. The phase portrait also reveals the presence of closed trajectories around elliptic points and separatrices connecting hyperbolic points. Closed trajectories correspond to nonlinear periodic solutions or nonlinear waves (see Fig. 12a), while separatrices correspond to localized kink-type vortex structures (see Fig. 12b), which are the most interesting localized solutions.
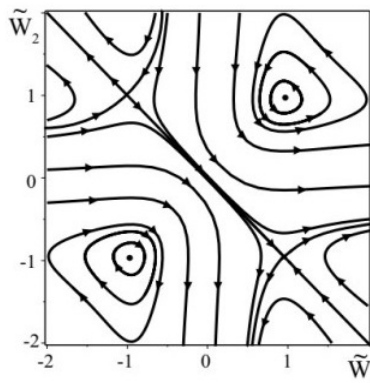

Figure 11. The phase plane for the dynamic system of equations (104)-(105) under the condition $C_1 = -1$ and $C_2 = 1$. Here you can see the presence of closed trajectories around elliptical points and separatrices that connect hyperbolic points.
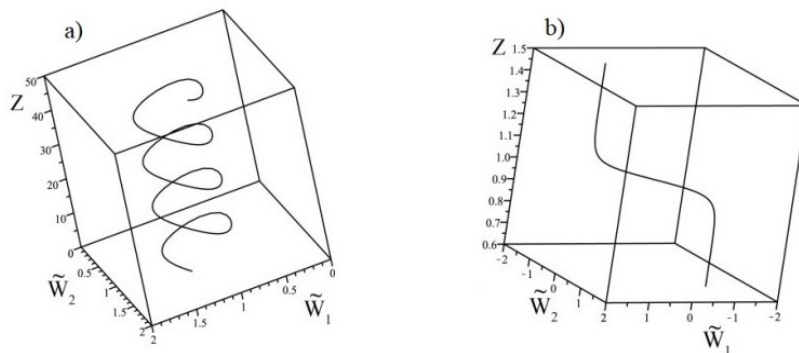

Figure 12. a) The phase plane displays a non-linear helical wave, which corresponds to a closed trajectory. b) Localized nonlinear vortex structure (kink), which corresponds to the separatrix on the phase plane ($C_1 = -1$, $C_2 = 1$, $D = Ra = 2$).

5. NONLINEAR VORTEX DYNAMO IN A ROTATING STRATIFIED MOIST ATMOSPHERE
A moist atmosphere is composed of dry air, water vapor, and fluid water droplets. If the specific humidity value is below saturation, the atmosphere behaves like a binary mixture of dry air and water vapor, following the usual

hydrodynamic equations. However, when the specific humidity reaches saturation, excess water vapor condenses and forms a new substance called water content. This process releases a large amount of energy, although we only consider its energy effect here as describing a phase transition is a difficult task. This section presents the results of large-scale instability in a rotating stratified moist atmosphere with small-scale helicity at low Reynolds numbers, as described in [31]. The small-scale helicity is induced by an external force that considers the influence of Coriolis force and stratification in a moist atmosphere. The method of multiscale asymptotic expansions was applied in [31], resulting in averaged nonlinear equations for large-scale fields in the third order of Reynolds number in a rotating moist atmosphere. The instability of the hydrodynamic α-effect was obtained for small amplitudes of large-scale velocity perturbations, and the criteria for the development of this instability were determined based on the rotation and stratification of the medium. The numerical estimates of the characteristic times and scales of instability given in [31] may explain the origin of the large-scale spiral structure of cloud mesovortices and typhoons at the initial stage of their development. Furthermore, a numerical analysis of the nonlinear equations in the stationary regime was conducted in [31], which revealed the existence of localized helical vortex structures of the kink type.

5.1. Statement of the problem and basic equations for large-scale vortex fields

The problem statement is as follows: Consider a layer of the atmosphere where the specific humidity is equal to the saturated humidity. The negative gradient of the saturated value of specific humidity in the atmosphere is determined by the stationary vertical gradients of temperature and pressure. When ascending air flows, twisted by the Coriolis force, condense water vapor and release latent thermal energy. In this medium, small-scale non-spiral turbulence is present, which is modeled by an external small-scale force. The main objective of this section is to understand how moisture phase transitions affect the dynamics of large-scale or averaged fields. To describe the process of wet convection, we use the well-known Boussinesq approximation to write hydrodynamic equations for perturbations of velocity V, temperature T, pressure P, and specific water content m in a rotating coordinate system.

$$\frac{\partial V_i}{\partial t} + V_k \frac{\partial V_i}{\partial x_k} = \nu \Delta V_i - \frac{1}{\rho} \frac{\partial P}{\partial x_i} + 2\varepsilon_{ijk} V_j W_k + g e_i \left(\beta T + \beta_1 m \right) + F_0^i \tag{107}$$

$$\frac{\partial T}{\partial t} + V_k \frac{\partial T}{\partial x_k} - A e_k V_k = \chi \Delta T + \frac{L}{c_p} K \tag{108}$$

$$\frac{\partial m}{\partial t} + V_k \frac{\partial m}{\partial x_k} - B e_k V_k = d \Delta m + K \tag{109}$$

$$\frac{\partial V_i}{\partial x_i} = 0 \tag{110}$$

The system of equations (107)-(110) describes the evolution of disturbances against the background of the main equilibrium state $\overline{T}(z)$, $\overline{\rho}(z)$, $\overline{m}(z)$, specified by a constant temperature gradient $\nabla \overline{T} = -A\vec{e}$ $(A > 0)$ (heating from below), an equilibrium gradient of specific water content $\nabla \overline{m} = -B\vec{e}$ $(B < 0)$, and hydrostatic pressure: $\nabla \overline{P} = \overline{\rho}\vec{g} - \left[\vec{\Omega} \times \left[\vec{\Omega} \times \vec{r} \right] \right]$, where $\vec{r}$ is the radius vector of the fluid element. Here $\vec{g} = (0, 0, -g)$ is the gravitational acceleration vector directed along the OZ axis. The angular velocity vector $\vec{\Omega}$ is constant, which means that the medium is rotating as a solid body around the OZ axis. The direction of the vector is also along the OZ axis, which means that the rotation is around a vertical axis. The constant rotation is an assumption of the problem, which simplifies the analysis of the equations and allows us to study the effects of moisture phase transitions on the large-scale dynamics. The heat balance equation (108) includes the source of latent heat release from saturated air condensation [18]:

$$Q = \frac{L}{c_p} K = \frac{L}{c_p} c A e_k v_k, \quad c = \frac{dq_n}{d\overline{T}}, \tag{111}$$

where L is the specific heat of condensation of water vapor, c_p is the heat capacity of dry air at constant pressure, K is the rate of condensation, and q_n is the specific saturated humidity or mass fraction of saturated steam. $e = (0, 0, 1)$ is a unit vector in the direction of the Z axis directed vertically upwards, β is the coefficient of thermal expansion, $\beta_1 = -\frac{1}{\overline{\rho}} \left(\frac{\partial \rho}{\partial m} \right)_{T,P}$ and d is the diffusion coefficient.

The Navier-Stokes equation (107) includes an external small-scale force F_0, which models the excitation source in the medium of small-scale and high-frequency pulsations of the velocity field v_0 with a small Reynolds number

$R = \dfrac{v_0 t_0}{\lambda_0} \ll 1$. The main role of this force is to maintain a small level of small-scale motions in the presence of dissipation. Here we consider a small-scale external force of the form (25) with properties (3). Applying the usual dimensionless procedure to the variables x, t, V, P, F_0, T as well as to perturbations of the specific water content $m \to m / \lambda_0 B$, we write equations (107)-(110) in a dimensionless form:

$$\frac{\partial V_i}{\partial t} + R V_k \frac{\partial V_i}{\partial x_k} = \Delta V_i - \frac{\partial P}{\partial x_i} + D\varepsilon_{ijk} V_j + e_i \left(\widetilde{Ra} T + \widetilde{R}_m m \right) + F_0^i \tag{112}$$

$$\frac{\partial T}{\partial t} + R V_k \frac{\partial T}{\partial x_k} - a e_k V_k = Pr^{-1} \Delta T \tag{113}$$

$$\frac{\partial m}{\partial t} + R V_k \frac{\partial m}{\partial x_k} - b e_k V_k = S^{-1} \Delta m \tag{114}$$

$$\frac{\partial V_i}{\partial x_i} = 0 \tag{115}$$

Here, new dimensionless parameters have appeared that are characteristic of a moist atmosphere: $\widetilde{R}_m = \dfrac{R_m}{S}$, $R_m = \dfrac{g \beta_1 B \lambda_0^4}{\nu d}$ is the diffusion analogue of the Rayleigh number on the scale λ_0; $S = \dfrac{\nu}{d}$ is the Schmidt number, $a = 1 + \dfrac{c}{c_p} L, b = 1 + \dfrac{cA}{B}$. The small parameter of the asymptotic expansion will be the Reynolds number R of small-scale motions, and the parameters Ra, R_m and D will be considered arbitrary, not affecting the expansion scheme.

Consider the problem statement below. Moist air found in certain parts of the atmosphere is made up of dry air, water vapor, and fluid water droplets. This environment experiences small-scale, high-frequency movements supported by an external force. The Coriolis force twists ascending airflows, leading to the condensation of water vapor into water and the release of latent thermal energy. The negative gradient of the saturated value of specific humidity in the atmosphere is determined by stationary vertical gradients of temperature and pressure. The impact of moisture phase transitions can significantly affect the dynamics of large-scale or averaged fields. To obtain equations for large-scale fields, the multiscale asymptotic expansion method is used. This method identifies the equations for large-scale perturbations by separating them from the hierarchy of perturbations. By using the technique described in the previous sections, the spatial and temporal derivatives in the system (112)-(115) are represented as an expansion (6). The variables $\vec{V}, P, T$ are represented as an asymptotic series (7) and (76). In constructing a nonlinear theory, perturbations of specific water content m are also represented as an asymptotic series.

$$m(x, t) = \frac{1}{R} M_{-1}(X) + m_0(x_0) + R m_1 + R^2 m_2 + R^3 m_3 + \cdots \tag{116}$$

The algebraic structure of the asymptotic expansion of equations (112)–(115) in various orders R is given in [31]. It is also shown that it is in order R^3 that the main secular equations, or equations for large-scale fields in a moist atmosphere, are obtained:

$$\partial_T W_{-1}^i - \Delta W_{-1}^i + \nabla_k \left(\overline{v_0^k v_0^i} \right) = -\nabla_i \overline{P}_1 \tag{117}$$

$$\partial_T T_{-1} - Pr^{-1} \Delta T_{-1} = -\nabla_k \left(\overline{v_0^k T_0} \right) \tag{118}$$

$$\partial_T M_{-1} - S^{-1} \Delta M_{-1} = -\nabla_k \left(\overline{v_0^k m_0} \right) \tag{119}$$

Equations (117)-(119) are supplemented by the following secular equations:

$$-\nabla_i P_{-3} + \widetilde{Ra} e_i T_{-1} + e_i \widetilde{R}_m M + D\varepsilon_{ijk} W_{-1}^k = 0, \ W_{-1}^k \nabla_k W_{-1}^i = -\nabla_i P_{-1}, \ W_{-1}^k \nabla_k T_{-1} = 0$$

$$W_{-1}^k \nabla_k M_{-1} = 0, \ \nabla_i W_{-1}^i = 0, \ W_{-1}^z = 0.$$

These equations are satisfied by large-scale fields of the Beltrami type:

$$\vec{W}_{-1} = \left(W_{-1}^x(Z), W_{-1}^y(Z), 0 \right), \quad M_{-1} = M_{-1}(Z), \quad T_{-1} = T_{-1}(Z), \quad P_{-1} = const \tag{120}$$

In the framework of the "quasi-two-dimensional" problem, when large-scale derivatives with Z are preferable

$$\nabla_Z \equiv \frac{\partial}{\partial Z} \gg \frac{\partial}{\partial X}, \frac{\partial}{\partial Y}$$

the system of equations (117)-(119) is simplified and takes the following form:

$$\partial_T W_1 - \nabla_Z^2 W_1 + \nabla_Z \left(\overline{v_0^z v_0^x} \right) = 0, \quad W_1 \equiv W_{-1}^x \tag{121}$$

$$\partial_T W_2 - \nabla_Z^2 W_2 + \nabla_Z \left(\overline{v_0^z v_0^y} \right) = 0, \quad W_2 \equiv W_{-1}^y \tag{122}$$

$$\partial_T T_{-1} - Pr^{-1} \Delta T_{-1} + \nabla_Z \left(\overline{v_0^z T_0} \right) = 0 \tag{123}$$

$$\partial_T M_{-1} - S^{-1} \Delta M_{-1} + \nabla_Z \left(\overline{v_0^z m_0} \right) = 0 \tag{124}$$

The system of equations (121)-(124) describes the evolution of large-scale disturbances in a rotating moist atmosphere within the framework of the condensation heat release model. To study the dynamics of a large-scale vortex field, it is necessary to obtain equations (121)–(122) in a closed form, i.e., to calculate the Reynolds stresses $\nabla_k \left(\overline{v_0^k v_0^i} \right)$. It is clear that in order to solve this problem, it is necessary to find solutions for a small-scale velocity field $\vec{v}_0$.

5.2. Small-scale fields in zero order by R
Let us consider the equations for zero order in R equations (112)-(115)

$$\widehat{D}_0 v_0^i = -\partial_i P_0 + D\varepsilon_{ijk} v_0^j e_k + \widetilde{Ra} e_i T_0 + \widetilde{R}_m e_i m_0 + F_0^i \tag{125}$$

$$\widehat{D}_m m_0 = b e_k v_0^k \tag{126}$$

$$\widehat{D}_\theta T_0 = a e_k v_0^k \tag{127}$$

where the notation for the operators is introduced

$$\widehat{D}_0 = \partial_t - \partial^2 + W_{-1}^k \partial_k, \quad \widehat{D}_m = \partial_t - S^{-1} \partial^2 + W_{-1}^k \partial_k, \quad \widehat{D}_\theta = \partial_t - Pr^{-1} \partial^2 + W_{-1}^k \partial_k.$$

Using the condition of solenoidality of the fields $\vec{v}_0$ and $\vec{F}_0$, we exclude from equation (125) the pressure P_0

$$P_0 = \frac{D \left(\partial_x v_0^y - \partial_y v_0^x \right)}{\partial^2} + \frac{\widetilde{Ra} \partial_z T_0}{\partial^2} + \frac{\widetilde{R}_m \partial_z m_0}{\partial^2} \tag{128}$$

From equations (126)-(127) we find expressions for small-scale temperature T_0 and specific water content m_0:

$$T_0 = \frac{a v_0^z}{\widehat{D}_\theta}, \quad m_0 = \frac{b v_0^z}{\widehat{D}_m}. \tag{129}$$

Putting (129) into (128), we get

$$P_0 = \frac{D \left(\partial_x v_0^y - \partial_y v_0^x \right)}{\partial^2} + \left(\frac{a \widetilde{Ra}}{\partial^2 \widehat{D}_\theta} + \frac{b \widetilde{R}_m}{\partial^2 \widehat{D}_m} \right) \partial_z v_0^z. \tag{130}$$

As a result of substituting (130) into (125), we obtain a system of equations for finding the velocity field of the zero approximation:

$$\begin{cases} \widehat{p}_{11}v_0^x + \widehat{p}_{12}v_0^y + \widehat{p}_{13}v_0^z = F_0^x \\ \widehat{p}_{21}v_0^x + \widehat{p}_{22}v_0^y + \widehat{p}_{23}v_0^z = F_0^y \\ \widehat{p}_{31}v_0^x + \widehat{p}_{32}v_0^y + \widehat{p}_{33}v_0^z = F_0^z \end{cases} \tag{131}$$

The tensor components $\widehat{p}_{ij}$ are as follows:

$$\widehat{p}_{11} = \widehat{D}_0 - D\frac{\partial_x\partial_y}{\partial^2}, \quad \widehat{p}_{12} = D\frac{\partial_x^2}{\partial^2} - D, \quad \widehat{p}_{13} = \left(\frac{a\widetilde{Ra}}{\widehat{D}_\theta} + \frac{b\widetilde{R}_m}{\widehat{D}_m}\right)\frac{\partial_x\partial_z}{\partial^2},$$

$$\widehat{p}_{22} = \widehat{D}_0 + D\frac{\partial_x\partial_y}{\partial^2}, \quad \widehat{p}_{23} = \left(\frac{a\widetilde{Ra}}{\widehat{D}_\theta} + \frac{b\widetilde{R}_m}{\widehat{D}_m}\right)\frac{\partial_y\partial_z}{\partial^2}, \quad \widehat{p}_{31} = -D\frac{\partial_z\partial_y}{\partial^2},$$

$$\widehat{p}_{21} = -\left(D\frac{\partial_y^2}{\partial^2} - D\right), \quad \widehat{p}_{32} = D\frac{\partial_z\partial_x}{\partial^2}, \quad \widehat{p}_{33} = \widehat{D}_0 + \left(\frac{a\widetilde{Ra}}{\widehat{D}_\theta} + \frac{b\widetilde{R}_m}{\widehat{D}_m}\right)\left(\frac{\partial_z^2}{\partial^2} - 1\right)$$

In equation system (131), we utilize the explicit form of the external helical force F_0, which is determined by expression (25). The small-scale velocity fields (v_0^x, v_0^y, v_0^z) are obtained by applying Cramer's rule to the components of the external helical force, as described in equations (26)-(28). Following similar procedures as in section 2.3, we determine the zero-approximation velocity field in R:

$$u_0 = C_1 e^{i\phi_1} + A_2 e^{i\phi_2} + c.c. = u_{01} + u_{02} + u_{03} + u_{04} \tag{132}$$

$$v_0 = A_1 e^{i\phi_1} - C_2 e^{i\phi_2} + c.c. = v_{01} + v_{02} + v_{03} + v_{04} \tag{133}$$

$$w_0 = -C_1 e^{i\phi_1} + C_2 e^{i\phi_2} + c.c. = w_{01} + w_{02} + w_{03} + w_{04} \tag{134}$$

Here $w_{02} = (w_{01})^*$, $w_{04} = (w_{03})^*$, $v_{02} = (v_{01})^*$, $v_{04} = (v_{03})^*$, $u_{02} = (u_{01})^*$, and new designations are introduced:

$$A_{1,2} = \frac{f_0}{2}\frac{\widehat{D}_{1,2}^* - \frac{1}{2}\left(\frac{a\widetilde{Ra}}{\widehat{D}_{\theta_{1,2}}^*} + \frac{b\widetilde{R}_m}{\widehat{D}_{m_{1,2}}^*}\right)}{\widehat{D}_{1,2}^*\left(\widehat{D}_{1,2}^* - \frac{1}{2}\left(\frac{a\widetilde{Ra}}{\widehat{D}_{\theta_{1,2}}^*} + \frac{b\widetilde{R}_m}{\widehat{D}_{m_{1,2}}^*}\right)\right) + \frac{D^2}{2}}, \quad C_{1,2} = \frac{f_0}{4}\frac{D}{\widehat{D}_{1,2}^*\left(\widehat{D}_{1,2}^* - \frac{1}{2}\left(\frac{a\widetilde{Ra}}{\widehat{D}_{\theta_{1,2}}^*} + \frac{b\widetilde{R}_m}{\widehat{D}_{m_{1,2}}^*}\right)\right) + \frac{D^2}{2}} \tag{135}$$

In contrast to the case of a homogeneous medium examined in Section 2, the small-scale velocity field (132)-(134) is influenced by the temperature gradient, specific water content gradient, and processes related to heat release during vapor condensation. This matter will be further addressed when analyzing the stability of small perturbations of a large-scale velocity field $\vec{W}$.

5.3. Nonlinear vortex dynamo equations and large-scale instability

To close the system of equations (121)-(122) describing the evolution of large-scale velocity fields $\vec{W}$, it is necessary to calculate the correlators of the following form:

$$T^{31} = \overline{w_0 u_0} = \overline{w_{01}(u_{01})^*} + \overline{(w_{01})^* u_{01}} + \overline{w_{03}(u_{03})^*} + \overline{(w_{03})^* u_{03}} \tag{136}$$

$$T^{32} = \overline{w_0 v_0} = \overline{w_{01}(v_{01})^*} + \overline{(w_{01})^* v_{01}} + \overline{w_{03}(v_{03})^*} + \overline{(w_{03})^* v_{03}} \tag{137}$$

Formulas (136), (137) determine the Reynolds stresses, for which we need expressions for small-scale velocity fields (132)-(134). After substituting these expressions into formulas (136)-(137), we find:

$$T^{31} = -2|C_1|^2 + C_2 A_2^* + C_2^* A_2, \qquad T^{32} = -2|C_2|^2 - (C_1 A_1^* + C_1^* A_1) \tag{138}$$

Substituting expressions (135) into formulas (138), we find expressions for the Reynolds stresses:

$$T^{31} = -\frac{f_0^2}{8} \frac{D^2}{\left|\hat{D}_1^2 + \frac{D^2}{2} - \left(\widetilde{Ra}\frac{a}{2}\frac{\hat{D}_1}{\hat{D}_{\theta_1}} + \tilde{R}_m\frac{b}{2}\frac{\hat{D}_1}{\hat{D}_{m_1}}\right)\right|^2} + \frac{f_0^2}{2} D \frac{\left(1 - \widetilde{Ra}\frac{a}{2}\frac{Pr^{-1}}{\left|\hat{D}_{\theta_2}\right|^2} - \tilde{R}_m\frac{b}{2}\frac{S^{-1}}{\left|\hat{D}_{m_2}\right|^2}\right)}{\left|\hat{D}_2^2 + \frac{D^2}{2} - \left(\widetilde{Ra}\frac{a}{2}\frac{\hat{D}_2}{\hat{D}_{\theta_2}} + \tilde{R}_m\frac{b}{2}\frac{\hat{D}_2}{\hat{D}_{m_2}}\right)\right|^2} \tag{139}$$

$$T^{32} = -\frac{f_0^2}{8} \frac{D^2}{\left|\hat{D}_2^2 + \frac{D^2}{2} - \left(\widetilde{Ra}\frac{a}{2}\frac{\hat{D}_2}{\hat{D}_{\theta_2}} + \tilde{R}_m\frac{b}{2}\frac{\hat{D}_2}{\hat{D}_{m_2}}\right)\right|^2} - \frac{f_0^2}{2} D \frac{\left(1 - \widetilde{Ra}\frac{a}{2}\frac{Pr^{-1}}{\left|\hat{D}_{\theta_1}\right|^2} - \tilde{R}_m\frac{b}{2}\frac{S^{-1}}{\left|\hat{D}_{m_1}\right|^2}\right)}{\left|\hat{D}_1^2 + \frac{D^2}{2} - \left(\widetilde{Ra}\frac{a}{2}\frac{\hat{D}_1}{\hat{D}_{\theta_1}} + \tilde{R}_m\frac{b}{2}\frac{\hat{D}_1}{\hat{D}_{m_1}}\right)\right|^2} \tag{140}$$

As a result, equations (121)-(122) take a closed form. If the properties of the medium are such that the Prandtl $Pr = \frac{\nu}{\chi}$

and Schmidt $S = \frac{\nu}{d}$ numbers are equal to one, we find

$$T^{31} = -\frac{f_0^2}{8} \frac{D^2\left(4+\tilde{W}_1^2\right)}{\left(4+\tilde{W}_1^2\right)\left[16\tilde{W}_1^2 + \left[\frac{D^2}{2}+4-\tilde{W}_1^2\right]^2 + \frac{\tilde{R}^2}{4}\right] - \tilde{R}\left(16-\tilde{W}_1^4\right) - D^2\frac{\tilde{R}}{2}\left(4-\tilde{W}_1^2\right)} +$$

$$+\frac{f_0^2}{2} \frac{D\left(4+\tilde{W}_2^2 - \frac{\tilde{R}}{2}\right)}{\left(4+\tilde{W}_2^2\right)\left[16\tilde{W}_2^2 + \left[\frac{D^2}{2}+4-\tilde{W}_2^2\right]^2 + \frac{\tilde{R}^2}{4}\right] - \tilde{R}\left(16-\tilde{W}_2^4\right) - D^2\frac{\tilde{R}}{2}\left(4-\tilde{W}_2^2\right)} \tag{141}$$

$$T^{32} = -\frac{f_0^2}{8} \frac{D^2\left(4+\tilde{W}_2^2\right)}{\left(4+\tilde{W}_2^2\right)\left[16\tilde{W}_2^2 + \left[\frac{D^2}{2}+4-\tilde{W}_2^2\right]^2 + \frac{\tilde{R}^2}{4}\right] - \tilde{R}\left(16-\tilde{W}_2^4\right) - D^2\frac{\tilde{R}}{2}\left(4-\tilde{W}_2^2\right)} -$$

$$-\frac{f_0^2}{2} \frac{D\left(4+\tilde{W}_1^2 - \frac{\tilde{R}}{2}\right)}{\left(4+\tilde{W}_1^2\right)\left[16\tilde{W}_1^2 + \left[\frac{D^2}{2}+4-\tilde{W}_1^2\right]^2 + \frac{\tilde{R}^2}{4}\right] - \tilde{R}\left(16-\tilde{W}_1^4\right) - D^2\frac{\tilde{R}}{2}\left(4-\tilde{W}_1^2\right)} \tag{142}$$

In formulas (141)-(142), the following designation is adopted: $\tilde{R} = aRa + bR_m$. As a rule, in atmospheric convection, the equilibrium gradient of specific water content is small $|B| \ll c|A|$ and taking into account that the expression $\left|\frac{L}{c_p}\right| \gg \left|\frac{\beta_1}{\beta}\right|$ for $\tilde{R}$ can be represented as a sum $\tilde{R} = \left(1 + L\frac{c}{c_p}\right)Ra = Ra + R_q$, where $Ra = \frac{g\beta A\lambda_0^4}{\nu^2}$ is the

Rayleigh number for "dry" convection at $\nu = \chi = d$, $R_q = \frac{g\beta(\gamma_m - \gamma_a)}{\nu^2}$ is a number characterizing the intensity of condensation heat release, and γ_m is a wet adiabatic and $\gamma_a = \frac{g}{c_p}$ is a dry adiabatic gradient related by the relation [19]:

$$\gamma_m = \gamma_a + \frac{L}{c_p}\frac{dq_n}{dz} \tag{143}$$

Please note that when the medium is homogeneous ($\widetilde{Ra} = \tilde{R}_m = 0$), equations (141)-(142) are equivalent to the findings presented in reference [30]. Equations (121)-(122) describe the nonlinear vortex dynamo equations in a humid,

rotating atmosphere with a small external force on a small scale. In case of the disappearance of the rotational effect ($\Omega = 0$) or the external force's amplitude is zero ($f_0 = 0$), the large-scale fields will undergo conventional diffusion spreading.

Initially, we examine the stability of small perturbations, followed by investigating the likelihood of stationary structures. When the $W_{1,2}$ values are small, the Reynolds stresses (141)-(142) can be expanded into a series in $W_{1,2}$, resulting in linearized equations (121)-(122).

$$\partial_T W_1 - \nabla_{\tilde{Z}}^2 W_1 = \alpha_1 \nabla_Z W_1 - \alpha_2 \nabla_Z W_2 \quad (144)$$

$$\partial_T W_2 - \nabla_{\tilde{Z}}^2 W_2 = \alpha_1 \nabla_Z W_2 + \alpha_2 \nabla_Z W_1 \quad (145)$$

Here

$$\alpha_1 = \frac{f_0^2}{8} D^2 \alpha \ , \ \alpha_2 = \frac{f_0^2}{2} D\left(\alpha \left(1 - \frac{\tilde{R}}{10} \right) - \alpha_0 \frac{\tilde{R}}{25} \right), \quad (146)$$

$$\alpha_0 = \frac{4}{\left(D^2 + 6 \right)^2 + 64 + \tilde{R}^2 - 12\tilde{R}\left(1 + \frac{D^2}{10} \right)}, \quad \alpha = \frac{32 D^2 \left[10 - D^2 + \tilde{R}\left(1 + \frac{D^2}{10} \right) + \frac{3}{50} \tilde{R} D^2 \right]}{\left(\left(D^2 + 6 \right)^2 + 64 + \tilde{R}^2 - 12\tilde{R}\left(1 + \frac{D^2}{10} \right) \right)^2}.$$

We seek a solution to the linear system of equations (144)-(145) in the form of plane waves with wave vector $\vec{K} \parallel OZ$. This results in a dispersion equation of the form (45). The solutions of this equation demonstrate the existence of unstable oscillatory solutions for large-scale vortex disturbances. It is important to note that the gain α_2 for small amplitudes of large-scale disturbances depends on the amplitude of the external force f_0 (turbulence intensity), the rotation parameter D, and the stratification parameter $\tilde{R}$, which takes into account the characteristics of Ra "dry" and R_q "wet" convection. To start, we examine how the values of coefficient α_2 change with the parameter $\tilde{R}$, for a fixed rotation parameter $D = 1$ and external force amplitude $f_0 = 10$. The functional dependence $\alpha_2(\tilde{R})$ is illustrated in Fig. 13a. The coefficient α_2 value at $\tilde{R} = 0$ corresponds to a homogeneous medium where the generation of large-scale vortex disturbances is caused by the Coriolis force and the action of an external small-scale force [30]. Fig. 13a illustrates that the presence of temperature stratification ($Ra \neq 0$) and an additional source of condensation heat release ($R_q \neq 0$) can increase the coefficient α_2, resulting in faster generation of large-scale vortex disturbances than in a homogeneous medium. At a critical value of the stratification parameter $\tilde{R} = \tilde{R}_0$, the generation of perturbations ceases because $\alpha_2 = 0$. Beyond this point, for $\tilde{R} > \tilde{R}_0$, the sign of the gain α_2 changes. The rising mode becomes damped, and vice versa. Additionally, we examine the influence of the medium's rotational effect on the gain or the process of generating large-scale disturbances by fixing the value of parameter $\tilde{R} = 2$ and the external force amplitude $f_0 = 10$. The functional dependence $\alpha_2(D)$ is illustrated on the right side of Fig. 13. An analysis of the dependence on the rotation parameter $\alpha_2(D)$ reveals that the coefficient $\alpha_2 \to 0$ decreases with "fast" rotation $D \to \infty$, implying that the α-effect is suppressed.

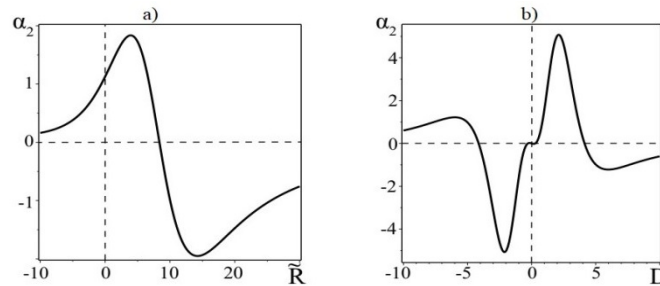**Figure 13.** a) Plot of dependence of α - effect on medium stratification parameter $\tilde{R}$. b) Plot of dependence of α - effect on medium rotation parameter D.

The graph depicting the dependency $\alpha_2(D)$ shows that there are certain parameter D values at which the generation of vortex disturbances ceases ($\alpha_2 = 0$). Fig. 14a illustrates a graphic representation of the combined

influence of rotation and stratification in the plane $(D, \widetilde{R})$, highlighting the region of instability $\alpha_2 > 0$ in gray. The maximum instability increment $\Gamma_{max} = \dfrac{\alpha_2^2}{4}$ is attained at the wavenumbers $K_{max} = \dfrac{\alpha_2}{2}$. The dependence graph (Fig. 14b) of the instability increment Γ on the wavenumbers K has a standard form, typical of the α-effect. As a consequence of the development of large-scale instability in a rotating humid atmosphere, large-scale spiral circularly polarized vortices of the Beltrami type are generated.
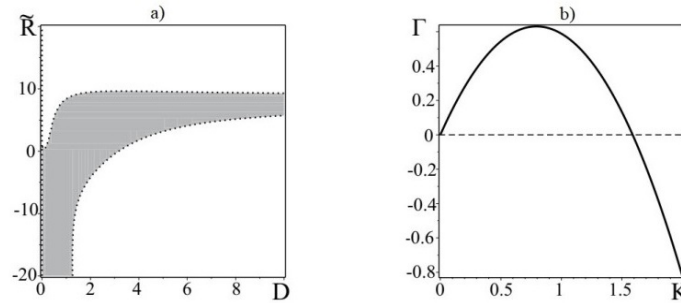
Figure 14. a) The plot illustrates the values of coefficient α_2 in the $(D, \widetilde{R})$ plane, where the area corresponding to unstable solutions (positive values of α_2) is shaded in gray, and the area corresponding to stable solutions (negative values of α_2) is shown in white. b) The plot shows the dependence of instability increment on wavenumbers K for parameters $D = 1$, $\widetilde{R} = 2$ and $f_0 = 10$.

In conclusion to this section, we can estimate the typical spatial $L_{max} \sim 1/\alpha_2$ and time $T_{max} \sim 1/\alpha_2^2$ scales of the unstable mode and its growth under the conditions of the hydrodynamic α-effect in a rotating moist atmosphere. To achieve this, we calculate the coefficient α_2 using the standard characteristics of atmospheric turbulence, such as the characteristic velocity $v_0 \approx 0.1$ in m/s, the scale of fluctuations $\lambda_0 \approx 10^3$ in meters, and the turbulent viscosity $\nu \approx 10^5$ in m/s, as described in references [5] and [18].

Hence the characteristic time of turbulent pulsations $t_0 = \lambda_0^2 / \nu \approx 10\,\text{s}$ and the value of the rotation parameter $D = 2\Omega\lambda_0^2 / \nu \approx 1.4 \cdot 10^{-3}$ (the angular velocity of the Earth's rotation $\Omega \approx 7 \cdot 10^{-5}\,\text{s}^{-1}$) and the Reynolds number $R = v_0\lambda_0 / \nu \approx 10^{-3}$. Let's compare the dimensionless parameters D, Ra, R_m with respect to the Reynolds number R:

$$D / R > 1, \quad Ra / R = \beta A \cdot 10^6 > 1, \quad R_m / R = \beta_1 B \cdot 10^6 > 1,$$

which is consistent with the asymptotic expansion scheme used here. The smallness of the rotation parameter D makes it possible to neglect the terms of order D^2 when estimating the coefficient α_2

$$\alpha_2 = \frac{f_0^2}{2} D\kappa, \tag{147}$$

where the value of $\kappa \approx 4.5 \cdot 10^{-2}$ is calculated according to formulas (146) for the stratification parameter $\widetilde{R} = 5$.

Let us express the hydrodynamic helicity $\alpha_v = (t_0 / 3)\overline{v_0 rot v_0}$ (see, for example, [11]) in terms of the dimensionless source amplitude:

$$\alpha_v = \frac{t_0 v_0^2}{3\lambda_0} f_0^2, \tag{148}$$

Here f_0 is the dimensionless amplitude of the external force included in formula (147). When deriving this formula, it is assumed that there is a balance between the source and dissipation, which corresponds to the stationary case. Substituting (148) into (147), we find expressions for the characteristic spatial and temporal scales:

$$L_{max} \approx \frac{2}{3} \frac{\alpha_v D\kappa}{v_0 R} = 106\,\text{km},$$

$$T_{max} \approx \frac{4}{9} \frac{t_0 v_0^2 R^2}{\alpha_v^2 D^2 \kappa^2} = 1.3\,\text{days}. \tag{149}$$

Here, the hydrodynamic helicity coefficient $\alpha_v \approx 10^{-2}$ m/s was considered [5]. Thus, quite acceptable estimates (149) of the characteristic scales of instability have been obtained, which can explain the origin of the large-scale spiral structure of cloudy mesovortices and typhoons at the initial stage of development.

5.4. Stationary nonlinear vortex structures

Clearly, with an increase in the amplitude of perturbations $W_{1,2}$, the nonlinear terms decrease and the instability saturates. As a result, nonlinear vortex structures are formed. Next, we put $\partial_T = 0$ in equations (121)-(122) and integrate the equations once over Z, and we get a system of nonlinear equations of the following form:

$$\frac{d\tilde{W}_1}{dZ} = -\frac{D^2 \frac{f_0^2}{8}\left(4+\tilde{W}_1^2\right)}{\left(4+\tilde{W}_1^2\right)\left[16\tilde{W}_1^2 + \left[\frac{D^2}{2}+4-\tilde{W}_1^2\right]^2 + \frac{\tilde{R}^2}{4}\right] - \tilde{R}\left(16-\tilde{W}_1^4\right) - D^2\frac{\tilde{R}}{2}\left(4-\tilde{W}_1^2\right)} +$$

$$+\frac{D\frac{f_0^2}{2}\left(4+\tilde{W}_2^2-\frac{\tilde{R}}{2}\right)}{\left(4+\tilde{W}_2^2\right)\left[16\tilde{W}_2^2 + \left[\frac{D^2}{2}+4-\tilde{W}_2^2\right]^2 + \frac{\tilde{R}^2}{4}\right] - \tilde{R}\left(16-\tilde{W}_2^4\right) - D^2\frac{\tilde{R}}{2}\left(4-\tilde{W}_2^2\right)} + C_1 \qquad (150)$$

$$\frac{d\tilde{W}_2}{dZ} = -\frac{D^2 \frac{f_0^2}{8}\left(4+\tilde{W}_2^2\right)}{\left(4+\tilde{W}_2^2\right)\left[16\left(1-\tilde{W}_2\right)^2 + \left[\frac{D^2}{2}+4-\tilde{W}_2^2\right]^2 + \frac{\tilde{R}^2}{4}\right] - \tilde{R}\left(16-\tilde{W}_2^4\right) - D^2\frac{\tilde{R}}{2}\left(4-\tilde{W}_2^2\right)} -$$

$$-\frac{D\frac{f_0^2}{2}\left(4+\tilde{W}_1^2-\frac{\tilde{R}}{2}\right)}{\left(4+\tilde{W}_1^2\right)\left[16\tilde{W}_1^2 + \left[\frac{D^2}{2}+4-\tilde{W}_1^2\right]^2 + \frac{\tilde{R}^2}{4}\right] - \tilde{R}\left(16-\tilde{W}_1^4\right) - D^2\frac{\tilde{R}}{2}\left(4-\tilde{W}_1^2\right)} + C_2 \qquad (151)$$

Here, C_1, C_2 are arbitrary constants of integration. Let us now find out what types of stationary vortex structures are described by the system of equations (150)-(151). Let's start a qualitative analysis of the system of equations (150)-(151), assuming for simplicity of calculations that the dimensionless parameters are $f_0 = D = 1$, $\tilde{R} = 2$.

For a given set of values of the parameters, the phase portrait of equations (150)-(151) can be determined based on the constants C_1 and C_2. It has been established using standard methods that the system of equations has four fixed points in the region shown in Fig. 15. No fixed points exist outside of this region, and degenerate cases are observed on the boundary, resulting in two fixed points. When the parameter values D are slightly modified, the region of existence of four fixed points is slightly deformed, altering its size and shape. Linearizing the vector field (150)-(151) in the neighborhood of the fixed points for the values of constants C_1 and C_2 (as shown in Fig. 15) where there are four fixed points, we can determine the type of fixed points. For four fixed points, two are hyperbolic, and the remaining two are stable and unstable focus. The position and type of the fixed points are used to construct the phase portrait of the system (150)-(151). The phase portrait enables us to describe all possible stationary vortex solutions qualitatively. Fig. 16 illustrates the phase portrait of the system of equations (150)-(151). The most interesting localized solutions are those that correspond to the phase portrait trajectories connecting fixed points on the phase plane. For instance, a separatrix linking a hyperbolic singular point with a stable focus corresponds to a solution for a localized kink-type vortex structure with rotation.
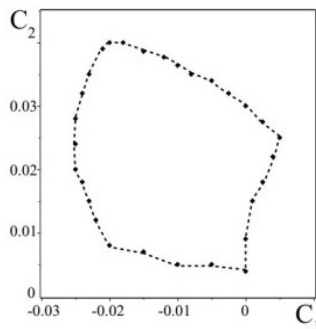

Figure 15. The boundary of the parameter region (C_1, C_2) in the phase portrait is marked by the dashed line. Within this region, there are two hyperbolic fixed points, as well as a stable and an unstable focus. Outside of this region, there are no fixed points. This area was constructed numerically for a value of $f_0 = D = 1$, $\tilde{R} = 2$.
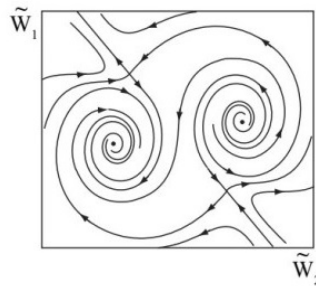
Figure 16. Phase portrait of the system of equations (150)-(151) at $f_0 = D = 1$, $\tilde{R} = 2$, $C_1 = -0.01$ and $C_2 = 0.01$. One can see the presence of two hyperbolic singular points and stable and unstable foci.

Fig. 17a illustrates the solution obtained through numerical integration. It corresponds to a spiral kink of one type. Another type of spiral kink is represented by the solution in Fig. 17b, for which the separatrix on the phase plane connects the unstable and stable focus. These solutions result in large-scale localized vortex structures, including kinks with rotation, which are produced by the instability of the α-effect.
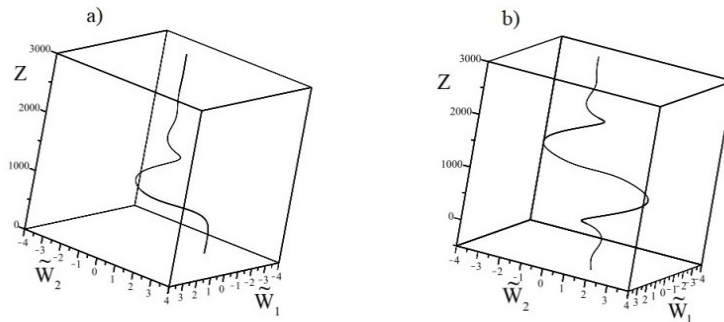
Figure 17. a) The image displays a kink that connects a hyperbolic point with a stable focus. As the stable focus is approached, the velocity field exhibits rotations. b) The picture illustrates the kink connecting the unstable and stable focus. It shows the internal helical structure of the kink. These solutions were obtained using the parameters: $f_0 = D = 1$, $\tilde{R} = 2$ and $C_1 = -0.01$, $C_2 = 0.01$.

6. VORTEX DYNAMO IN A ROTATING MOIST ATMOSPHERE WITH A SMALL-SCALE NON-HELICAL FORCE

This section presents the findings of a study conducted in [35] on a large-scale instability in a rotating stratified humid atmosphere subjected to a small-scale non-helical force. The previous section explored helical turbulence. Helical turbulence in natural conditions is typically attributed to the influence of the Coriolis force on the previously uniform, isotropic, and mirror-symmetric (non-spiral) turbulent motion of the medium. This raises a question about the origin of helicity itself. The natural hypothesis is that helicity arises due to the Coriolis force acting on convective turbulence. In this scenario, large-scale instabilities in the atmosphere should emerge self-consistently, without additional assumptions.

The turbulence in reference [35] was simulated by utilizing an external small-scale force that had no helicity $\vec{F}_0 rot \vec{F}_0 = 0$ and induced velocity fluctuations with a low Reynolds number $R = \dfrac{v_0 t_0}{\lambda_0} \ll 1$. Additionally, the medium's rotation axis was assumed to deviate from the vertical direction. The authors employed the method of multiscale asymptotic expansions and derived the equations of a nonlinear vortex dynamo. The study investigated linear instability and stationary nonlinear regimes and resulted in the discovery of localized vortex structures, namely nonlinear Beltrami waves and kinks.

6.1. Closed equations for large-scale vortex fields

We utilize equations (112)-(115) in the Boussinesq approximation with an external non-helical force $\vec{F}_0$ to describe the generation of large-scale vortex structures, such as tropical cyclones. This approach differs from the method used in Section 5, which involved a helical force as the source of turbulence for a vortex dynamo in a moist atmosphere (see Fig. 18).

Instead, we use an external non-helical force of the form (49) with properties (50). To understand how the small-scale motions created by this non-helical force influence the dynamics of large-scale perturbations, we apply the method of multiscale asymptotic expansion. The algebraic structure of the asymptotic expansion of equations (112)-(115) in different orders in is presented in [35]. By considering the third order of the asymptotic expansion in the Reynolds number R, we obtain the basic equations for the evolution of the vortex field in "quasi-two-dimensional" geometry, which take the form (121)-(124).
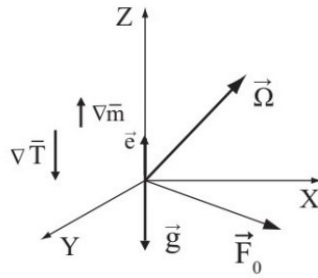
Figure 18. The angular velocity $\vec{\Omega}$ is inclined with respect to the plane (X,Y) in which the external force $\vec{F}_0$ is located.

To derive these equations in a closed form, it is necessary to calculate the Reynolds stresses $\nabla_k \left(\overline{v_0^k v_0^i} \right)$ by first obtaining solutions for a small-scale velocity field $\vec{v}_0$. It is important to note that this velocity field will differ from the one found in Section 5.2 for two reasons. Firstly, because a non-helical external force is being considered, and secondly, because all projections of the Coriolis force (oblique rotation) are taken into account. To reflect this difference, the term $D\varepsilon_{ijk} v_0^j e_k$ in equation (125) is replaced with $\varepsilon_{ijk} v_0^j D_k$. By performing the same mathematical operations as in Section 5.2, we obtain the zero approximation velocity field:

$$u_0 = \frac{f_0}{2} \frac{\widehat{A}_2^*}{\widehat{A}_2^* \widehat{D}_2^* + D_2^2} e^{i\phi_2} + c.c. = u_{03} + u_{04} \tag{152}$$

$$v_0 = \frac{f_0}{2} \frac{\widehat{A}_1^*}{\widehat{A}_1^* \widehat{D}_1^* + D_1^2} e^{i\phi_1} + c.c. = v_{01} + v_{02} \tag{153}$$

$$w_0 = -\frac{f_0}{2} \frac{D_1}{\widehat{A}_1^* \widehat{D}_1^* + D_1^2} e^{i\phi_1} + \frac{f_0}{2} \frac{D_2}{\widehat{A}_2^* \widehat{D}_2^* + D_2^2} e^{i\phi_2} + c.c. = w_{01} + w_{02} + w_{03} + w_{04} \tag{154}$$

where

$$\widehat{A}_{1,2}^* = \widehat{D}_{1,2}^* - \frac{a\widetilde{Ra}}{\widehat{D}_{\theta_{1,2}}^*} - \frac{b\widetilde{R}_m}{\widehat{D}_{m_{1,2}}^*} \tag{155}$$

This indicates that the component of the rotation parameter D_3 is eliminated due to the choice of an external force of the form (49). The resulting small-scale velocity field $\vec{v}_0$ (152)-(154) has a non-trivial topology due to the rotation of the medium, which gives rise to the topological characteristic of helicity $H = \overline{\vec{v}_0 rot \vec{v}_0}$. Helicity is a measure of the "knotting" of the field lines of force [5]. We will now demonstrate that an external force without helicity $\vec{F}_0 rot \vec{F}_0 = 0$, when combined with the Coriolis force, generates an average helicity $H \neq 0$. In coordinate representation, the average helicity is defined as follows:

$$H = \overline{u_0 \frac{\partial w_0}{\partial y}} - \overline{w_0 \frac{\partial u_0}{\partial y}} + \overline{w_0 \frac{\partial v_0}{\partial x}} - \overline{v_0 \frac{\partial w_0}{\partial x}},$$

or after substituting formulas (152)-(154)

$$H = 2i(u_{04}w_{03} - u_{03}w_{04} + w_{02}v_{01} - v_{02}w_{01}) = \frac{if_0^2}{2} \cdot \left(\frac{D_2(\widehat{A}_2 - \widehat{A}_2^*)}{\left| \widehat{A}_2 \widehat{D}_2 + D_2^2 \right|^2} + \frac{D_1(\widehat{A}_1 - \widehat{A}_1^*)}{\left| \widehat{A}_1 \widehat{D}_1 + D_1^2 \right|^2} \right).$$

For the Prandtl and Schmidt numbers $Pr = S = 1$, the average helicity H takes the form:

$$H = -f_0^2 \cdot \left(\frac{D_1(1 + \widetilde{W}_1^2 + \widetilde{R})}{(1 + \widetilde{W}_1^2)\left((1 + \widetilde{W}_1^2)^2 + 2(D_1^2 - \widetilde{R})(1 - \widetilde{W}_1^2) + (D_1^2 - \widetilde{R})^2 \right)} + \right.$$

$$\left. + \frac{D_2(1 + \widetilde{W}_2^2 + \widetilde{R})}{(1 + \widetilde{W}_2^2)\left((1 + \widetilde{W}_2^2)^2 + 2(D_2^2 - \widetilde{R})(1 - \widetilde{W}_2^2) + (D_2^2 - \widetilde{R})^2 \right)} \right) \tag{156}$$

Reynolds stresses are calculated by formulas (136)-(137), using expressions (152)-(155) we obtain

$$T^{31} = \frac{f_0^2}{4} \frac{D_2(\hat{A}_2 + \hat{A}_2^*)}{\left| \hat{A}_2 \hat{D}_2 + D_2^2 \right|^2}, \qquad T^{32} = -\frac{f_0^2}{4} \frac{D_1(\hat{A}_1 + \hat{A}_1^*)}{\left| \hat{A}_1 \hat{D}_1 + D_1^2 \right|^2} \tag{157}$$

If the properties of the medium are such that the Prandtl number Pr and the Schmidt number S are equal to one, then the expressions for the Reynolds stress components will be simplified:

$$T^{31} = \frac{f_0^2}{2} D_2 \frac{(1 + \tilde{W}_2^2 - \tilde{R})}{(1 + \tilde{W}_2^2)((1 + \tilde{W}_2^2)^2 + 2(D_2^2 - \tilde{R})(1 - \tilde{W}_2^2) + (D_2^2 - \tilde{R})^2)} \tag{158}$$

$$T^{32} = -\frac{f_0^2}{2} D_1 \frac{(1 + \tilde{W}_1^2 - \tilde{R})}{(1 + \tilde{W}_1^2)((1 + \tilde{W}_1^2)^2 + 2(D_1^2 - \tilde{R})(1 - \tilde{W}_1^2) + (D_1^2 - \tilde{R})^2)}, \tag{159}$$

where $\tilde{R} = aRa + bR_m$.

As a result, the equations for the components of the large-scale velocity field $\vec{W}$ take a closed form:

$$(\partial_T - \nabla_Z^2)\tilde{W}_1 = \frac{f_0^2}{2} D_2 \nabla_Z \left[\frac{1 + \tilde{W}_2^2 - \tilde{R}}{(1 + \tilde{W}_2^2)((1 + \tilde{W}_2^2)^2 + 2(D_2^2 - \tilde{R})(1 - \tilde{W}_2^2) + (D_2^2 - \tilde{R})^2)} \right] \tag{160}$$

$$(\partial_T - \nabla_Z^2)\tilde{W}_2 = -\frac{f_0^2}{2} D_1 \nabla_Z \left[\frac{1 + \tilde{W}_1^2 - \tilde{R}}{(1 + \tilde{W}_1^2)((1 + \tilde{W}_1^2)^2 + 2(D_1^2 - \tilde{R})(1 - \tilde{W}_1^2) + (D_1^2 - \tilde{R})^2)} \right] \tag{161}$$

Equations (160)-(161) represent the equations of a nonlinear vortex dynamo in a rotating stratified moist atmosphere with a small-scale non-helical force. It is important to note that this vortex dynamo effect occurs only in a turbulent medium that is undergoing rotation. Equations (160)-(161) have a similar form to equations (98)-(99), except that the stratification parameter in equations (160)-(161) contains the parameters of both dry and wet convection: $\tilde{R} = \left(1 + L \frac{c}{c_p}\right) Ra = Ra + R_q$. When there is no rotation ($\Omega = 0$) or external force ($F_0 = 0$), the large-scale fields are dampened by viscous dissipation. In the limit of a dry atmosphere $R_q = 0$, equations (160)-(161) are identical to equations (98)-(99), and in the limit of a homogeneous fluid $\tilde{R} = 0$, equations (160)-(161) are identical to equations (60) when $f_0 = 1$.

6.2. Large scale instability
Let us consider the initial stage of the evolution of vortex disturbances $W_{1,2}$. Then, for small perturbations (W_1, W_2), expression (156) can be linearized:

$$H = H_{01} + H_{02} - f_0^2 2D_1 \cdot \frac{(-D_1^2 + \tilde{R} + 2)(\tilde{R} + 2) + \frac{\tilde{R}}{4}(4 + (D_1^2 - \tilde{R})^2)}{(4 + (D_1^2 - \tilde{R})^2)^2} \cdot W_1 -$$

$$- f_0^2 2D_2 \cdot \frac{(-D_2^2 + \tilde{R} + 2)(\tilde{R} + 2) + \frac{\tilde{R}}{4}(4 + (D_2^2 - \tilde{R})^2)}{(4 + (D_2^2 - \tilde{R})^2)^2} \cdot W_2,$$

where $H_{01} + H_{02}$ is the constant average helicity of the small-scale field for very small perturbations $(W_1, W_2) \to 0$:

$$H_{01} + H_{02} = -\frac{f_0^2}{2} \left(D_1 \cdot \frac{\tilde{R} + 2}{4 + (D_1^2 - \tilde{R})^2} + D_2 \cdot \frac{\tilde{R} + 2}{4 + (D_2^2 - \tilde{R})^2} \right) \tag{162}$$

This indicates that the helicity of a velocity field on a small scale in a moist atmosphere that is rotating is influenced by both the Coriolis force and an external force that lacks helicity. As a result, the rotation of the medium produces helicity and suggests the emergence of a hydrodynamic α-effect, which is responsible for creating large-scale vortices. When the values are small $W_{1,2}$, equations (160)-(161) become linearized, reducing to the following set of linear equations:

$$\begin{cases} \partial_T W_1 - \nabla_Z^2 W_1 - \alpha_2 \nabla_Z W_2 = 0 \\ \partial_T W_2 - \nabla_Z^2 W_2 + \alpha_1 \nabla_Z W_1 = 0 \end{cases} \tag{163}$$

where the following notation is introduced for the coefficients

$$\alpha_1 = -2H_{01} \left[\frac{(D_1^2 - \tilde{R} - 2)(2 - \tilde{R}) + \frac{\tilde{R}}{4}(4 + (D_1^2 - \tilde{R})^2)}{(\tilde{R} + 2)(4 + (D_1^2 - \tilde{R})^2)} \right], \quad \alpha_2 = -2H_{02} \left[\frac{(D_2^2 - \tilde{R} - 2)(2 - \tilde{R}) + \frac{\tilde{R}}{4}(4 + (D_2^2 - \tilde{R})^2)}{(\tilde{R} + 2)(4 + (D_2^2 - \tilde{R})^2)} \right] \tag{164}$$

The above statement suggests that the amplification coefficients $\alpha_{1,2}$ consist of a fixed average helicity $H_{01,02}$. Equations (163) bear a resemblance to the equations used to describe vortex dynamos in media that have helical turbulence [5]. In order to analyze the large-scale instability that is described by the system of equations (163), we opt to use perturbations in the form of plane waves that have a wave vector $\vec{K} \parallel OZ$, which can be represented as $W_{1,2} \sim \exp(-i\omega t + iKZ)$. By applying this approach to the system of equations (163), we derive the dispersion equation.

$$\left(-i\omega + K^2 \right)^2 - \alpha_1 \alpha_2 K^2 = 0 \tag{165}$$

Representing $\omega = \omega_0 + i\Gamma$, from equation (165) we find

$$\Gamma = Im\omega = \pm\sqrt{\alpha_1 \alpha_2} K - K^2 \tag{166}$$

The solutions presented in (166) demonstrate that large-scale vortex disturbances exhibit instability when $\alpha_1 \alpha_2 > 0$. On the other hand, if $\alpha_1 \alpha_2 < 0$, damped oscillations with frequency $\omega_0 = \sqrt{\alpha_1 \alpha_2} K$ are observed instead of instabilities. Positive feedback between the velocity components is established through the projections of the Coriolis force, facilitated by the coefficients α_1 and α_2. It is worth noting that in the linear theory being discussed here, the coefficients α_1 and α_2 are independent of the field amplitudes but rather depend on the rotation parameters $D_{1,2}$, the total Rayleigh number $\tilde{R}$, and the amplitude of the external force f_0. When examining the coefficients α_1 and α_2, it is convenient to switch from Cartesian projections to their projections in the spherical coordinate system (D, φ, θ), where the coordinate surface $D = const$ represents a sphere, with θ representing latitude ($\theta \in [0, \pi]$) and φ representing longitude ($\phi \in [0, 2\pi]$). In this case, the rotation parameters D_1 and D_2 in the amplification coefficients of vortex disturbances α_1 and α_2 are

$$D_1 = D\sin\theta\cos\varphi, \quad D_2 = D\sin\theta\sin\varphi.$$

By setting the rotation parameter D, the stratification parameter $\tilde{R}$, and the amplitude of the external force f_0 to fixed values, we can determine the relationship between the gain and the latitude θ and longitude φ (as shown in Figure 19).
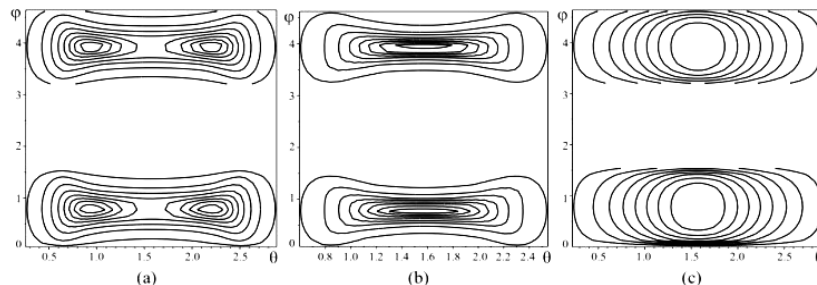

Figure 19. Contour plot for gain α versus longitude φ and latitude θ with increasing stratification parameters: a) $\tilde{R} = 3$; b) $\tilde{R} = 5$; c) $\tilde{R} = 15$. The calculations were carried out for $D = 2$ and $f_0 = 10$.

Figure 19 indicates that as the stratification parameter $\tilde{R}$ increases, the maximum gain α shifts towards the equator (latitude $\theta = \pi/2$) and longitude $\varphi = \pi/4$. It is less effective to generate large-scale vortex disturbances at the poles ($\theta = 0, \theta = \pi$) (where $\alpha \to 0$), which is consistent with meteorological observations [4], [8] that indicate the absence of large-scale cyclones at the Earth's poles. Subsequent calculations will focus on latitude $\theta = \pi/2$ and

longitude $\varphi = \pi / 4$ Next, we will examine the impact of the medium rotation D on the gain α or the process of generating large-scale perturbations by setting the value of the number $\tilde{R} = 5$.

On the left side of Fig. 20a it is shown that at a certain value of the rotation parameter D, the coefficient α reaches its maximum value α_{max}. Further, as the number D increases, the coefficient α gradually tends to zero, i.e., the α-effect is suppressed. The dependence of the coefficient α on the medium stratification parameter $\tilde{R}$ at a fixed value of the number $D = 3$ is also shown in Fig. 20. The case of a homogeneous medium $\tilde{R} = 0$ is shown in Fig. 20b, where the generation of large-scale vortex disturbances is due to the action of an external small-scale non-helical force and the Coriolis force [32]. From Fig. 20c we see that the presence of stratification for "dry" and "wet" convection ($\tilde{R} \neq 0$) can lead to a significant increase in the coefficient α and, as a result, faster generation of large-scale vortex disturbances than in a homogeneous medium. Further, with an increase in the Rayleigh numbers $\tilde{R}$, a decrease in the values of the coefficient α is observed. Fig. 21 is a graph showing the combined effect of rotation and stratification in the $(D, \tilde{R})$ plane. Here, the region of instability $\alpha > 0$ is highlighted in grey. The graph of the dependence (see the right side of Fig. 21) of the instability increment Γ on the wave numbers K has a standard form, typical for the α-effect.
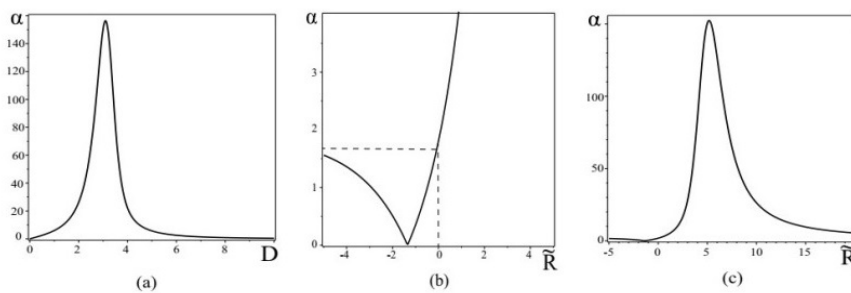

Figure 20. a) plot of the dependence of the α-effect on medium rotation parameter D; b) the graph shows the value in the case of a homogeneous medium $\tilde{R} = 0$; c) plot of the α-effect versus the medium stratification parameter $\tilde{R}$. The calculations were carried out for $f_0 = 10$.
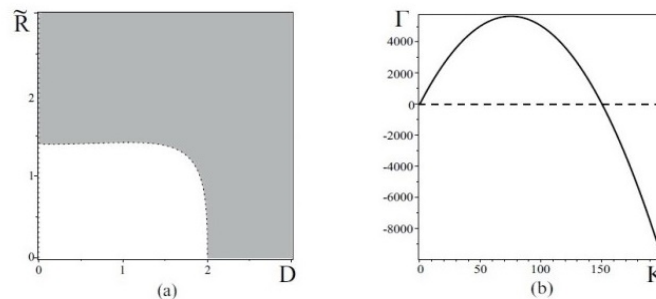

Figure 21. On the left is a graph for α in the $(D, \tilde{R})$ plane, where the area corresponding to positive values of α (unstable solutions) is shown in grey and the area corresponding to negative values of α is shown in white; on the right is a graph of the dependence of the instability increment Γ on the wave numbers K for the parameters $D = 3$, $\tilde{R} = 5$.

6.3. Stationary nonlinear vortex structures

It is evident that the exponential growth of small perturbations $W_{1,2}$ resulting from the development of large-scale instability eventually saturates. This is attributed to the emergence of nonlinear effects, which weaken the coefficient of the nonlinear α-effect ($\alpha \sim 1/W_{1,2}^4$) and increase the amplitude of perturbations. Consequently, nonlinear vortex structures are formed. To search for stationary structures, we substitute into equations (160)-(161) $\partial_T = 0$ and integrate these equations once over Z. We focus on the case of the maximum value of α_{max}, where latitude $\theta = \pi / 2$ and longitude $\varphi = \pi / 4$ This results in a system of nonlinear equations in the following form:

$$\frac{d\tilde{W}_1}{dZ} = -f_0^2 D\sqrt{2} \frac{1 + \tilde{W}_2^2 - \tilde{R}}{(1 + \tilde{W}_2^2)(4(1 + \tilde{W}_2^2)^2 + 4(D^2 - 2\tilde{R})(1 - \tilde{W}_2^2) + (D^2 - 2\tilde{R})^2)} + C_1 \tag{167}$$

$$\frac{d\tilde{W}_2}{dZ} = f_0^2 D\sqrt{2} \frac{1 + \tilde{W}_1^2 - \tilde{R}}{(1 + \tilde{W}_1^2)(4(1 + \tilde{W}_1^2)^2 + 4(D^2 - 2\tilde{R})(1 - \tilde{W}_1^2) + (D^2 - 2\tilde{R})^2)} + C_2 \tag{168}$$

Here C_1, C_2 are arbitrary constants of integration. Note that the dynamic system of equations (167)-(168) is conservative and therefore Hamiltonian. It is easy to find it by writing equations (167)-(168) in the Hamiltonian form:

$$\frac{d\widetilde{W}_1}{dZ} = -\frac{dH}{d\widetilde{W}_2}, \quad \frac{d\widetilde{W}_2}{dZ} = \frac{dH}{d\widetilde{W}_1}$$

where the Hamiltonian H has the form:

$$\mathrm{H} = H_1(\widetilde{W}_1) + H_2(\widetilde{W}_2) + C_2\widetilde{W}_1 - C_1\widetilde{W}_2 \tag{169}$$

the functions $\mathrm{H}_{1,2}$ are

$$\mathrm{H}_{1,2} = f_0^2 D\sqrt{2}\int \frac{(1+\tilde{W}_{1,2}^2 - \widetilde{R})d\tilde{W}_{1,2}}{(1+\tilde{W}_{1,2}^2)(4(1+\tilde{W}_{1,2}^2)^2 + 4(D^2 - 2\widetilde{R})(1-\tilde{W}_{1,2}^2) + (D^2 - 2\widetilde{R})^2)}$$

The integral in the Hamiltonian $\mathrm{H}_{1,2}$ is not calculated exactly in quadratures, so we calculate it for fixed rotation parameters $D = \sqrt{10}$ and stratification $\widetilde{R} = 5$, which were used in the linear theory. Under these conditions, Hamiltonian (169) takes the form:

$$\mathrm{H} = -\frac{25}{4}\sqrt{5}\left(\frac{\widetilde{W}_1(11\widetilde{W}_1^2 + 21)}{(\widetilde{W}_1^2 + 1)^2} + \frac{\widetilde{W}_2(11\widetilde{W}_2^2 + 21)}{(\widetilde{W}_2^2 + 1)^2} + 11(arctg\widetilde{W}_1 + arctg\widetilde{W}_2)\right) + C_2\widetilde{W}_1 - C_1\widetilde{W}_2$$

After performing a qualitative analysis of the system of equations (167)-(168), we found that only two types of fixed points can be observed in the phase space: elliptic and hyperbolic fixed points. By linearizing the right-hand side of equations (167)-(168) in the vicinity of fixed points, we determined their type and constructed a phase portrait. Through this analysis, we identified the presence of four fixed points, two of which are hyperbolic and two are elliptic. The phase portrait of the dynamic system of equations (167)-(168) for constants $C_1 = -0.05$, $C_2 = 0.05$ and parameters $D = \sqrt{10}$, $\widetilde{R} = 5$ and $f_0 = 10$ is displayed in Fig. 22. This figure shows the existence of closed trajectories on the phase plane around elliptic points and separatrices that link hyperbolic points. The closed trajectories correspond to nonlinear periodic solutions or nonlinear waves, while the separatrices correspond to localized kink-type vortex structures (as depicted in Fig. 23).
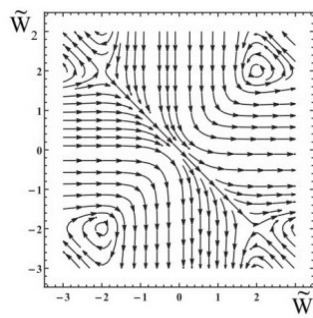

Figure 22. Phase plane for the dynamic system of equations (167)-(168) under the conditions $C_1 = -0.05$ and $C_2 = 0.05$. Here you can see the presence of closed trajectories around elliptical points and separatrices that connect hyperbolic points.
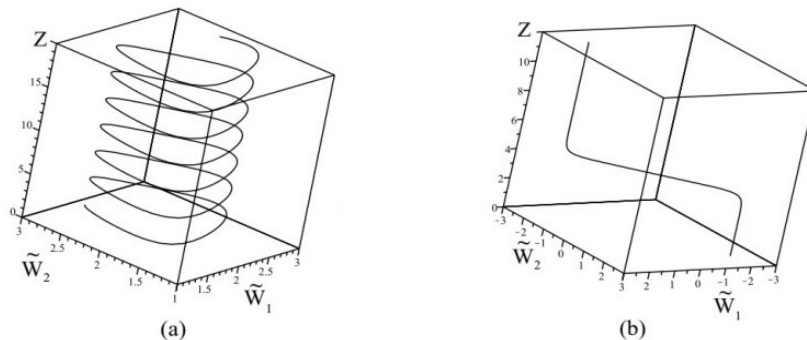

Figure 23. On the left is a non-linear spiral wave that corresponds to a closed trajectory on the phase plane; on the right is a localized non-linear vortex structure (kink), which corresponds to a separatrix on the phase plane.

7. VORTEX DYNAMO IN AN OBLIQUELY ROTATING STRATIFIED NANOFLUID WITH A SMALL-SCALE NON-HELICAL FORCE

An important factor to consider is the impact of small particles present in the hydrodynamic medium, which is of interest due to its prevalence in both technological and natural environments. The presence of nanoparticles in the medium results in what is commonly referred to as a nanofluid. One issue that arises with nanofluids is the generation of large-scale structures, which is discussed in this section based on the results of a study (reference [36]). The study revealed the occurrence of a large-scale instability in an obliquely rotating stratified nanofluid, caused by an external small-scale non-helical force. Nonlinear equations for large-scale motions were obtained using a method of multiscale asymptotic expansions, and a linear large-scale instability was examined as a function of rotation parameters D, temperature stratification $\widetilde{Ra}$, and nanoparticle concentration $\widetilde{R}_n$. The study also discovered a new effect of LSVS generation in a nanofluid associated with an increase in nanoparticle concentration. This effect resulted in the formation of circularly polarized Beltrami vortices. The saturation mode of the large-scale instability was studied, and a dynamic system of equations for large-scale perturbations of the velocity field was obtained in the stationary regime. Numerical solutions of this system of equations were found, which showed the existence of localized vortex structures in the form of nonlinear Beltrami waves and kinks.

7.1. Equations and Statement of the Problem

The system being considered is an infinite horizontal layer of an incompressible nanofluid that undergoes constant rotation at a fixed angular velocity $\vec{\Omega} = (\Omega_1, \Omega_2, \Omega_3)$, with inclination in relation to the (X, Y) plane, as illustrated in Fig. 24.
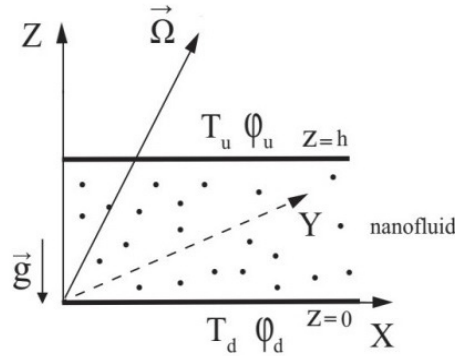

Figure 24. The angular velocity $\vec{\Omega}$ is inclined with respect to the plane (X, Y) in which the external force $\vec{F}_{0\perp}$ is located.

The nanofluid is contained between two parallel planes, $z = 0$ and $z = h$, where the temperature and volume fraction of nanoparticles remain constant:

$$T = T_d, \phi = \phi_d \quad \text{при} \quad z = 0,$$
$$T = T_u, \phi = \phi_u \quad \text{при} \quad z = h, \tag{170}$$

at $T_d > T_u, \phi_u > \phi_d$. Both boundary surfaces are assumed to be free. The hydrodynamic equations governing the behavior of a viscous, incompressible, rotating nanofluid under the Boussinesq approximation are given by the following expressions (as seen, for instance, in references [40]-[41]):

$$\rho_{00}\left(\frac{\partial \vec{V}}{\partial t} + \vec{V} \cdot \nabla \vec{V}\right) = -\nabla P + \mu \nabla^2 \vec{V} + [\phi \rho_p + (1-\phi)\rho_{00}(1 - \beta(T - T_u))]\vec{g} + 2\rho_{00}\vec{V} \times \vec{\Omega} + \vec{F}_0 \tag{171}$$

$$(\rho c)_f\left(\frac{\partial T}{\partial t} + \vec{V} \cdot \nabla T\right) = k_f \nabla^2 T + (\rho c)_p\left(D_B \nabla \phi \cdot \nabla T + D_T \frac{\nabla T \cdot \nabla T}{T_u}\right) \tag{172}$$

$$\frac{\partial \phi}{\partial t} + \vec{V} \cdot \nabla \phi = D_B \nabla^2 \phi + \frac{D_T}{T_u} \nabla^2 T \tag{173}$$

$$\nabla \vec{V} = 0 \tag{174}$$

Equations (171)-(174) are accompanied by boundary conditions for the velocity of the nanofluid. The vertical impermeability condition of the layer boundaries and the absence of tangential stresses at these boundaries result in the following boundary conditions for the velocity:

$$V_z = 0, \quad \frac{\partial^2 V_z}{dz^2} = 0, \quad \text{при} \quad z = 0, h \tag{175}$$

Here, $\rho_{00} = \phi\rho_p + (1-\phi)\rho_f$ is the density of the nanofluid at the control temperature T_u, ρ_p is the density of the nanoparticles, ρ_f is the density of the base fluid at the temperature T_u, ϕ is the volume fraction of the nanoparticles, and β is the coefficient of thermal expansion. The unit vector $\vec{e} = (0,0,1)$ is directed towards the positive Z axis. Gravity is directed vertically downwards $\vec{g} = (0,0,-g)$; $(\rho c)_f, (\rho c)_p$ is the effective heat capacity of the base fluid and nanoparticles; D_B - Brownian diffusion coefficient, D_T - thermophoretic diffusion coefficient. The signs of the coefficients and are positive, and they are respectively equal:

$$D_B = \frac{k_B T}{3\pi\mu d_p}, \quad D_T = \left(\frac{\mu_f}{\rho_f}\right)\left(\frac{0.26 k_f}{2 k_f + k_p}\right),$$

where d_p is the diameter of the nanoparticles, k_B is the Boltzmann constant, k_f, k_p is the thermal conductivity of the base fluid and nanoparticles, and μ_f is the viscosity of the base fluid. Equation (171) includes an external force $\vec{F}_0$, which simulates an excitation source in the medium of small-scale and high-frequency fluctuations of the velocity field with a small Reynolds number $R = \frac{v_0 t_0}{\lambda_0} \ll 1$, where λ_0 is the characteristic scale, t_0 is the characteristic time. Let us pass in equations (171)-(174) and boundary conditions (170), (175) to dimensionless variables, which we denote by an asterisk (*):

$$(x^*, y^*, z^*) = \frac{(x,y,z)}{h}, \vec{V} = (V_x^*, V_y^*, V_z^*) = (V_x, V_y, V_z)\frac{h}{\chi_f}, t^* = \frac{t \cdot \chi_f}{h^2}, P^* = \frac{P \cdot h^2}{\chi_f \mu},$$

$$\vec{\Omega}^* = \frac{\vec{\Omega}}{\Omega_0}, \phi^* = \frac{\phi - \phi_d}{\phi_u - \phi_d}, T^* = \frac{T - T_u}{T_d - T_u}, F_0^* = F_0\frac{h^3}{\chi_f \mu}, \chi_f = \frac{k_f}{(\rho c)_f}.$$

Omitting the asterisk (*) in the system of dimensionless equations (176)-(179) and boundary conditions (180), we get

$$\frac{1}{\text{Pr}}\left(\frac{\partial \vec{V}}{\partial t} + \vec{V} \cdot \nabla \vec{V}\right) = -\nabla P + \nabla^2 \vec{V} - \vec{e} R_n \phi - \vec{e} R_m + \vec{e} Ra T + \sqrt{Ta}(\vec{V} \times \vec{\Omega}) + \vec{F}_0 \tag{176}$$

$$\frac{\partial T}{\partial t} + \vec{V} \cdot \nabla T = \nabla^2 T + \frac{N_B}{L_e}(\nabla \phi \cdot \nabla T) + \frac{N_A N_B}{L_e}(\nabla T \cdot \nabla T) \tag{177}$$

$$\frac{\partial \phi}{\partial t} + \vec{V} \cdot \nabla \phi = \frac{1}{L_e}\nabla^2 \phi + \frac{N_A}{L_e}\nabla^2 T \tag{178}$$

$$\nabla \cdot \vec{V} = 0 \tag{179}$$

$$T_d = 1, \phi_d = 0, V_z = \frac{\partial^2 V_z}{\partial z^2} = 0 \quad \text{при} \quad z = 0,$$

$$T_u = 0, \phi_u = 1, V_z = \frac{\partial^2 V_z}{\partial z^2} = 0 \quad \text{при} \quad z = 1, \tag{180}$$

where $\text{Pr} = \mu / \rho_{00}\chi_f$ is the Prandtl number, $R_n = (\rho_p - \rho_f)(\phi_u - \phi_d)gh^3 / \mu\chi_f$ is the concentration Rayleigh number, $R_m = (\rho_p\phi_d + \rho_f(1-\phi_d))gh^3 / \mu\chi_f$ is the Rayleigh number of the base density, $Ra = (T_d - T_u)\rho_{00}g\beta h^3 / \mu\chi_f$ is the Rayleigh number, $Ta = 4\Omega_0^2 h^4 \rho_{00}^2 / \mu^2$ is the Taylor number, $L_e = \chi_f / D_B$ is the Lewis number, $N_B = (\phi_u - \phi_d) \cdot \dfrac{(\rho c)_p}{(\rho c)_f}$ is the coefficient characterizing the increase in the density of nanoparticles, and $N_A = D_T(T_d - T_u) / D_B T_u(\phi_u - \phi_d)$ is the modified diffusion coefficient. Let us represent all the quantities in equations (176)-(179) as the sum of the ground (stationary) state and the perturbed one:

$$\vec{V} = \vec{V}', T = T_b(z) + T', \phi = \phi_b(z) + \phi', P = P_b(z) + P'. \tag{181}$$

After substituting (181) into equations (176)-(179), we find the evolution equations for the perturbed quantities $\vec{V}', T', \phi'$:

$$\frac{1}{\text{Pr}}\left(\frac{\partial \vec{V}'}{\partial t} + \vec{V}' \cdot \nabla \vec{V}'\right) = -\nabla P' + \nabla^2 \vec{V}' - \vec{e} R_n \phi' + \vec{e} Ra T' + \sqrt{Ta}(\vec{V}' \times \vec{\Omega}) + \vec{F}_0$$

$$\frac{\partial T'}{\partial t} + \vec{V}' \cdot \nabla T' + V_z' \frac{dT_b}{dz} = \nabla^2 T' + \frac{N_B}{L_e}(\nabla \phi' \cdot \nabla T') + \frac{N_B}{L_e}\left(\frac{d\phi_b}{dz}\frac{dT'}{dz} + \frac{d\phi'}{dz}\frac{dT_b}{dz}\right) +$$

$$+ \frac{N_A N_B}{L_e}(\nabla T' \cdot \nabla T') + \frac{2N_A N_B}{L_e}\frac{dT'}{dz}\frac{dT_b}{dz} \tag{182}$$

$$\frac{\partial \phi'}{\partial t} + \vec{V}' \cdot \nabla \phi' + V_z' \frac{d\phi_b}{dz} = \frac{1}{L_e}\nabla^2 \phi' + \frac{N_A}{L_e}\nabla^2 T'$$

against the background of the main equilibrium state, set by constant gradients of temperature and volume fraction of nanoparticles:

$$0 = -\frac{dP_b}{dz} - R_m - R_n \phi_b + Ra T_b$$

$$0 = \frac{d^2 T_b}{dz^2} + \frac{N_B}{L_e}\left(\frac{d\phi_b}{dz}\frac{dT_b}{dz}\right) + \frac{N_A N_B}{L_e}\left(\frac{dT_b}{dz}\right)^2 \tag{183}$$

$$0 = \frac{d^2 \phi_b}{dz^2} + N_A \frac{d^2 T_b}{dz^2}.$$

Using boundary conditions (180), from equations (183) we find solutions for $T_b = 1 - z$ and $\phi_b = z$, which have a linear dependence on z.

Let the external force $\vec{F}_0$ have the form (49) and satisfy the properties (50). The simple physical form of the external force (49) can be easily implemented in laboratory experiments. Let us rescale the variables in the equations for perturbations (182):

$$\vec{x} \to \frac{\vec{x}}{\lambda_0}, t \to \frac{t}{t_0}, \vec{V} \to \frac{\vec{V}'}{v_0}, P \to \frac{P'}{p_0}, F_0 \to \frac{F_0}{f_0}, T \to \frac{T'}{R}, \phi \to \frac{\phi'}{R}, \frac{p_0 t_0}{\lambda_0 v_0} = \frac{f_0 t_0}{v_0} = \frac{t_0}{\lambda_0^2} = 1.$$

As a result, we obtain the following system of equations for perturbations:

$$\frac{1}{\Pr}\left(\frac{\partial \vec{V}}{\partial t} + R\vec{V} \cdot \nabla \vec{V}\right) = -\nabla P + \nabla^2 \vec{V} - \vec{e}\widetilde{R_n}\phi + \vec{e}\widetilde{Ra}T + \vec{V} \times \vec{D} + \vec{F}_0 \tag{184}$$

$$\frac{\partial T}{\partial t} + R\vec{V} \cdot \nabla T - V_z = \nabla^2 T + R\frac{N_B}{L_e}(\nabla \phi \cdot \nabla T) + \frac{N_B}{L_e}\left(\frac{dT}{dz} - \frac{d\phi}{dz}\right) + \tag{185}$$

$$+ R\frac{N_A N_B}{L_e}(\nabla T \cdot \nabla T) - \frac{2N_A N_B}{L_e}\frac{dT}{dz}$$

$$\frac{\partial \phi}{\partial t} + R\vec{V} \cdot \nabla \phi + V_z = \frac{1}{L_e}\nabla^2 \phi + \frac{N_A}{L_e}\nabla^2 T \tag{186}$$

where new designations are introduced

$$D = \frac{2h^2}{\mu}\rho_{00}\lambda_0^2 \Omega, \quad \widetilde{R_n} = R_n \cdot \lambda_0^3, \quad \widetilde{Ra} = Ra \cdot \lambda_0^3.$$

In equations (184)-(186), we treat the Reynolds number $R = \frac{v_0 t_0}{\lambda_0} \ll 1$ as a small parameter for the purpose of

asymptotic expansion, while considering the other parameters $D, \widetilde{R_n}, \widetilde{Ra}$ as arbitrary and not impacting the expansion scheme. An external force acting on the equilibrium state results in small-scale and high-frequency velocity oscillations. Although the average values of these oscillations are zero, nonlinear interactions generate terms in certain orders of the perturbation theory that do not cancel out upon averaging.

7.2. Large scale instability

By employing the method of multiscale asymptotic expansions in the context of the "quasi-two-dimensional" problem, we derived a closed system of equations for the large-scale velocity field $\vec{W}$. This system has the form of equations (80)-(81), and the expressions for the Reynolds stress components at $Pr = 1$ are given by:

$$T^{31} = \frac{f_0^2 D_2 k_0^2 (k_0^4 + \widetilde{\omega}_2^2 - \widetilde{Ra} - l_{n_2})}{2(k_0^4 + \widetilde{\omega}_2^2)((k_0^4 + \widetilde{\omega}_2^2)^2 + 2(D_2^2 - \widetilde{Ra})(k_0^4 - \widetilde{\omega}_2^2) + (D_2^2 - \widetilde{Ra})^2 + r_{n_2}(k_0^4 + \widetilde{\omega}_2^2) + 2p_{n_2} D_2^2)},$$

$$T^{32} = -\frac{f_0^2 D_1 k_0^2 (k_0^4 + \widetilde{\omega}_1^2 - \widetilde{Ra} - l_{n_1})}{2(k_0^4 + \widetilde{\omega}_1^2)((k_0^4 + \widetilde{\omega}_1^2)^2 + 2(D_1^2 - \widetilde{Ra})(k_0^4 - \widetilde{\omega}_1^2) + (D_1^2 - \widetilde{Ra})^2 + r_{n_1}(k_0^4 + \widetilde{\omega}_1^2) + 2p_{n_1} D_1^2)}, \qquad (187)$$

where $\widetilde{\omega}_{1,2} = \omega_0 - k_0 W_{1,2}$. The expressions for the coefficients $l_{n_{1,2}}$, $p_{n_{1,2}}$, $r_{n_{1,2}}$ have a very cumbersome form and are given in [36].

When the amplitude (W_1, W_2) is small, the nonlinear equations for $\vec{W}$ can be approximated by linear vortex dynamo equations similar to system (100). The solutions of this linear system describe circularly polarized plane waves, known as Beltrami waves. The amplitude of these waves grows exponentially over time. The large-scale velocity field satisfies the Beltrami flow, which satisfies the following condition:

$$\vec{W} \times rot \vec{W} = 0$$

To determine the conditions under which a large-scale vortex instability occurs, we first examine the dependence of the amplification α_{nf} on the angle θ of inclination of the axis of rotation of the nanofluid. The solid line in Fig. 25 represents this dependence for fixed values of

$$D = 2, \widetilde{Ra} = 2, k_0 = \omega_0 = 1, \Pr = 5, \widetilde{R}_n = 0.122, N_A = 5, L_e = 5000.$$
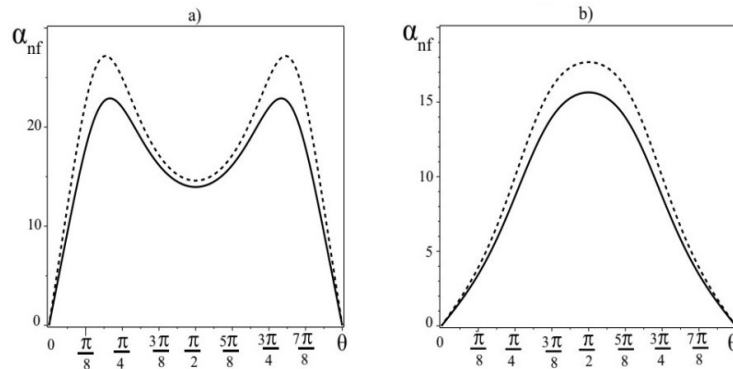

Figure 25. The solid line shows the dependence of the gain α_{nf} for a nanofluid on the angle of inclination θ, and the dashed line shows the dependence of the gain α_b for a pure fluid on the angle of inclination θ. Graphs a) are built for the Prandtl number $\Pr = 5$, and graphs b) for $\Pr = 1$.

The values of the nanofluid parameters $\Pr, \widetilde{R}_n, N_A, L_e$ (Al_2O_3-water) are taken from [40]. As can be seen from Fig. 25a, the maximum value α_{nf} for a nanofluid is the angle of inclination $\theta_{max} \approx \pi/5 + \pi n$, and the minimum value is $\theta_{min} \approx \pi/2 + \pi n$. The dashed line in Fig. 25a corresponds to the dependence $\alpha_b(\theta)$ in the case of a "pure" fluid with the Prandtl number $\Pr = 5$. The graphs in Fig. 25a show that the maximum amplification coefficient $\alpha_b = (\alpha_{nf})_{\widetilde{R}_n = 0}$ for a "pure" fluid is greater than that for a nanofluid. The same conclusion remains valid for the Prandtl numbers $\Pr = 1$. In this case, the maximum gains in nano- and "pure" fluids are at the deflection angles $\theta \approx \pi/2 + \pi n$ (see Fig. 25b). Hence, it follows that the characteristic time T_{nf} and characteristic scale L_{nf} of large-scale vortices generated in a nanofluid exceed the corresponding scales T_b, L_b in a "pure" fluid:

$$T_{nf} \gg T_b, \quad L_{nf} \gg L_b, T_{nf} \approx (\alpha_{nf}^2/4)^{-1}, L_{nf} \approx (\alpha_{nf}/2)^{-1}, T_b \approx (\alpha_b^2/4)^{-1}, L_b \approx (\alpha_b/2)^{-1}$$

Let us consider the influence of the nanofluid rotation effect on the amplification factor α_{nf} or the process of large-scale vortex generation. For these purposes, we fix the nanofluid parameters $\Pr, \widetilde{R}_n, N_A, L_e$, and the Rayleigh number $\widetilde{Ra} = 2$.

The incline angle chosen is $\theta_{max} \approx 0.645 \sim \pi/5$, which corresponds to the maximum values of the gain (see Fig. 26a). As can be seen from Fig. 26a, at a certain value of the rotation parameter D, the coefficient $\alpha_{nf}(\alpha_b)$

reaches its maximum value $\alpha_{max}^{(nf,b)}$. Further, as the number D increases, the gains gradually tend to zero, i.e., the α -effect is suppressed.
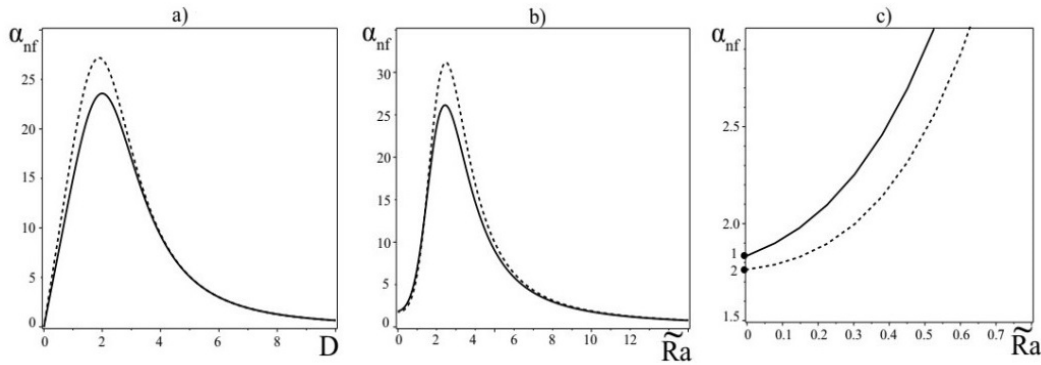

Figure 26. a) The solid line shows the dependence of the gain α_{nf} for a nanofluid on the rotation parameter D, and the dashed line shows the dependence of the gain α_b for a pure fluid on the rotation parameter D; b) The solid line shows the dependence of the gain α_{nf} for a nanofluid on the Rayleigh number $\widetilde{Ra}$, and the dashed line shows the dependence of the gain α_b for a "pure" fluid on the Rayleigh number $\widetilde{Ra}$; c) Point 1 corresponds to the value α_{nf} (nanofluid) at $\widetilde{Ra} = 0$, and Point 2 corresponds to the value α_b ("pure" fluid) at $\widetilde{Ra} = 0$.

Further, fixing the nanofluid parameters $\Pr, \widetilde{R}_n, N_A, L_e$, rotation $D = 2$ and tilt angle $\theta_{max} \approx 0.645$, we determine the dependence of the coefficient α_{nf} on the Rayleigh number $\widetilde{Ra}$. It can be seen from Fig. 26b that the maximum value of the gain $\alpha_{nf}(\alpha_b)$ corresponds to small Rayleigh numbers $\widetilde{Ra}$. Large-scale vortices are efficiently generated in the range of Rayleigh numbers $\widetilde{Ra} \in [0,3]$; this means that at high Rayleigh numbers $\widetilde{Ra}$, large-scale instability does not occur in nano- and ordinary fluids, but ordinary convective instability arises. Under the condition when there is no heating $\widetilde{Ra} = 0$, the amplification factor in pure fluid α_b (point 2 in Fig. 26c) is less than that in nanofluid α_{nf} (point 1 in Fig. 26c): $\alpha_{nf} > \alpha_b$. On Figs. 26a-26b it is also observed that the maximum gain $\alpha_b = (\alpha_{nf})_{\widetilde{R}_n=0}$ for a "pure" liquid is greater than that for a nanofluid. On Fig. 27a is a graph showing the combined effect of rotation and temperature stratification in the $(D, \widetilde{Ra})$ plane. Here, the region of instability $\alpha_{nf} > 0$ is highlighted in grey. Curve 1 corresponds to the instability boundary for a nanofluid ($\widetilde{R}_n = 0.122$), and curve 2 corresponds to the instability boundary for a pure fluid ($\widetilde{R}_n = 0$).
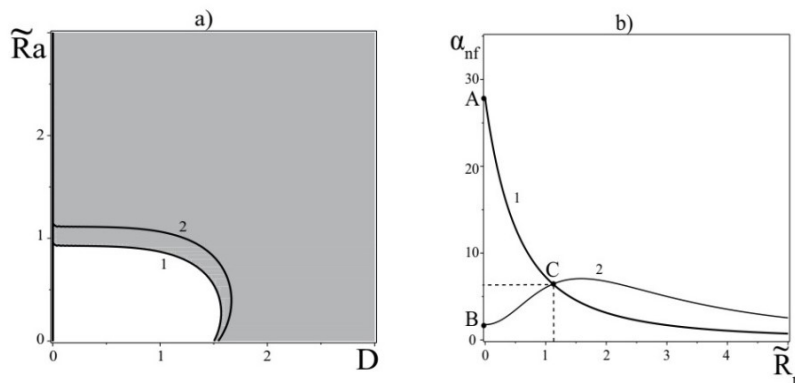

Figure 27. a) Plot α_{nf} in the plane $(D, \widetilde{Ra})$, where the area corresponding to positive values α_{nf} (unstable solutions) is shown in grey and negative values are shown in white. Curve 1 corresponds to the instability boundary for a nanofluid ($\widetilde{R}_n = 0.122$), and curve 2 corresponds to the instability boundary for a pure fluid ($\widetilde{R}_n = 0$). b) A graph of the α_{nf} -effect versus the Rayleigh concentration number $\widetilde{R}_n$.

Now let's analyze the influence of the Rayleigh concentration number $\widetilde{R}_n$ on the gain or generation of the LSVS for the following fixed parameters: $D = 2, \widetilde{Ra} = 3, k_0 = \omega_0 = 1, \Pr = 5, N_A = 5, L_e = 5000, \theta \approx 0.645$. On Fig. 27b, the intersection of the graphs (curve 1 and curve 2) is at point $C(\widetilde{R}_n^{(0)}, \alpha_{nf}^{(0)})$. Curve 1 is constructed for the case when there

is a temperature gradient $\widetilde{Ra} = 3$. At $\widetilde{R}_n = 0$, curve 1 shows the maximum value α_b^{st} (point A) which corresponds to a "pure" stratified fluid. A further increase in the concentration of nanoparticles leads to a decrease in α_{nf}. Curve 2 is plotted for the case when there is no temperature gradient. It can be seen from the behaviour of curve 2 that an increase in the concentration of nanoparticles first leads to an increase α_{nf} and then to a decrease. At $\widetilde{R}_n = 0$, curve 2 shows the maximum value α_b^h (point B) corresponding to the amplification factor for a homogeneous fluid [32]. Here we see that in a "pure" stratified fluid, the generation of LSVSs is more efficient than in a homogeneous fluid, which is consistent with the conclusions of [34]. Thus, at a certain value of the number $\widetilde{R}_n^{(0)}$ (the concentration of nanoparticles), we obtain equal rates of LSVS generation (point C in Fig. 27b) in the nanofluid both with $\widetilde{Ra} \neq 0$ and without a temperature gradient $\widetilde{Ra} = 0$. Physically, this process can be explained as follows. An increase in the concentration of nanoparticles on the upper surface layer leads to the appearance of a flow due to the gravitational segregation of nanoparticles on the lower surface. In turn, in the presence of a temperature gradient, a heat flux $\vec{q} \sim \vec{e}(T_d - T_u)/h$ arises that prevents the nanoparticles from settling on the lower surface layer. With an increase in the concentration of nanoparticles $\widetilde{R}_n$, a decrease in the proportion of heat flux occurs and, as a result, a decrease in the gain α_{nf}. On the charts in Fig. 28, the dependence of the instability increment Γ on the wave numbers K for the hydrodynamic α_{nf}-effect in a nanofluid at constant parameters $D = 2, \widetilde{Ra} = 2, \Pr = 5, \widetilde{R}_n = 0.122, N_A = 5, L_e = 5000, \theta \approx 0.645$ is shown.

As can be seen from Fig. 28a, with an increase in the frequency ω_0 of the external force F_0 at $k_0 = 1$, the maximum growth rate Γ_{max} of large-scale vortex disturbances decreases. Fixing the frequency of the external force at $\omega_0 = 1$, we plot the growth rate (see Fig. 28b) as the small-scale wavenumber k_0 changes. For numbers $k_0 < 1$, one can observe both an increase in the maximum growth rate Γ_{max} of large-scale vortex disturbances ($k_0 = 0.8$) relative to the level Γ_{max} at $k_0 = 1$, and a decrease in the maximum growth rate of large-scale vortex disturbances at $k_0 = 0.5$. This behavior is due to the structural dependence of the coefficient α_{nf} on small-scale parameters of the external force (ω_0, k_0).
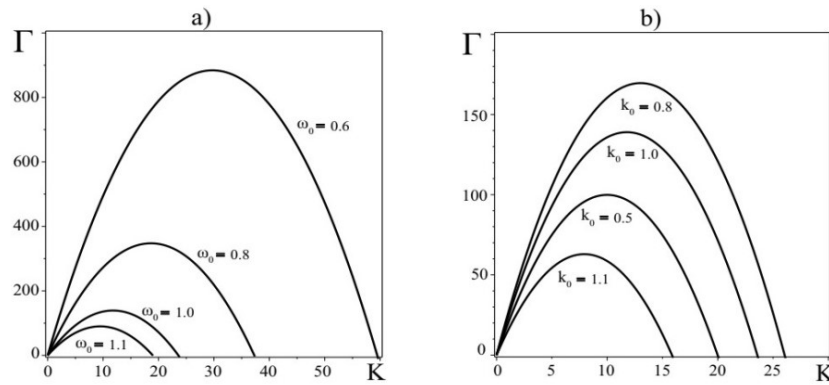

Figure 28. a) Plot of the dependence of the instability increment Γ on the wave numbers for different frequencies ω_0 of the external force $\vec{F}_0$ at $k_0 = 1$. b) Plot of the dependence of the instability increment Γ on the wave numbers K for different wave numbers k_0 of the external force $\vec{F}_0$ at $\omega_0 = 1$.

7.3. Instability saturation and nonlinear structures

An increase in W_1 and W_2 leads to saturation of the instability. As a result of the development and stabilization of the instability, nonlinear structures arise. In the stationary case, these structures are described by nonlinear equations in the Hamiltonian form

$$\frac{dW_1}{dZ} = \frac{dH}{dW_2}, \quad \frac{dW_2}{dZ} = -\frac{dH}{dW_1} \tag{188}$$

where the Hamiltonian H has the form:

$$H = H_1(W_1) + H_2(W_2) + C_2 W_1 - C_1 W_2$$

and the functions $H_{1,2}$ are

$$H_{1,2} = \frac{f_0^2 \sqrt{2}}{4} D \sin\theta \int \frac{k_0^2 (k_0^4 + \widetilde{\omega}_{1,2}^2 - \widetilde{Ra} - l_{n_{1,2}}) \mathrm{d}W_{1,2}}{2 \Pr(k_0^4 + \widetilde{\omega}_2^2)\Lambda_{1,2}} \ . \tag{189}$$

The integral in the Hamiltonian $H_{1,2}$ is not calculated exactly in quadratures. We used the values of nanofluid parameters $\Pr = 1, \widetilde{R}_n = 0.122, N_A = 5, L_e = 5000$ (Al_2O_3 -water) [40]. As a result of the analysis of nonlinear equations, four fixed points were found, two of which are of the hyperbolic type and two of the elliptic type.

The figure in Fig. 29 depicts the phase portrait of a dynamic system of equations, which bears resemblance to equations (104)-(105), given certain constants $C_1 = -0.005$ and $C_2 = 0.005$ parameters $D = \widetilde{Ra} = 2$, $k_0 = \omega_0 = 1$, $f_0 = 10$. Through the phase portrait, we can qualitatively describe potential stationary solutions. Of particular interest are localized solutions that can be found in the phase portrait trajectories connecting fixed (singular) points on the phase plane. As shown in Fig. 29, closed trajectories are present on the phase plane surrounding elliptical points and separatrices that link hyperbolic points. Nonlinear periodic solutions, such as nonlinear waves, correspond to closed trajectories, while localized kink-type vortex structures (as seen in Fig. 30) correspond to separatrices.
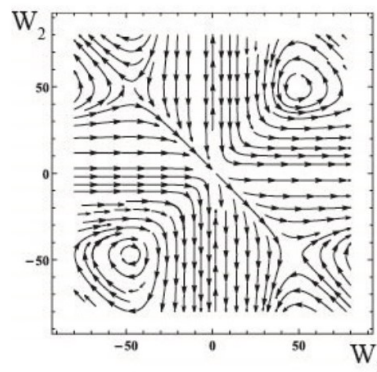

Figure 29. Phase plane of the dynamic system of equations (188) for constants $C_1 = -0.05$ and $C_2 = 0.05$. Here you can see the presence of closed trajectories around elliptical points and separatrices that connect hyperbolic points.
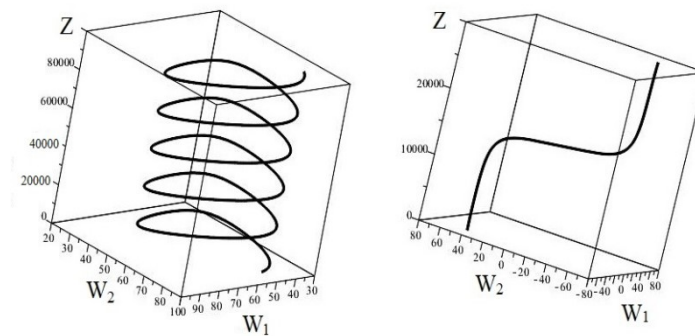

Figure 30. On the left is a non-linear spiral wave that corresponds to a closed trajectory on the phase plane; on the right is a localized non-linear vortex structure (kink), which corresponds to a separatrix on the phase plane.

8. CONCLUSIONS

The review paper presents the theoretical findings of the authors [30]-[36] in the area of vortex dynamo in rotating media. The focus is on the mechanisms behind the generation of large-scale vortex structures resulting from both non-helical external forces and the Coriolis force. A comprehensive analysis of closed systems of nonlinear equations describing the linear and nonlinear stages of the growth of large-scale vortex flows in rotating turbulent media has been conducted. The authors have obtained reasonable estimates of the characteristic scales of instability in a rotating moist atmosphere, which can explain the formation of the large-scale spiral structure of cloudy mesovortices and typhoons at the initial stage of their development. A promising direction in the development of the vortex dynamo theory for rotating nanofluid media containing floating microorganisms. For these media, the theory of large-scale instability can also be developed using the asymptotic method of multiscale expansions. We can anticipate the discovery of new large-scale stationary vortex structures in rotating porous media saturated with nanofluids. The investigation of these structures is not only useful for geophysical applications but also for a variety of technological problems.

ORCID IDs
Michael I. Kopp, https://orcid.org/0000-0001-7457-3272, **Volodymyr V. Yanovsky,** https://orcid.org/0000-0003-0461-749X

REFERENCES

[1] H. P. Greenspan, *The Theory of Rotating Fluids* (Cambridge University Press, 1968).

[2] V.I. Petviashvili, and O.A. Pohkotelov, *Solitary Waves in Plasmas and in the Atmosphere* (London, 1992). https://doi.org/10.4324/9781315075556

[3] M.Ya. Marov, and A.V. Kolesnichenko, *Turbulence and Self-Organization. Modeling Astrophysical Objects* (Springer, New York, 2013). https://doi.org/10.1007/978-1-4614-5155-6

[4] A.S. Monin, *Theoretical Geophysical Fluid Dynamics* (Springer Dordrecht, 1990). https://doi.org/10.1007/978-94-009-1880-1

[5] Anatoli Tur, and Vladimir Yanovsky, *Coherent Vortex Structures in Fluids and Plasmas* (Springer, 2017). https://doi.org/10.1007/978-3-319-52733-8

[6] M.V. Nezlin, and E.N. Snezhkin, *Rossby Vortices, Spiral Structures, Solitons* (Springer Series in Nonlinear Dynamics, 1993).

[7] A.M. Fridman, and A.V. Khoperskov, *Physics of Galactic Disks* (Cambridge International Science Publishing, 2013).

[8] A.S. Monin, *An Introduction to the Theory of Climate* (Springer Dordrecht, 1986). https://doi.org/10.1007/978-94-009-4506-7

[9] O. Onishchenko, V. Fedun, W. Horton et al., "The stationary concentrated vortex model", Climate, **9**, 39-52 (2021). https://doi.org/10.3390/cli9030039

[10] M. Steenbeck, F. Krause, and K.H. Rädler, "Berechnung der mittleren Lorentz Feldstärke $\overline{\vec{v} \times \vec{b}}$ für ein elektrisch leitendes Medium in turbulenter, durch Coriolis-Kräfte beeinfluß ter Bewegung", Z. Naturforsch **21**, 369-376 (1966). https://doi.org/10.1515/zna-1966-0401

[11] S.M. Tobias, "The turbulent dynamo", J. Fluid Mech. **912**, P1 (2021). https://doi.org/10.1017/jfm.2020.1055

[12] F. Rincon, "Dynamo theories", J. Plasma Phys. **85**, 205850401 (2019) https://doi.org/10.1017/S0022377819000539

[13] S.S. Moiseev, R.Z. Sagdeev, A.V. Tur, G.A. Khomenko, and V.V. Yanovsky, "A theory of large-scale structure origination in hydrodynamic turbulence", Sov. Phys. JETP, **58**, 1144 (1983).

[14] G. Khomenko, S. Moiseev, & A. Tur, The hydrodynamical alpha-effect in a compressible medium, J. Fluid Mech. **225**, 355-369 (1991). https://doi.org/10.1017/S0022112091002082

[15] F. Krause, and G. Rüdiger, "On the Reynolds stresses in mean-field hydrodynamics. I. Incompressible homogeneous isotropic turbulence", Astron. Nachr. **295**, 93-99 (1974). https://doi.org/10.1002/asna.19742950205

[16] V.V. Gvaramadze, G.A. Khomenko, and A.V. Tur, "Large-scale vortices in helical turbulence of incompressible fluid", Geophys. Astrophys. Fluid Dyn. **46**, 53-69 (1989). https://doi.org/10.1080/03091928908208904

[17] S.S. Moiseev, P.B. Rutkevich, A.V. Tur, and V.V. Yanovsky, "Vortex dynamos in a helical turbulent convection", Sov. Phys. JETP, **67**, 294-299 (1988).

[18] S.S. Moiseev, K.R. Oganyan, P.B. Rutkevich et al., "An eddy dynamo and spiral turbulence", in: *Integrability and Kinetic Equations for Solitons*, edited by V.G. Bar'yachtar, (Naukova Dumka, Kiev, 1990), pp. 280-332.

[19] B.Ya. Shmerlin, and M.V. Kalashnik, "Rayleigh convective instability in the presence of phase transitions of water vapor. The formation of large-scale eddies and cloud structures", Phys. Usp. **56**, 473-485 (2013). https://doi.org/10.3367/UFNe.0183.201305d.0497

[20] G.V. Levina, S.S. Moiseev, and P.B. Rutkevich, "Hydrodynamic alpha-effect in a convective system," in: *Nonlinear Instability, Chaos and Turbulence, Adv. Fluid Mech. Series*, edited by L. Debnath, D.N. Riahi, (WIT Press, Southampton, Boston, UK, USA, 2000), Vol. 2, pp. 111-161 (2000).

[21] P.B. Rutkevich, "Equation for vortex instability caused by convective turbulence and coriolis force", JETF **77**, 933-938 (1993).

[22] L.L. Kitchatinov, G. Rüdiger, and G. Khomenko, "Large-scale vortices in rotating stratified disks", Astron. Astrophys. **287**, 320-324 (1994). https://adsabs.harvard.edu/full/1994A%26A...287..320K

[23] L.M. Smith, and F. Waleffe, "Generation of slow large scales in forced rotating stratified turbulence", J. Fluid Mech. **451**, 145-168 (2002). https://doi.org/10.1017/S0022112001006309

[24] N. Kleeorin, and I. Rogachevskii, "Generation of large-scale vorticity in rotating stratified turbulence with inhomogeneous helicity: mean-field theory", J. Plasma Phys. **84**, 735840303 (2018). https://doi.org/10.1017/S0022377818000417

[25] U. Frisch, Z.S. She, and P.L. Sulem, "Large scale flow driven by the anisotropic kinetic alpha effect", Physica D, **28**, 382-392 (1987). https://doi.org/10.1016/0167-2789(87)90026-1

[26] P.L. Sulem, Z.S. She, H. Scholl, and U. Frisch, "Generation of Large-Scale Structures in Three-Dimensional Flow Lacking Parity-Invariance. Journal of Fluid Mechanics", J. Fluid Mech. **205**, 341-358 (1989). https://doi.org/10.1017/S0022112089002065

[27] B. Dubrulle, and U. Frisch, "Eddy viscosity of parity-invariant flow", Phys. Rev. A **43**, 5355-5364 (1991). https://doi.org/10.1103/physreva.43.5355

[28] A.V. Tur, and V.V. Yanovsky, "Large-scale instability in hydrodynamics with stable temperature stratification driven by small-scale helical force," (2012). https://doi.org/10.48550/arXiv.1204.5024

[29] A.V. Tur, and V.V. Yanovsky, "Non-Linear Vortex Structure in Stratified Fluid Driven by Small-scale Helical Force", Open J. Fluid Dyn. **3**, 64-74 (2013). https://doi.org/10.4236/ojfd.2013.32009

[30] M.I. Kopp, A.V. Tur, and V.V. Yanovsky, "The Large-scale instability in rotating fluid with small scale force", Open J. Fluid Dyn. **5**, 128-138 (2015). https://doi.org/10.4236/ojfd.2015.52015.

[31] M.I. Kopp, A.V. Tur, and V.V. Yanovsky, "Nonlinear vortex dynamo in a rotating stratified moist atmosphere", J. Exp. Theor. Phys. **124**, 1010-1022 (2017). https://doi.org/10.1134/S1063776117060127

[32] M.I. Kopp, A.V. Tur, and V.V. Yanovsky, "Nonlinear Vortex Structures in Obliquely Rotating Fluid", Open J. Fluid Dyn. **5**, 311-321 (2015). https://doi.org/10.4236/ojfd.2015.54032

[33] M.I. Kopp, A.V. Tur, and V.V. Yanovsky, "The large-scale instability and nonlinear vortex structures in obliquely rotating fluid with small scale non spiral force", VANT, **4**, 264-269 (2015).

[34] M.I. Kopp, A.V. Tur, and V.V. Yanovsky, "Nonlinear vortex structures in obliquely rotating stratified fluids driven by small scale non helical forces", Ukr. J. Phys. **66**, 478-488 (2021). https://doi.org/10.15407/ujpe66.6.478

[35] M.I. Kopp, A.V. Tur, and V.V. Yanovsky, "Vortex Dynamo in a Rotating Stratified Moist Atmosphere driven by Small-scale Non-helical Forces", Geophys. Astrophys. Fluid Dyn. **115**, 551-576 (2021). https://doi.org/10.1080/03091929.2021.1946802

[36] M.I. Kopp, A.V. Tur, and V.V. Yanovsky, "Vortex Dynamo in an obliquely rotating stratified nanofluid by small-scale non-helical forces," East Eur. J. Phys. **2**, 51-72 (2021). https://doi.org/10.26565/2312-4334-2021-2-02

[37] G.V. Levina, and M.T. Montgomeri, "The first examination of the helical nature of tropical cyclogenesis", Doklady Earth Sciences, **434**, 1285-1289 (2010). https://doi.org/10.1134/S1028334X1009031X

[38] G.V. Levina, "On the Path from the Turbulent Vortex Dynamo Theory to Diagnosis of Tropical Cyclogenesis", Open J. Fluid Dyn. **8**, 86-114 (2018). https://doi.org/10.4236/ojfd.2018.81008.

[39] G. Rüdiger, "On the α-Effect for Slow and Fast Rotation", Astron. Nachr. **299**, 217-222 (1978). https://doi.org/10.1002/asna.19782990408

[40] D. Yadav, G.S. Agrawal, and R. Bhargava, "Thermal instability of rotating nanofluid layer", Int. J. Eng. Sci. **49**, 1171-1184 (2011). https://doi.org/10.1016/j.ijengsci.2011.07.002

[41] S. Agarwal, and B.S. Bhadauria, "Unsteady heat and mass transfer in a rotating nanofluid layer", Continuum Mech. Thermodyn. **26**, 437-445 (2014). https://doi.org/10.1007/s00161-013-0309-6

ВИХРОВЕ ДИНАМО У СЕРЕДОВИЩАХ, ЩО ОБЕРТАЮТЬСЯ
Михайло Й. Копп[a], Володимир В. Яновський[a,b]
[a]Інститут монокристалів, Національна Академія Наук України, пр. Леніна 60, 61072 Харків, Україна
[b]Харківський національний університет імені В.Н. Каразіна, майдан Свободи, 4, 61022, Харків, Україна

В огляді висвітлено основні досягнення теорії вихрового динамо в середовищах, що обертаються. Обговорюються різні моделі вихрового динамо в таких середовищах: однорідна в'язка рідина, температурно-стратифікована рідина, волога атмосфера і стратифікована нанорідина. Наведено основні аналітичні та чисельні результати для цих моделей, що отримані методом багатомасштабних асимптотичних розкладів. Головна увага приділяється моделям із неспіральною зовнішньою силою. Для вологої атмосфери, що обертається, отримані характерні оцінки просторового і часового масштабів вихрових структур. Виявлено нові ефекти вихрового динамо у стратифікованій нанорідині, що обертається, які виникають за рахунок термофорезу та броунівського руху наночастинок. Результати аналізу нелінійних рівнянь вихрового динамо у стаціонарному режимі приводять до існування спіральних кінків, періодичних нелінійних хвиль та солітонів.

Ключові слова: *теорія динамо; великомасштабна нестійкість; сила Коріоліса; багатомасштабні асимптотичні розкладання; α-ефект; солітони; кінки*